NTNU

Norwegian University of
Science and Technology

Dynamic Simulations of Simultaneous HVDC Contingencies in the Nordic Power System Considering System Integrity Protection Schemes

Espen Hafstad Solvang

Master of Energy and Environmental Engineering
Submission date: June 2018
Supervisor: Kjetil Uhlen, IEL
Co-supervisor: Iver Bakken Sperstad, SINTEF Energi
Sigurd Hofsmo Jakobsen, IEL

Norwegian University of Science and Technology
Department of Electric Power Engineering

Problem description

HVDC links carrying gigawatts of power such as the under construction North Sea Link and NordLink introduces new challenges to the Nordic power system. The possibility of contingencies of one or several such links possibly represents a significant risk to the Nordic transmission system operators, especially if the extraordinary event of simultaneous HVDC link contingencies is considered. Such an outage may be of several gigawatts in size, far exceeding the dimensioning fault of 1450 MW of the Nordic power system.

The possible consequences, barriers and vulnerabilities of the power grid following large HVDC link outages must be identified. Specifically, the consequences at the transmission level for the Nordic power system if multiple outages occur simultaneously at HVDC links importing power should be illuminated. The sufficiency of existing barriers such as Under-Frequency Load Shedding, HVDC Emergency Power and generator primary response to hinder severe system states following such large HVDC link should be considered, along with the potential of the possible future barrier, Demand-Side Response, to improve the frequency response of the power grid. The extent to which the reduced inertia in the future power system affects the system's ability to withstand such HVDC contingencies should be quantified. Finally, vulnerabilities in the Nordic grid that limit the ability of the Nordic power system to withstand simultaneous HVDC contingencies should be identified.

Preface

This thesis concludes my degree Master of Science at the Norwegian University of Science and Technology (NTNU) after 5 years at the study program Energy and Environmental Engineering under the department of Electrical Engineering. The thesis is credited 30 ECTS points and is written in co-operation with SINTEF Energy Research as part of the HILP-project [1]. This thesis is a continuation of my project work in the previous semester, presented in [2].

I would like to thank my supervisor Kjetil Uhlen at NTNU for his guidance and supervision throughout the work done for this thesis. His insights and constructive criticism have proven helpful many times and is genuinely appreciated for navigating the many challenges encountered. I would also like to thank my co-supervisors Iver Bakken Sperstad at SINTEF Energy Research and Sigurd Hofsmo Jakobsen at NTNU. They have both continuously been available at short notice to answer questions big and small, and I look forward to working with both of them when we will be colleagues at SINTEF Energy Research in the near future.

Trondheim, 2018-06-11

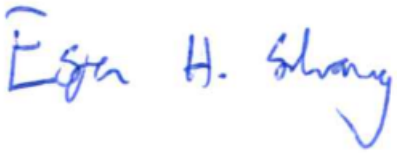

Espen Hafstad Solvang

Abstract

Individual HVDC links connecting the Nordic power system to other synchronous systems may carry gigawatts of power. For the transmission system operators, who must maintain power balance to operate the grid at 50.0 Hz, the outage of such HVDC links may lead to large, undesirable frequency swings due to large power imbalances after an outage, where lower system inertia will lead to larger frequency swings.

The extraordinary event of simultaneous outages of multiple HVDC links is highly unlikely, but may lead to consequences in the power grid that are unacceptable. In this thesis, the consequences of such an event are considered for the Nordic power system with an emphasis on system frequency response and the ability of barriers in the form of System Integrity Protection Schemes, or corrective actions, to curb the most critical frequency excursions. The ability of generator primary response as well as corrective actions such as Under-Frequency Load Shedding, HVDC Emergency Power and Demand-Side Response to improve the frequency response is considered. Only outages of links that are importing power are examined.

The model used is the aggregated network model Nordic 44. The PSS®E software performs the simulations interfaced with Python using the Psspy API. An assortment of cases are studied; first, event trees are used with corrective actions to identify the ability of different corrective actions to affect the system frequency response for higher and lower inertia scenarios following outages of North Sea Link and NordLink. Thereafter, the impact of locality in terms of where the simultaneous HVDC link outages occur is studied in an attempt to identify critical consequences and vulnerabilities of the power system.

Results indicate that the frequency drop will be very large and perhaps unmanageable when the system inertia decreases. If there are insufficient primary reserves, the system is bound to collapse. However, Demand-Side Response has significant potential to contain the frequency decline if time-delay for Demand-Side Response is low. In several cases, voltage decline in the south of Sweden leads to system separation and limits ability of the power system to withstand the simultaneous HVDC outages. Current construction of HVDC links may thus be contributing to future voltage instability in Sweden. Use of frequency-based corrective actions does not affect the voltage issues in southern Sweden, and voltage-based corrective

actions or extra measures for voltage stabilization in Sweden may be necessary.

A recommendation following the obtained results is to emphasize low activation time-delay in projects and future implementation of Demand-Side Response, as this will allow realization of the potential of Demand-Side Response in frequency containment. As construction of new HVDC links may increase the rate of occurrence of large HVDC link outages, it is also recommended that investments in construction of HVDC links are accompanied by investments in voltage stabilizing measures in the south of Sweden. The results should be verified by tuning of the N44 model towards voltage response and by the detailed network models of the transmission system operators.

Sammendrag

HVDC-forbindelser mellom det nordise kraftsystem og andre synkronnett overfører mye effekt. For systemoperatørene, som må balansere effekten i kraftsystemet for å opprettholde 50.0 Hz nettfrekvens, kan utfall av slike HVDC-forbindelser føre til store, uønskede frekvenssvingninger grunnet effektubalanse etter utfallet hvor mindre systemtreghet fører til større frekvenssvingninger.

Den ekstraordinære hendelsen samtidige utfall av flere HVDC-forbindelser er høyst usannsynlig, men kan føre til konsekvenser i kraftsystemet som er uakseptable. Konsekvensene av en slik hendelse er i denne oppgaven betraktet for det nordiske kraftsystemet, med vekting på frekvensrespons. Evnen til systemvern, eller korrektive tiltak, i å motvirke de mest kritiske frekvensforløpene er blitt vurdert. Dette inkluderer primærrespons, frekvensstyrt belastningsfrakobling, HVDC nødeffekt og storskala laststyring hos forbruker. I tillegg blir spenningsstyrt belastningsfrakobling vurdert i noen simuleringer. Kun utfall av HVDC-forbindelser som importerer strøm er betraktet. Modellen brukt for simuleringer er den aggregerte nettverksmodellen Nordic 44. Programvaren PSS®E utfører simuleringer via en kobling med Python og Psspy API-et. Forskjellige simuleringer utføres; først blir hendelsestrær nyttet med korrektive tiltak for å illustrere frekvenspåvirkningsevnen til de ulike korrektive tiltakene i scenario med høy treghet og med lav treghet etter samtidige utfall av HVDC-forbindelsene North Sea Link og NordLink. Deretter blir effekten av lokasjon av HVDC-utfall betraktet ved å simulere samtidige utfall i henholdsvis Norge, Sverige og Finland.

Resultater indikerer at frekvensfallet etter samtidige HVDC-utfall blir veldig stort og kanskje uhåndterbart ved lavere treghet i systemet. Systemet vil ikke takle et utfall om det er utilstrekkelige primærreserver. Storskala laststyring har potensialet til å motvirke frekvensfall hvis tidsforsinkelsen til aktivering etter frekvensfall er lav. Spenningsfall i Sør-Sverige virker ut til å være et problem og fører til øydrift samt tap av synkronisme for generatorer, noe som i stor grad begrenser systemets evne til å håndtere samtidige HVDC-utfall. Utbyggelse av HVDC-forbindelser kan derfor være medvirkende til fremtidige spenningsfall i Sverige. Frekvensbaserte korrektive tiltak virker ut til å ha noen innvirkning på spenningen i Sør-Sverige, og spenningsstabiliserende tiltak kan derfor være nødvendig.

To anbefalinger til systemoperatørene følger. Den første er å vektlegge lav aktiveringstid eller

responstid av frekvensrespons for laststyring i framtidige prosjekter og implementering av storskala laststyring. Den andre, i takt med investeringer i HVDC-forbindelser, å investere i spenningsstabilisering for Sør-Sverige. Resultatene bør kontrolleres ved å kalibrere N44-modellen til spenningsrespons eller ved å bruke mer detaljerte nettmodeller.

Contents

0.1 Acronyms

DSR Demand-Side Response

FCR Frequency Containment Reserves

HVDC High-Voltage Direct Current

HILP High Impact, Low Probability

N44 Nordic 44

NL NordLink

NSL North Sea Link

OSF Outage Scaling Factor

PGU Programmable Generation Unit

ROCOF Rate of change of frequency

SSF Steady-State Frequency

SIPS System Integrity Protection Scheme

UFLS Under-Frequency Load Shedding

UVLS Under-Voltage Load Shedding

VSC Voltage Source Converter

Chapter 1

Introduction

The power system is changing. While traditionally there have been relatively few, centralized generators, generation is becoming decentralized as renewable energy is replacing traditional generation units. This development is anticipated to lead to decreased inertia in the future power system due to a lack of rotating mass in some types of renewable energy, such as photovoltaics. Possibly decreased inertia is described in [3]:

> *In 2025 the inertia, measured as kinetic energy, is estimated to be below the required volume of 120–145 GWs 1–19 per cent of the time depending on the climate year (based on analyses with historical reference period 1962–2012). The lowest kinetic energy values are observed during summer nights with high wind production. In the current Nordic power system (2010–2015), the estimated kinetic energy was below 140 GWs 4 per cent of the time or less; however, in 2009 the duration was approximately 12 per cent.*

At the same time, solar and wind power is variable, causing lower predictability of the operating states of the grid, and expansion and strengthening of the grid is more difficult than before due to increased political opposition. HVDC links are becoming more prevalent, causing increased interdependency between different synchronous systems. Together, these factors lead to a more complex grid and require Transmission System Operators (TSO) to operate under stricter constraints where the grid is operated closer to its limits. In such an operating state, individual faults, compared to a less constrained power system, may lead to more severe consequences when they occur.

To ensure a stable power system frequency for all components in the grid, the power balance in the system must be maintained. Disturbances such as outages of generators or loss of load frequently influence the power balance in the system causing frequency transients, where lower inertia will lead to larger frequency swings. One type of power system element that may face disturbances are HVDC links. HVDC links are today used to interconnect different synchronous areas and to provide a controllable power transfer between regions. As each link carries large amounts of power, disturbances to HVDC links pose a problem to TSO who are responsible to maintain the system frequency and active power balance. If an HVDC link is disconnected, there is temporarily a large power imbalance in the system which may cause large frequency swings as kinetic energy is taken from rotating masses. HVDC link outages are a limited problem in the present power system, but the Nordic system sees increasing HVDC interconnection to the continental European power system: today, the total transfer capacity of Nordic HVDC links is 8 GW [3] but another 4 GW is already under construction [4]. The newer links carry larger amounts of power than previous links. Both NordLink [5] and North Sea Link [6] will carry 1400 MW each, which alone approaches the dimensioning fault of 1450 MW in the Nordic system. The dimensioning fault is the maximum instantaneous generation loss the system is built to withstand and is also referred to as the reference incident. An outage of either link will thus be considered a possibly critical disturbance with large consequences. China has similar issues in regions that have little generation and are reliant on HVDC power import [7]. With decreasing inertia, such disturbances may be even more critical in the future. A future summer scenario might be imagined, where the Nordic TSOs are importing high amounts of cheap renewable energy from Continental-Europe while hydro generators are offline, leading to low amounts of rotating mass and low inertia in the Nordic power system. If an unlikely event should then occur, such as a contingency to not only one but multiple several HVDC-links, what would be the consequences? Such an event would be considered High Impact, Low Probability (HILP) event or an extraordinary event. In some cases only two simultaneous outages are necessary to far exceed the dimensioning fault, as illustrated in fig. 1.1.

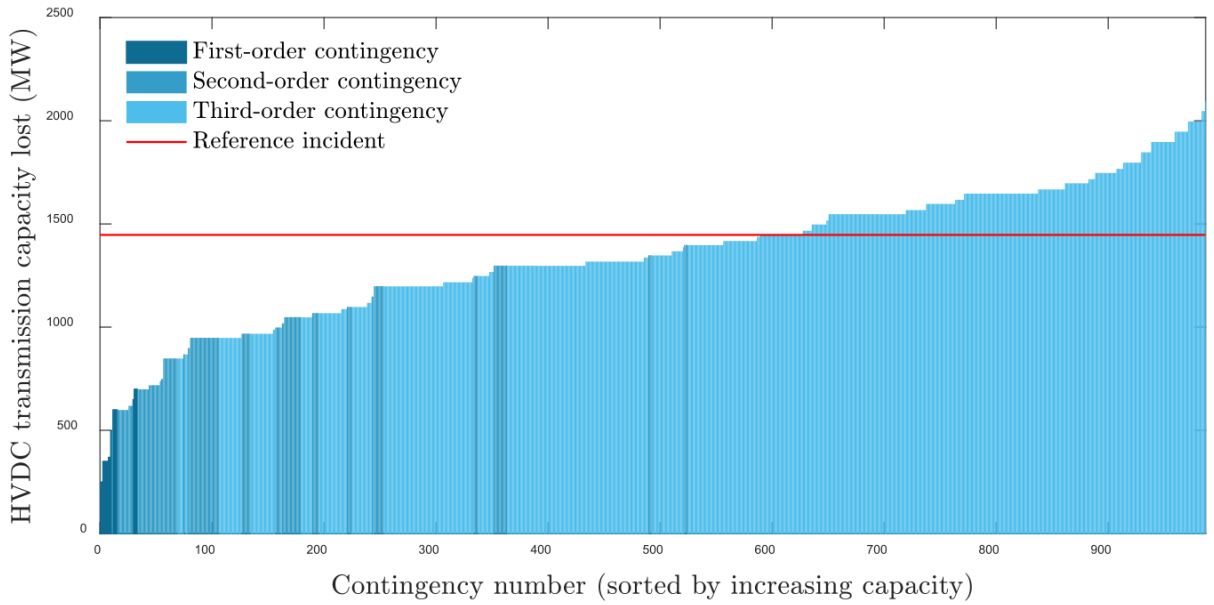

Figure 1.1: Size of power loss due to simultaneous outage of combinations of HVDC links. First-order, second-order and third-order contingencies indicate simultaneous outages of 1, 2 or 3 HVDC links respectively[8]. The transmission capacity lost is for the 2018 power system, and with future HVDC links carrying large amounts of power, far more contingency combinations may exceed the dimensioning fault size

1.1 High Impact, Low Probability

HVDC contingencies is one category of HILP events that may lead to especially large consequences due to the large amounts of power transferred over HVDC links. The HILP project [1] attempts to learn to identify, understand and assess such extraordinary events, as well as to increase awareness of extraordinary events and competence in handling them. The low probability of such events may cause them to be entirely neglected if operators are unaware of the possibility of them occurring, while at the same time an aware operator may overestimate the probability of such an event occurring [9]. A framework for handling such extraordinary events is thus necessary for incorporation in cost-benefit analyses by TSOs for power system planning. Perhaps an even greater benefit is the possible increased preparedness for the unthinkable; for a society critically dependant on electric power supply, the consequences of such an extraordinary event may be too severe to be permitted at all.

1.2 System Integrity Protection Schemes

To hinder severe consequences from faults in a power system operating close to its limit, rapidly acting control mechanisms called System Integrity Protection Schemes (SIPS) may quickly act to save the power system. Primarily, the SIPS in this thesis are concerned with restoring the power balance of the system to hinder large frequency drops in the study of contingencies of HVDC-links importing power. Two types of SIPS are concerned with reducing the load of the system: Under-Frequency Load Shedding (UFLS) and Demand-Side Response (DSR). UFLS may disconnect any load as the frequency drops very low and is considered the final frontier in a power system to avoid blackout. DSR also disconnects loads as frequency drops, but only loads that are enabled for DSR. These loads are typically less visible to the user that load is being disconnected and DSR may thus possibly be used more aggressively as a power system control action without reduced quality of life for the end customer. Examples of such DSR-enabled equipment may be electric car batteries, which when charging may contribute to DSR by reducing load or even supplying power in response to a control signal. A third type of SIPS, HVDC Emergency Power, responds to frequency drops or specific events by increasing import at online HVDC links to reduce power system active power generation deficit. SIPS differ from primary response, which over several seconds gradually increase power output depending on generation unit dynamics, as SIPS are typically activated in response to larger disturbances and are not continuously acting on the system during normal operation.

1.3 HVDC-links in the Nordic system

The HVDC links currently operational in the Nordic power grid are shown in tab. 1.1 along with NordLink and North Sea Link. The geographical placement of these links is shown in fig. 1.2. In this thesis, the Nordic system refers to Norway, Sweden and Finland and only the HVDC links in these countries are considered. Study of contingencies of these HVDC links is performed using the Nordic44 [10] aggregated network model in Siemens PSS®E software [11]. Several combinations of HVDC link contingencies may be considered for studies of consequences of simultaneous outages, as is obvious from the numerous links in the power

grid. Simultaneous outages of North Sea Link and NordLink importing maximum amount of power are the primary objects of study in this thesis. Simultaneous outages of North Sea Link and NordLink lead to a potentially massive outage of 2.8 GW if both links are importing power at their rated capacity. Additional studies of simultaneous outages are performed for Southern Sweden with simultaneous outages of KontiSkan, Baltic Cable and SwePol, as well as for Finland with simultaneous outages of EstLink and Vyborg Link.

Table 1.1: HVDC links in the Nordic system

Cable name	Countries	Capacity [MW]
NorNed	NO-NE	700
Skagerak 1	NO-DK	250
Skagerak 2	NO-DK	250
Skagerak 3	NO-DK	500
Skagerak 4	NO-DK	700
KontiSkan 1	SE-DK	380
KontiSkan 2	SE-DK	360
Baltic Cable	SE-GE	600
SwePol	SE-PO	600
Nordbalt	SE-LI	700
FennoSkan	SE-FI	500
Estlink 1	FI-EE	350
Estlink 2	FI-EE	650
Vyborg Link	FI-RU	1420
NordLink (2019)	NO-GE	1400
North Sea Link (2020)	NO-GB	1400

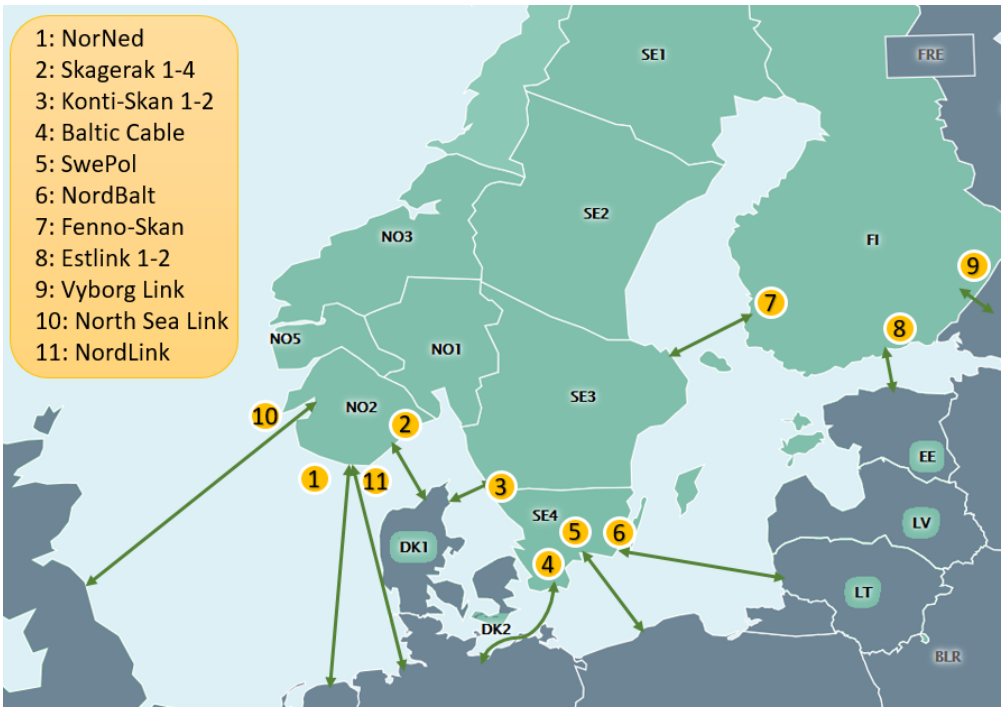

Figure 1.2: Geographical placement of HVDC links in the Nordic system

1.4 Scope of work

Considerations are made as to the effects of simultaneous HVDC-outages of high import HVDC links in the Nordic grid in operating states with high and low inertia. The possible failure or lacking activation of SIPS is evaluated using event trees. The ability of SIPS such as UFLS, DSR and HVDC Emergency Power to mitigate frequency drops resulting from power imbalances are tested, and the results of each type of SIPS is compared using performance indicators such as steady-state frequency and frequency nadir by running separate case studies. DSR in particular is extensively tested with different response speeds as well as response size, as DSR is a potentially new type of SIPS that may be implemented in the future Nordic power system. System states such as generator angles, frequencies, voltages and active power generation among others, are presented in plots for individual case studies. Limiting factors for the Nordic power system to be able to withstand extraordinary outages are considered by case studies of outages in Norway, Sweden and Finland. The considered outages are all for HVDC links importing power. Consequences are considered primarily in terms of large signal frequency stability, but also in rotor angle and voltage stability.

1.5 Thesis outline

The thesis is organized in 11 chapters. A framework for the study of extraordinary events is presented in chapter 2 along with background for the development for such a framework and the challenges of modelling rare events. In chapter 3, the concepts of power system stability is introduced along with the four stages of frequency dynamics in the grid following a generation outage. In chapter 4 power system security is explored with a focus on corrective actions and SIPS. Chapter 5 describes modelling and methodology to simulate simultaneous HVDC-outages with emergency power mechanisms in the Nordic grid including software, modelling and descriptions of case studies. Chapter 6 verifies that the multitude of scripts written and models used for this thesis are behaving as intended. Thereafter, chapters 7, 8 and 9 cover results for the described case studies. A summary of results along with discussion and conclusions follow in chapter 10 and with suggestions for further work in chapter 11.

Chapter 2

Extraordinary Events

An event that is both unforeseen and unforeseeable may be considered as an extraordinary event. If the extraordinary event has a large influence or impact, it may be considered a high impact, low probability (HILP) event. HILP events have been underestimated or neglected in traditional risk analyses [9], necessitating a method to include HILP events in risk analyses.

Studying the impact of HILP events such as simultaneous outages of HVDC links may seem like a purely academic pursuit due to the unforeseeable nature of such events. As [12] and [13] argue, the human mind is not suited for considering the unlikely events that may occur. On the contrary, when planning towards the future, humans are primarily concerned with what is more likely to happen and base future expectations partially on what has happened before. Acknowledgement of the unpredictability of what the future may hold and the associated planning for the unpredictable is thus necessary. For example, it is shown in [14] that power system upgrades which reduce the frequency of blackouts may in the long term increase the frequency of *large* blackouts. The frequency of large blackouts may still be small, but the highly improbable already contributes significantly to the total blackout risk [15]. An increase of large blackouts will possibly drastically increase the risk associated with these unlikely events and a framework for tackling them is needed.

2.1 Vulnerability analysis

A framework for tackling extraordinary events is currently being developed in the HILP-project [1]. Central to the understanding of HILP-events is the understanding of the terms *risk* and *vulnerability*. Risk combines both probability and cost and may be considered as the product of probability and consequences of an unwanted event occurring. Vulnerability describes the susceptibility to unwanted events occurring and the coping capacity after the event has occurred. This makes vulnerability a part of risk [16].

To gain insight in the vulnerability of the power system, a vulnerability analysis can be performed. The vulnerability analysis approach may be considered a reversed approach to the risk analysis described in [9]. The steps of vulnerability analysis can be described as follows [8]:

1. Identify critical consequences
2. Identify critical contingencies potentially leading to critical consequences
3. Identify threats that can cause the critical contingencies
4. Identify vulnerabilities associated with the power system's susceptibility and coping capacity
5. Identify factors influencing the power system's coping capacity
6. Identify existing and missing barriers against critical contingencies

Vulnerability analysis may used for HVDC link contingencies, as is illustrated in fig. 2.1. This vulnerability analysis for HVDC link contingencies is carried out step by step in [8], limited to the frequency drop following loss of import. It is briefly covered as follows. Critical consequences are identified as large amounts of power interrupted or power interruptions over longer duration. Large frequency drops following HVDC contingencies may lead to load shedding. Massive load shedding which successfully prevents a blackout may still be considered a critical consequence. Critical contingencies are listed HVDC contingencies of combinations of HVDC links exceeding the system reference incident of loss of 1450 MW active power, and are compared to the reference incident as in fig. 1.1. Threats that may cause critical contingencies are identified as blackouts in neighbouring synchronous areas, local

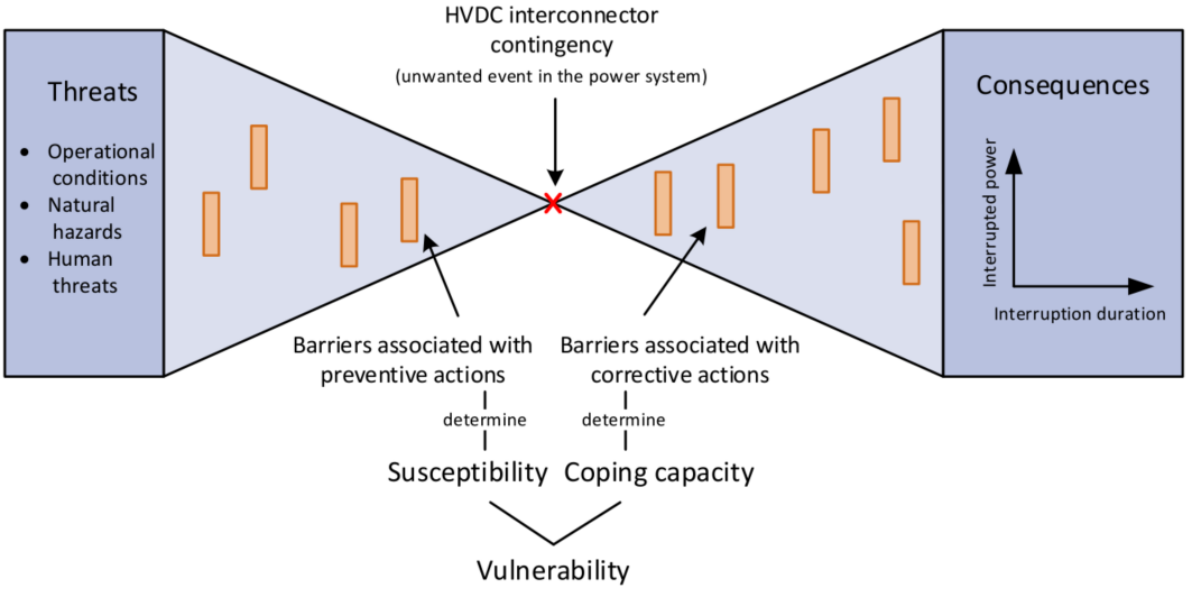

Figure 2.1: Bow-tie model for vulnerability analysis [8]

threats to converter stations and threats to HVDC transmission lines. Vulnerabilities are then identified with regards to the proximity of individual converter stations to one another and which converter contingencies may be considered critical. The factor influencing coping capacity is primarily the inertia of the system, which may be low when HVDC import is high and the frequency drops from HVDC contingencies are potentially the most severe. The system operator situational awareness also affects coping capacity. Lastly, several barriers are identified. This includes the system inertial response, load shedding schemes, frequency and voltage dependence of loads among other barriers. The barriers of interest in this thesis are the corrective actions.

2.2 Challenges related to cascading failures and corrective actions

When dealing with active power interruptions of gigawatts such as with HVDC contingencies and the Nordic power system reference incident of 1450 MW, study of single unit failures may be insufficient. The dynamics initiated by a large event may lead to cascading failures, where single unit failures weaken other units and cause successive failures, further weakening other units. The disturbances do not need be large as small disturbances may propagate and cause larger blackouts due to the stochastic nature of disturbances and pro-

tection mechanisms, which is evident from the heavy tail in the probability distribution in [17]. A large outage may for example change the power flow significantly, which overloads a branch causing disconnection, which successively overloads another branch due to reduced transfer capacity and causing further disconnection. The cascades may be due to several different weaknesses of the grid including insufficient reactive power resources, generator rotor dynamic instability, motor stalling due to off-nominal frequencies or voltages, hidden failures or random unit failures [15].

An issue is then that, given equal operating states and case studies, deterministic simulation tools will follow a single path given that the initial operating state is the same. The probabilistic characteristic of cascading failures is lost as corrective controls and emergency controls will always activate in the same manner for each simulation leading to the same simulation results. Cascading failure tools which incorporate random variables seek to alleviate this issue. The hidden yet possible sequences of events that did not occur in the deterministic simulation may then be revealed along with the associated consequences. As power system tools and simulations are increasingly being utilized to make large investment decisions and due to the challenges described in the previous paragraph, there is a need to include cascading failure analysis tools and to ensure the accuracy and usefulness of results provided. As cascading failures are complex (it may take months after a blackout has occurred to gather data and analyze the sequence of events leading up to the blackout [14]) as well as rare (little historical data to utilize for development and validation), it is demanding to create such analysis tools. In [17], some of the challenges identified relate to verification and validation of such tools. Ensuring accurate and correct results for cascading failure simulations is difficult because the large variety of possible event sequences may lead to wildly varying results. The cascading failures following large simultaneous outages of HVDC links are largely influenced by the corrective actions' activation. Corrective actions failure is one type of stochastic variable which may be considered for extraordinary events.

2.2.1 Failures of corrective actions

Failure of corrective actions increases the possibility of cascading failures [15] and leads to possibly larger outages. The relevance of corrective actions modelling is increasingly relevant as market forces seek to minimize the limits or preventive actions the power grid and

the system operators impose on power trading between regions while rather increasingly utilizing corrective actions to operate the power system closer to its limits [15]. In cascading failure tools, the stochasticity of corrective actions failures is necessary to include but data collection of corrective actions failures is a topic that has been largely overlooked[18] to develop probabilistic and cascading failure models of the power grid. As [18] continues, corrective actions failures may come in several forms: actions failing to activate when it should (missing operation), activation of corrective actions when it should not be initiated (unwanted operation) and slow responses which may be deemed as failures due to time-critical demands of operation. While lacking the data for the likelihood of corrective actions failures, the consequences of related to HVDC contingency failure cascades may still be studied using event trees.

2.2.1.1 Event trees

Event trees are a useful tool when considering cascading failures. An example event tree is shown in fig.2.2. While the shown event tree has probabilities and alternatives, a simple Yes/No for each event suffice in some cases. Event trees with Yes/No options are used for corrective actions in section 5.5.1. In this context, event trees are useful to track the successful or unsuccessful activation of corrective actions in deterministic simulations; that is, only the cascades which the user of the deterministic simulation tool is aware of will be simulated. A cascading failure analysis tool will have the potential to expose new unconsidered event sequences but at the cost of requiring far more data. Failures of corrective actions may not be considered as cascading failures by themselves when run in deterministic simulations using event trees, but the consequences of different corrective actions failures are surely likely to lead to widely different cascading failures.

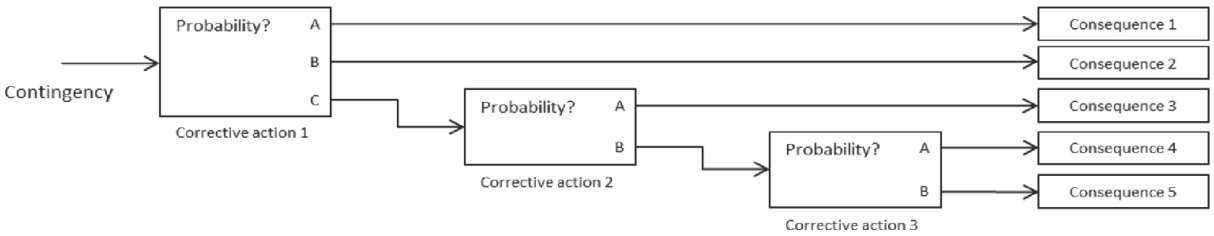

Figure 2.2: Example event tree from [18]

2.2.2 Use of cascading failure tools and extraordinary events

Cascading failure tools encounter many of the same challenges as analyses of extraordinary events. Useful terms in this regard are verification and validation. Verification is concerned with ensuring software integrity, while validation is about ensuring the correctness of results resulting from use of the software. Some approaches useful to validation are listed in [17]: Checking for internal validity (that internal modelling and approximations are valid), comparing simulation results with real data, comparing the performance of one tool with another tool, checking for reproducibility (that use of stochastic variables do not lead to significantly different results from one run to another) and sensitivity analysis (how much the results change when varying the input parameters). Validation requires the use of test case data for some power system in a given power system state, and such test data is often hard to come by [17]. Test case data for HVDC contingencies is no exception. Further, as individual studies often seek to study specific phenomena that are not included in the test cases in the specific manner that is intended for the study, augmentation of existing test cases may be necessary. In such instances, thorough documentation of used datasets and methods used should be made publicly available along with the study as indicated by [17], in addition to restrictions constraints of the methods and datasets.

Chapter 3

Power system stability

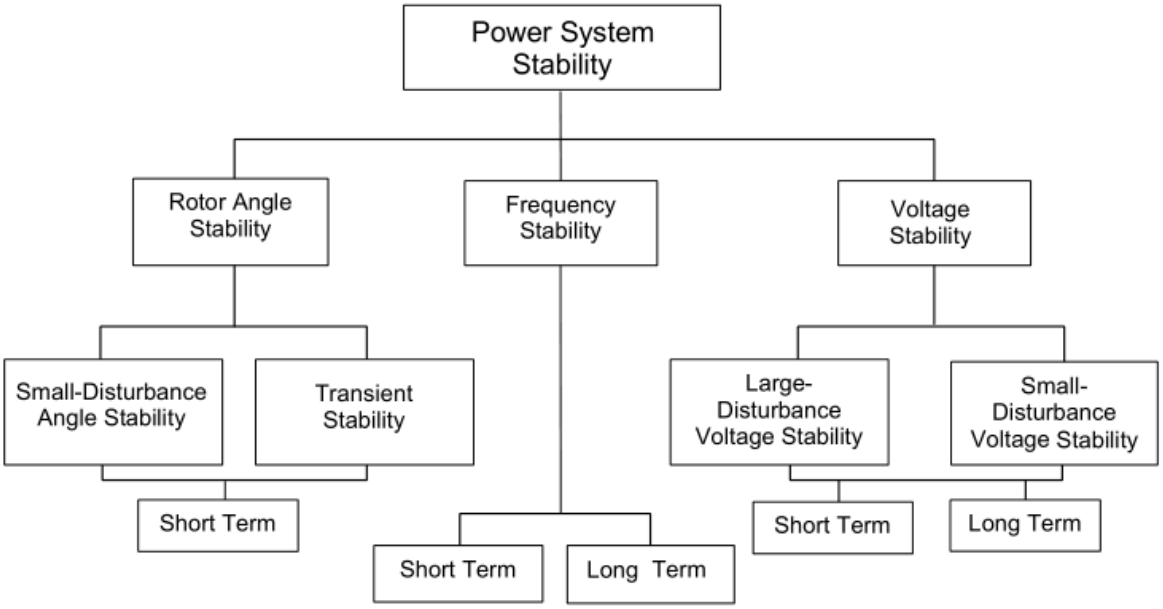

Figure 3.1: Overview of power system stability [19]

Power system stability is a broad term and encompasses several topics such as frequency stability, voltage stability and rotor angle stability, as seen in fig. 3.1. Frequency stability relates to the active power balance of the system, voltage stability relates to the reactive power balance of individual locations and rotor angle stability refers to generators' ability to stay in synchronism with the grid. All the categories of stability will influence the sequence of events after a contingency occurs. The system wide properties of frequency stability will be the focus of this thesis, while voltage and rotor angle-based phenomena serve as a supplement to explaining the sequence of events that occur for different scenarios.

There is a need to maintain a grid frequency close to nominal frequency, as equipment connected to the grid is designed to operate within a certain frequency range. Frequency deviating significantly from nominal may lead to equipment damage. The nominal frequency of the European system is 50.0 Hz and frequency quality parameters for the Nordic system are shown in tab. 3.1. As this thesis is concerned with the consequences of a HVDC contingency in which large power import is lost, the frequency dynamics following such a loss must be described. The frequency of the system will depend on the frequencies of the generators in the system, and as such, generator dynamics must be described. The duration of the dynamics occurring are divided into four stages: rotor swings in the generators, frequency drop, primary response and secondary response [20].

Table 3.1: ENTSO-E frequency quality parameters for the Nordic system [21]

Nominal system frequency	**50.0 Hz**
Standard frequency range	±100 mHz
Maximum instantaneous frequency deviation	1000 mHz
Maximum steady-state frequency deviation	500 mHz

3.1 Stage 1: Rotor swings in the generators

The first few seconds after the contingency, the generators close to the lost generation unit will experience large rotor swings, while generators farther away[1] will experience smaller rotor swings. It is best understood by an example from [20]; two equal generators are operating in parallel connected to a stiff grid. An illustration is seen in fig. 3.2, where X'_d is the generator transient reactance, X_T is the transformer reactance and X_s is the system reactance. As the two units are similar, they are represented by the same emf $\underline{E}'$ connected in parallel to a stiff grid through the system reactance. When one of them is disconnected, the reactance as seen from the online generator is increased, shown in eq. 3.1. The increased reactance causes a decrease in the amplitude of active power output while simultaneously the mechanical power input is halved due to the disconnected generator unit. This is illustrated by the help of the equal area criterion in fig. 3.3, where $P_-(\delta')$ and $P_+(\delta')$ represent the

[1] Farther away refers to electrical distance

power-angle characteristics before and after disturbance and P_{m-} and P_{m+} represents the mechanical power input before and after the disturbance. The figure includes a series of operating points which help illustrate the movements in the rotor. As the rotor angle is unable to change instantaneously after the disturbance, the operating point moves from 1 to 2, at which point the difference $P_+(\delta'_0) - P_{m+}$ shows that the electrical power output exceeds the mechanical power input. This decelerates the rotor, and due to momentum, it swings past point 4 until point 3, oscillating back and forth for a few moments until reaching steady-state operating point 4. The mechanical power input is shown as a flat line due to the large time-constants of changing the turbine input relative to the electrical response of the rotor. This two-machine example could be generalized to a multi-machine system with similar results [20]. The equal area criterion may here be used to explain rotor angle stability. For readers unfamiliar with the equal-area criterion, it can be said that if the power-angle becames large enough such that $P(\delta') < P_m$, the rotor will not swing back to a stable position but instead accelerate uncontrollably and lose synchronism with the grid.

$$P_-(\delta'_0) = \frac{E'V_s}{\frac{X'_d+X_T}{2}+X_s}\sin\delta'_0 \qquad P_+(\delta'_0) = \frac{E'V_s}{X'_d+X_T+X_s}\sin\delta'_0 \tag{3.1}$$

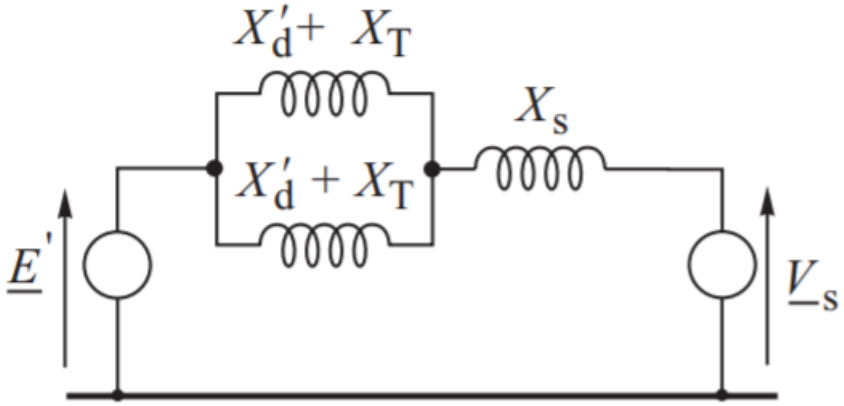

Figure 3.2: Stage 1 circuit diagram [20]

The disconnected generator has caused the electrical power supplied to the system to be decreased. The load demand of the system does not immediately react so the drawn power of the system remains the same. As there is always power balance in the system, the lacking power is supplied by other generating units in the power system leading to stage 2, frequency drop.

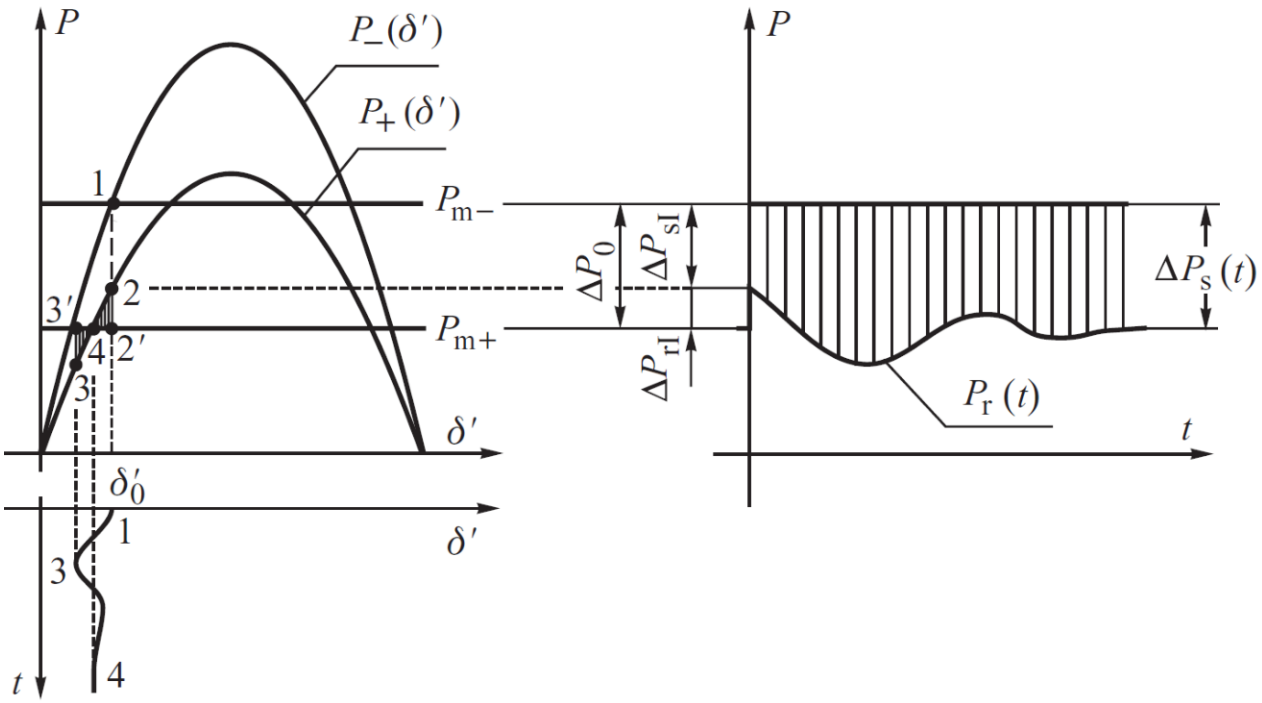

Figure 3.3: Power angle dynamics for the loss of one of two parallell generation units [20]

3.2 Stage 2: Frequency drop

Where stage 1 is primarily concerned with transient rotor angle stability, stage 2 is concerned with frequency stability. The *swing equation* is central to understand the phenomena of stage 2.

3.2.1 Swing equation

The swing equation relates the power system active power balance to the frequency. As described in [20], the swing equation is a central equation in power system dynamics, describing the rotor dynamics of a single generator supplying power to the grid. Eq. 3.2 describes the swing equation for an electrical machine running at nominal speed, where M_m is the angular momentum of the rotor at synchronous speed, δ_m is the angle deviation of the mechanical shaft from the angle of the nominal frequency, P_m is the mechanical power input by the turbine shaft, P_e the active power output by the generator and D_m is a damping coef-

ficient.

$$M_m \frac{d^2\delta_m}{dt^2} = P_m - P_e - D_m \frac{d\delta_m}{dt} \tag{3.2}$$

Using the swing equation and neglecting the damping term D_m for all further considerations, it is seen that an active power output exceeding the mechanical power input will decrease the frequency of the generator, and vice-versa. As described for stage 1, after an outage of generating unit the loads will still draw the same amount of power as before the outage. Assuming no power system security mechanisms are activated, the remaining online generators will almost instantaneously see an increased power drawn from the grid, corresponding to an increase of P_e in eq. 3.2. The power difference $P_a = P_m - P_e$ is considered the accelerating power. With P_m remaining constant in the timescales involved, there is a negative accelerating power P_a supplied by the generator rotating mass kinetic energy. As kinetic energy is depleted, there is an angular deceleration and generator frequency starts to drop.

The rate at which the frequency drops, or the Rate of Change of Frequency (RoCoF), depends on inertia. Inertia may be thought of as resistance to change of motion where generators with a higher mass have more inertia, which means the absolute value of RoCoF will be lower after an outage. The swing equation can be altered by introducing the inertia constant $H = \frac{\text{Kinetic energy of rotating mass}}{\text{Machine rated power}} = \frac{1}{2}\frac{J\omega_{sm}^2}{S_n}$ where J is the inertia of the turbine and rotor and ω_{sm} is the rotor synchronous speed. H is given in seconds and describes the length of time the rotating mass could in theory deliver rated power using only the stored kinetic energy of the rotating mass, going from an angular velocity at nominal speed to standstill, at which all kinetic energy would be depleted. As the power imbalance of the system shortly after the disturbance will have to be covered by the kinetic energy stored in the rotating masses (given that there are no other measures in place, see chap. 4), it is obvious that high inertia is beneficial to the system frequency stability. Using the definition of angular momentum $M_m = J\omega_{sm}$ and rewriting it using H, we get $M_m = \frac{2HS_n}{\omega_{sm}}$. Thereafter using $\omega = \frac{d\delta}{dt}$ and $\omega = 2\pi f$ we have gone from eq. 3.2 to eq. 3.3, another form of the swing equation.

$$H\frac{df}{dt} = \frac{1}{2}\frac{f_s}{S_n}(P_m - P_e) \tag{3.3}$$

Eq. 3.3 is helpful in explaining frequency behaviour after contingencies, and can also be used to approximate inertia and inertia constants by measuring the RoCoF $\frac{df}{dt}$ and solving for H. While H is given in seconds [s], a more popular measure of inertia for system considerations is megawatt seconds [MWs] [22]. The system inertia given in megawatt seconds can be found solving for $E_{k,sys}$ in eq. 3.5. If the unit for inertia is given in seconds, it is a theoretical measurement of how long the system could deliver the system rated power $S_{n,sys} = \sum_{i=1}^{N} S_{n,i}$ if depleting all the kinetic energy stored in the system. If given in megawatt seconds, it is a measure of the stored kinetic energy in the system rotating mass. $E_{k,sys}$ is most commonly used because it takes into account the ratings of the individual machines to calculate the energy stored and thus can be used to find the resulting steady-state system frequency after some load change in the system.

$$H_{sys} = \frac{\sum_{i=1}^{N} S_{n,i} H_i}{S_{n,sys}} \tag{3.4}$$

$$E_{k,sys} = S_{n,sys} H_{sys} = \sum_{i=1}^{N} S_{n,i} H_i \tag{3.5}$$

3.2.2 Centre of Inertia-Frequency

Despite talk of a system frequency, there is no readily defined system frequency: the power system consists of several generators, each of which is operating at individual frequencies. By weighting the individual generators' frequency according to different criteria, an approximation or a virtual system frequency can be calculated. One such weighted frequency is the Centre of Inertia (COI) frequency shown in eq. 3.6. The COI-frequency weighs frequencies using the inertia constant of individual machines. According to [22], the COI-frequency is relatively accurate when used for estimating system inertia and is used for this reason. The COI-frequency may be seen as different from the machines' frequencies. Individual generator frequencies describe the power balance of individual generator at given locations, while the COI-frequency describes an aggregated active power balance of the entire system. A plot of several generators swinging about the COI-frequency is shown in tab. 3.4.

$$f_{COI} = \frac{\sum_{i=1}^{n} H_i f_i}{\sum_{i=1}^{n} H_i} \tag{3.6}$$

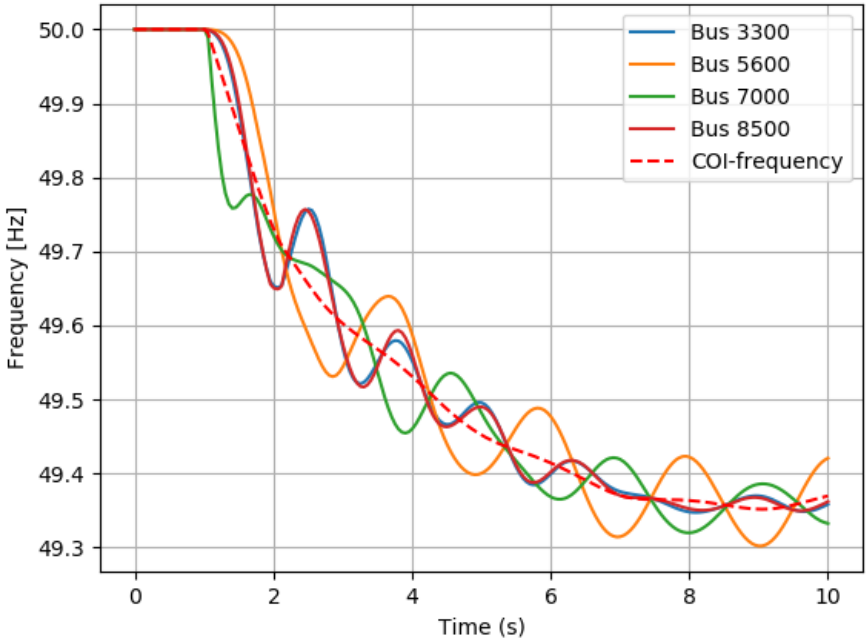

Figure 3.4: Frequency falling after a generation outage. Individual generators at buses 3300, 5600, 7000 and 8500 can be seen swinging about the COI-frequency

3.2.3 Inertial response

The frequency drop stage is characterized by the inertial response of the generators. While in stage 1 the electrical distance to the disturbance was essential, the inertia of the generators is now deciding how much power each generator contributes to the power imbalance. Despite contributing different amounts of active power in the inertial response, the generators will at this stage slow down at approximately the same rate. High inertia is in this regard desirable as a generator with high inertia can during the inertial response supply the same amount of power with a lower RoCoF. The frequency then dips more slowly. Higher inertia means higher amounts of kinetic energy stored in the rotating masses of the system, which lets the system generators release a larger amount of energy before slowing down significantly. A lower RoCoF allows slower power system protection mechanisms to react and attempt to save the power system before cascading outages or system blackout occurs. A comparison of cases with high and low inertia is shown in fig. 3.5, where the high inertia case $H = 6$ oscillates with a lower frequency and amplitude than the lower inertia cases.

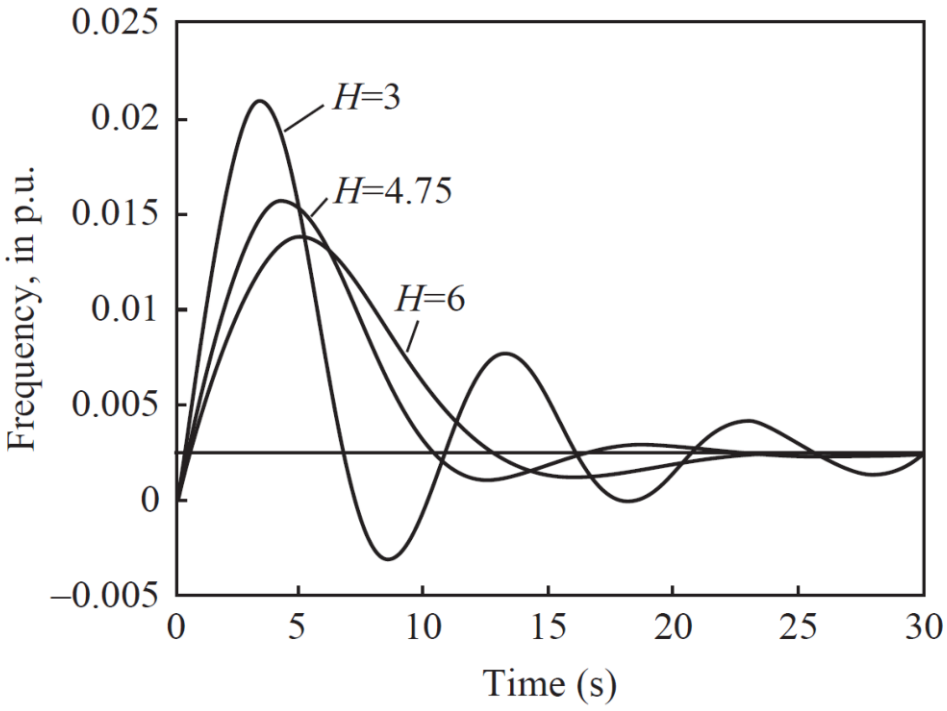

Figure 3.5: Increased inertia reduces the frequency response oscillation [19]

As power electronics-based renewable energy increases in use in the Nordic grid [3], there will be fewer rotating machines contributing rotating mass to the system inertia. In the context of extraordinary events, there may then be extremely large frequency swings. Sufficient inertia or supplementary control mechanisms such as synthetic inertia or HVDC Emergency Power are a necessity.

3.3 Stage 3: Primary control

The primary control decides how generators change their generation setpoints when the frequency changes. Droop S is a central concept in primary control. The droop setting of the turbine governor decides how much the active power output setpoint of the generator changes as the frequency changes. The setpoint changes are used by the governor to adjust valve openings to change the mechanical power input P_m to the turbine. Droop setting is illustrated in figs. 3.6 and 3.7. In the former figure, turbine shaft frequency f is measured and the frequency deviation Δf from nominal is calculated by the use of the nominal system frequency f_0 (50 Hz). The active power setpoint of the generator P^{set,tot_m} is then changed from the reference value P_{m0}^{set} by adding ΔP_m^{set} based on the droop setting and the frequency

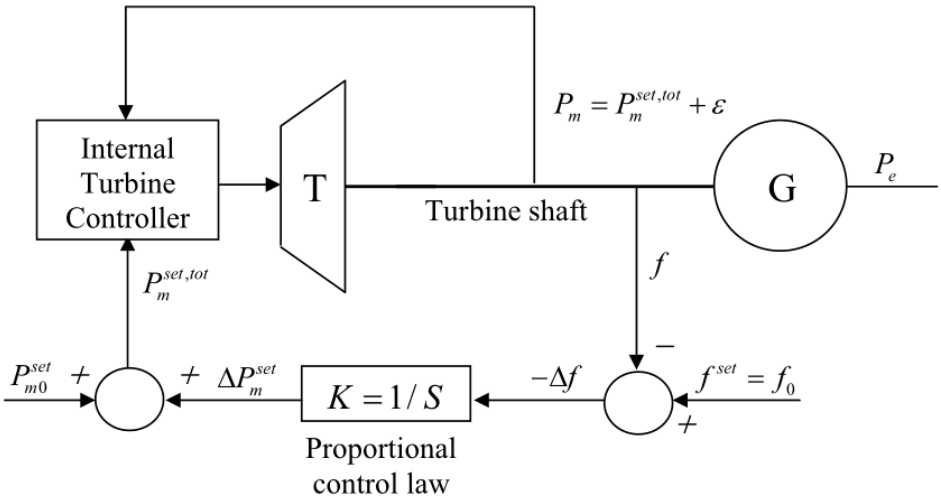

Figure 3.6: Governor controlling the generator power setpoint based on frequency deviations and droop setting S [19]

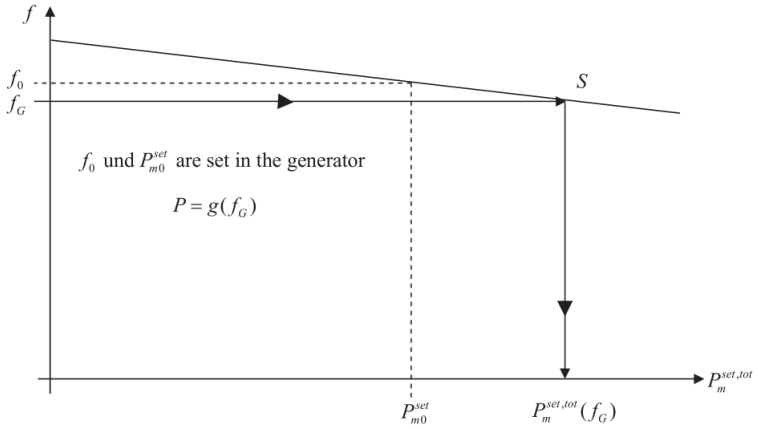

Figure 3.7: Change of generator power setpoint due to droop control [19]

deviation. In the latter figure, the power setpoint change from the reference value is based on the measured frequency deviation is shown. The power setpoint changes with frequency depending on the slope S as seen in the figure. The equation for setting droop is given in eq. 3.7

$$S = -\frac{f - f_0}{P_m^{set,tot} - P_{m0}^{set}} \tag{3.7}$$

The power output response of individual generators will be inversely proportional to the droop setting of the turbine. The primary response dynamics to a frequency drop are shown in fig. 3.8, where P_L is the electrical load seen by the generator, P_T is the mechanical power input from the turbine and ΔP_0 is lost power following the loss of a generation unit con-

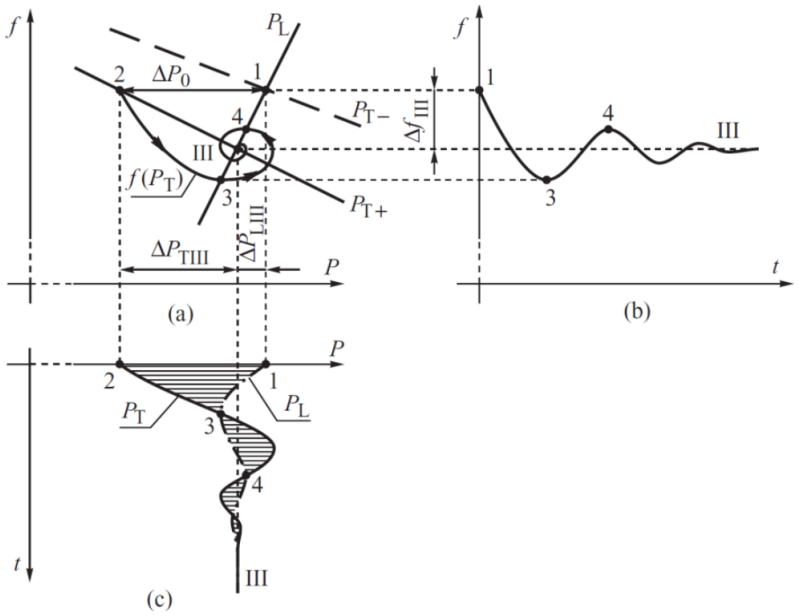

Figure 3.8: Primary response dynamics [20]

nected in parallel similar to sec. 3.1. Initially, the generator is operating with both mechanical input and electrical output at point 1, but the mechanical power input P_T is changed by ΔP_0 to point 2 as one of the two generating units is lost. The frequency then drops in accord with dynamics related to the swing equation as the electrical load exceeds the mechanical power input, but now the setpoint of the generator also changes to counteract the dropping frequency; mechanical power input is increased as the frequency drops. At point 3, the RoCoF is zero as the load demand is equal to the mechanical input. The load demand drops and the primary response controls is overshot and reaches point 4. For some moments there are interactions between governor mechanical power input and load power demand before the frequency settles at the steady-state frequency in the centre of the spiral if fig. 3.8 a). The load P_L varies slightly in the figure and mechanisms behind load demand response is briefly covered in sec. 3.6.

Note that primary control does not restore the frequency to nominal: it only helps contain the frequency drop and primary reserves are thus called Frequency Containment Reserves. The Nordic system operates with two kinds of FCR: FCR-N, the normal reserve, and FCR-D, the disturbance reserve. FCR-N is the normal reserve, which operates between 50.0 ±0.1 Hz during normal operation and has a response time of 2-3 minutes. For the Nordic region this reserve is at approximately 600 MW, where the Norwegian share is just above 200 MW [23]. FCR-D is the disturbance reserve, which is set to respond to disturbances in the power grid

and operates between 49.9-49.5 Hz and 50.1-50.5 Hz. The disturbance reserve in the Nordic system is at approximately 1200 MW, of which the Norwegian share is at 350 MW. FCR-D has a response time of up to 30 seconds[23].

3.4 Stage 4: Secondary control

Stage 4 dynamics or secondary control are not included in the simulations and are thus only covered shortly. The role of the secondary reserve is to restore scheduled inter-area power flows, bring the frequency back to nominal and to free the faster primary reserves. Restoring scheduled inter-area power flows is necessary as there will be primary control response all across the power system, which disturbs the scheduled power interchanges. Secondary control must also recover the system frequency to nominal, as the primary control has been shown to not restore the system frequency to nominal. Freeing the faster primary reserves is necessary so they can respond quickly to further disturbances, as the secondary control is slower: In the Nordic system time to full activation of secondary control is 15 minutes and should be able to run for up to 30 minutes [24].

Secondary control is also referred to as Automatic Generation Control (AGC). AGC operates by using the tie-line power flows and using the frequency to change the generator setpoints over given areas separated by tie-lines. An illustration of a two-area system is given in fig. 3.9. It does so by utilizing an *Area Control Error* (ACE). ACE can be written as in eq. 3.8

$$ACE_i = \Delta P_{Ti} + B_i \Delta f \tag{3.8}$$

for which the subscript i is for each area, ΔP_{Ti} is the sum of the tie-line power flow difference from scheduled flow, B_i is the frequency bias factor for the area and Δf is the frequency deviation from nominal. Further details are omitted and the reader is referred to other sources such as [19]. The time constants for secondary control are larger than primary response as to not interfere with the primary response control. In the Nordic system, secondary reserves are called Frequency Restoration Reserve Automatic (FRR-A) and will automatically operate by increasing the power output of devices configured for secondary control. The amount of power available for secondary response is varying.

The stages of frequency dynamics are summarized in fig. 3.10.

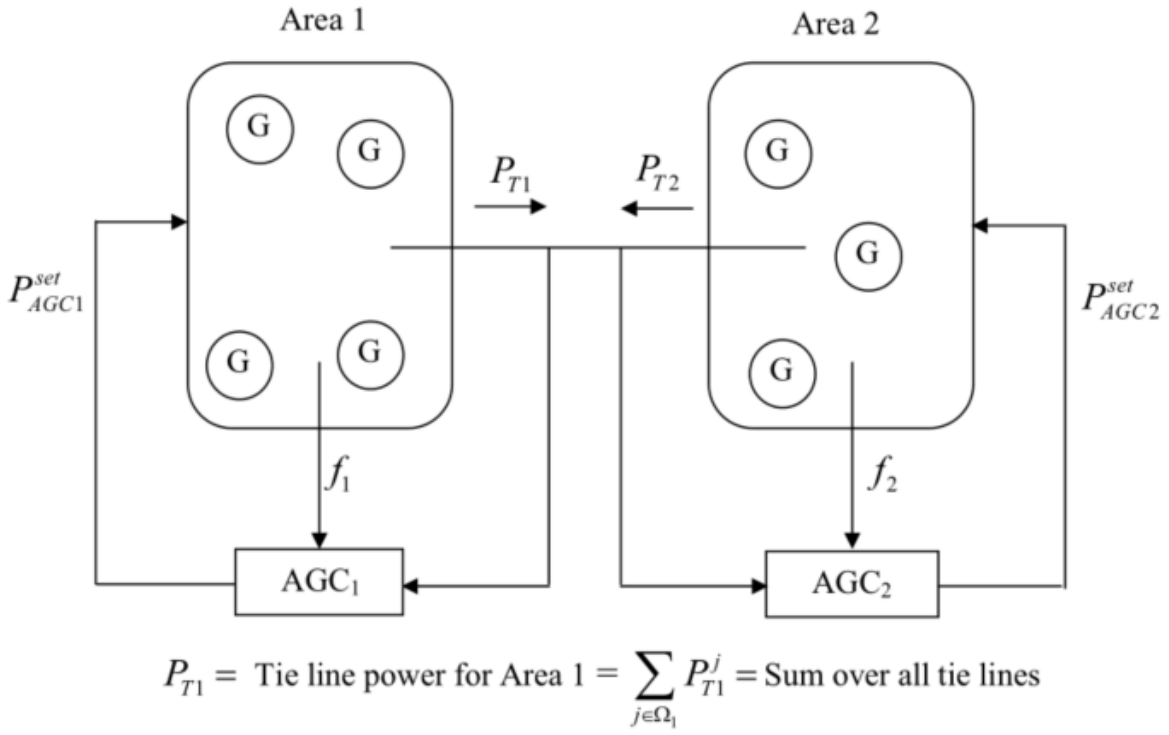

Figure 3.9: Two area AGC [19]

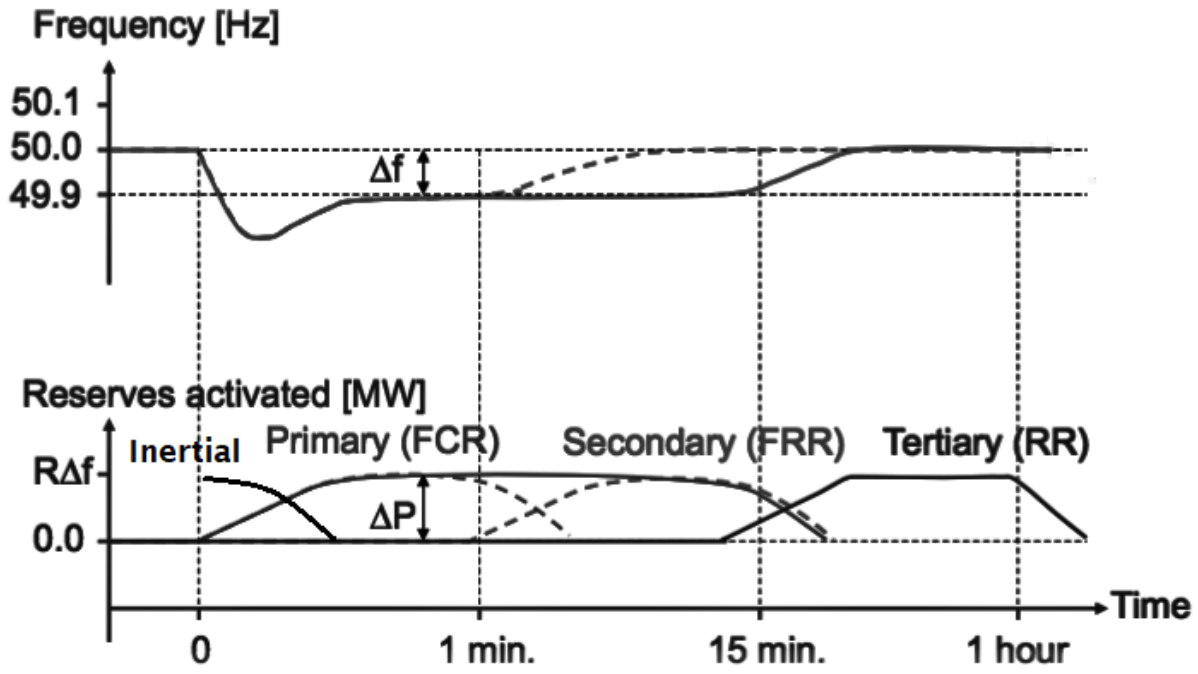

Figure 3.10: The stages of frequency dynamics[19], with modifications. The inertial response occurs almost instantaneously as the frequency starts dropping, while primary response and secondary response are gradually activated

3.5 Power transfer capability

Maintaining a stable voltage in the power system is important to permit connected equipment to operate within the technical specifications they were designed for, which ensures safety and operating efficiency. Bus voltages affect the power transfer capabilities of the system, which can be illustrated by the 2-bus sample system [25] in fig. 3.11. A mathematical equation relating to this simple model is seen in eq. 3.9, where P_1 and P_2 is the power flow into the line seen from buses 1 and 2, $|V_1|$ and $|V_2|$ are the bus voltage magnitudes at buses 1 and 2, X is the line reactance and θ_{12} is the voltage angle difference between the two buses. The equation shows that a reduction in voltage at either end of the line will hamper the maximum active power flow over the line. Potential power system issues arising from low power transfer capabilities is separation of the grid, in which different regions run at a different frequency, as seen in [2]. Voltage is dependent on reactive power and is considered a local grid property so reactive power balance must be ensured at each bus. Typical issues causing voltage instability may be incorrect settings of the Automatic Voltage Regulator (AVR) or the load models used [19].

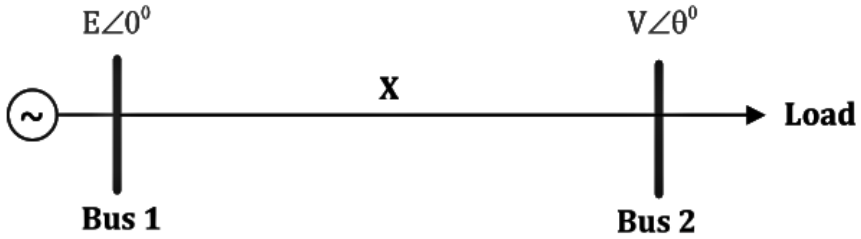

Figure 3.11: 2-bus system for illustrating power transfer capability

$$P_1 = P_2 = \left(\frac{|V_1| \cdot |V_2|}{|X|}\right) \sin\theta_{12} \tag{3.9}$$

3.6 Load models

While large resources are used to model generators, wind turbines and similar generation equipment in the power grid, not as much emphasis has been put on loads [19]. There is a significant need for proper load representation. However, load representation in system wide studies is difficult due to the aggregated nature of the loads as perceived from the high

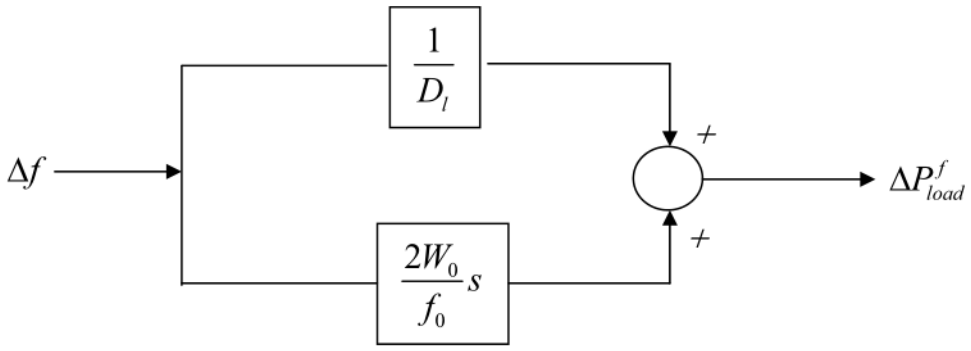

Figure 3.12: Block diagram for frequency response of loads. The default ZIP load models in PSS/E do not capture this characteristic.

voltage grid. As different buses may have different load compositions which vary throughout the year, different load models must often be used. The loads connected also vary year to year. For example, increased use of power electronics using converter interfaces drawing constant power may cause constant power models to be more applicable. As any student learning electrical engineering knows , loads have typically been modelled as resistive.

Loads in the system may respond to frequency changes. As some loads are be rotating masses, these will contribute an inertial response. In addition, there may be a frequency dependency of the load power consumption. Control blocks for load frequency dependence are seen in 3.12, where the upper block $\frac{1}{D_l}$ is the constant frequency dependency of the load and the lower block $\frac{2W_0}{f_0}s$ is the inertial response of the load rotating mass. Both effects aid in stabilizing the frequency in the frequency containment phase, but are not included in the PSS/E simulations soon to be presented as the default ZIP load model is used instead.

3.6.1 ZIP load model

The ZIP load model is the default load type in PSS/E dynamic simulations and is described in eqs. 3.10 and 3.11 [26] . Eq. 3.10 describes the active power consumption of a load and consists of three terms. The $\alpha_1\left(\frac{V}{V_0}\right)^2$ term describes the voltage dependent power output of the ZIP-model, the $\alpha_2\left(\frac{V}{V_0}\right)$ term describes the current dependent power output and the final term α_3 term describes the constant power part of the load. α_1, α_2 and α_3 can be varied to represent different load characteristics. In eq. 3.11, Q is reactive power and the modelling is

similar to that of the active power component. The ZIP load model is a static[2] load model. Static load models include the exponential load model, frequency load model and the polynomial (ZIP) model.

$$P = P_0 \left[\alpha_1 \left(\frac{V}{V_0} \right)^2 + \alpha_2 \left(\frac{V}{V_0} \right) + \alpha_3 \right] \tag{3.10}$$

$$Q = Q_0 \left[\alpha_4 \left(\frac{V}{V_0} \right)^2 + \alpha_5 \left(\frac{V}{V_0} \right) + \alpha_6 \right] \tag{3.11}$$

A high voltage dependence of the active power may aid in stabilizing the power system if the voltage falls along with the frequency drop after a generator outage, as the load active power consumption would be reduced. Similarly, a high voltage dependence of reactive power may aid the voltage stability of the system by reducing reactive power consumption as voltage falls.

[2] Static load models are load models based on algebraic equations

Chapter 4

Power System Security

Power system security is defined by [25] as the ability of the system to operate within constraints in the event of an outage of a component. Constraints include operating constraints and load demand constraints. Not violating system constraints is important to attempt to avoid contingencies, defined as [25]:

> A contingency is an unplanned outage of one or more primary equipment components, i.e. one or more primary equipment components are in the outage state.

An outage is when a component is unavailable and thus can not perform its intended function, for example when a power line has an outage and can not be used to transfer power. Outages change the operating state of the system, where operating states refers to the electrical topology of the network, load and generation in the system, as well as import and export. By electrical topology, it is meant the breaker positions and other switches that decide the connections in the network.

4.1 Operating state transition diagram

Power system operating states are classified into five different operating states: normal, alert, emergency, in extremis and restorative states [19]. The five states relate to load demand constraints and operating constraints. Load demand constraints is the constraint requiring TSOs and DSOs to supply power corresponding to the load demand of customers connected to the

grid. Operating constraints is a safety constraint to not exceed component ratings during operation as this may harm power grid equipment. In the normal state, the system fulfills operating constraints and load demand constraints, and is also N-1 secure. The alert state also fulfills both constraints, but is not N-1 secure and will go into emergency state should a contingency occur. In the emergency state, all loads are still supplied, but operating constraints are not satisfied and the system can only operate at this level temporarily. If control actions are not taken, the system will deteriorate further into in extremis state, where equipment starts to be disconnected to protect itself, and load demand constraints are no longer satisfied. At this point, emergency actions must be taken to bring the system into restorative state and to avoid a total system blackout. In restorative state, the system is being energized in a controlled manner, bringing loads back online while remaining within operating constraints. It is important to note that the purpose of the different operating states differ: in the normal state, optimization of socioeconomic benefits is the main priority. In emergency, in extremis and restorative states security is the primary concern. In the alert state there is a combination of both security and socioeconomic optimization. The transition between states can be better understood by a conceptual tool called an *operating state transition diagram*. The diagram is shown in fig. 4.1.

The transitions between the different operating states are categorized into transitions caused by disturbances or by control actions. Disturbances may bring the system from the normal state to the alert state, and further to the emergency state and the in extremis state. This is indicated by the red arrows in fig. 4.1. Deliberate control actions, indicated by the green arrows, may bring the system in the direction back towards the normal state. Different control actions carry different names, depending on which transitions they describe. The type of control we are interested in for the purpose of this thesis are the corrective controls and the emergency controls, or more precisely the System Integrity Protection Schemes (SIPS). The use of SIPS in this thesis is limited to use of frequency-based corrective controls and emergency controls. These controls differ from primary reserves in that they are not continuously acting on the power system to maintain power balance, but usually respond to larger disturbances instead.

Corrective controls and emergency controls are numerous; fast HVDC active power setpoint changes, opening of tie-lines between regions to contain frequency deviations, restricting transformer tap changers, insertion of braking resistors and many more [19]. The more dras-

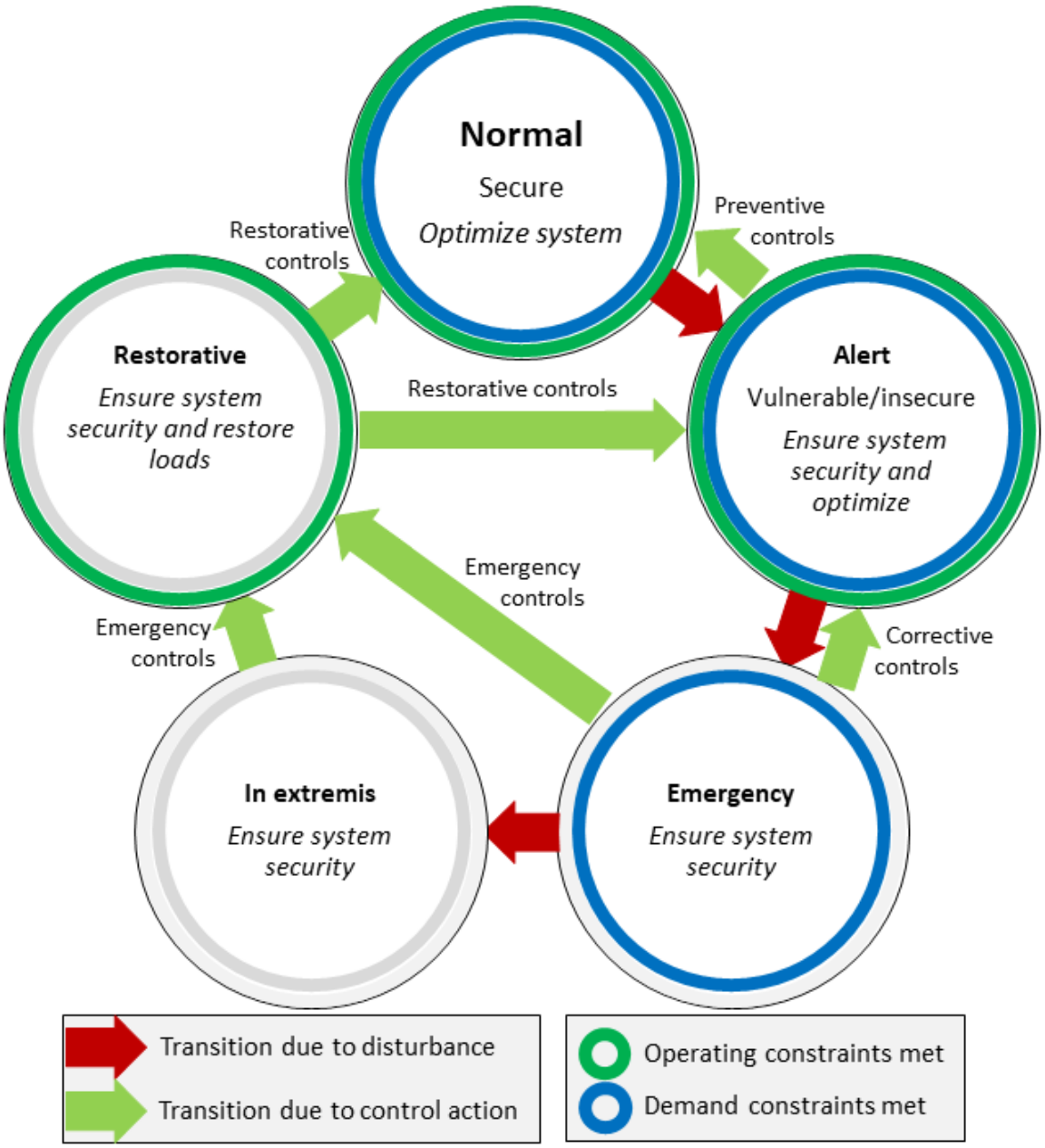

Figure 4.1: Operating state transition diagram, modified from [25]

tic measures include load shedding and tripping of generators. The corrective and emergency controls seek to arrest the sequence of events that would occur if the system were free to operate on its own. Current practice on corrective actions is that corrective actions are either manually activated by operators at a central or automatically activated by preconfigured settings [27]. Different events may occur in the power system leading to a large variety of consequences. A small subset of contingencies (unit failure and line failure) and a sequence of events thereafter is shown in fig. 4.2. Further cascades after losses of lines, generators disconnecting or other random unit failures may be arrested thus avoiding or

mitigating issues such as large frequency swings, voltage fluctuations or even system partitioning.

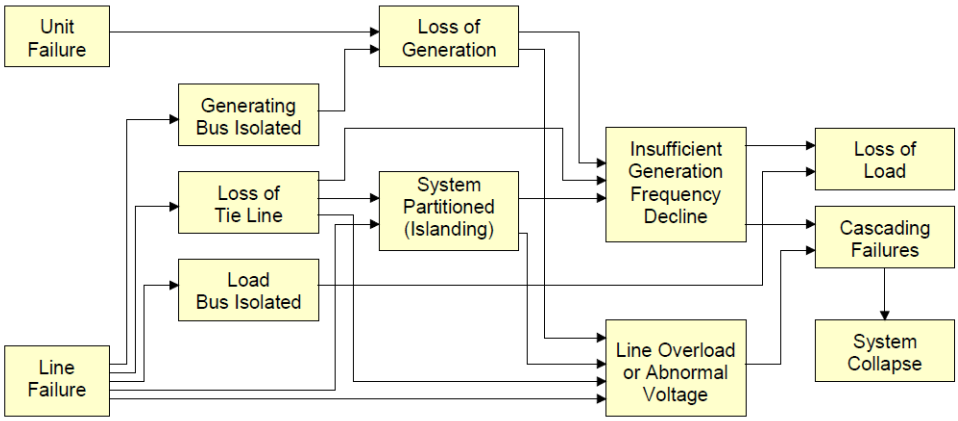

Figure 4.2: Possible effects of contingencies [25], where the sequence of events may be arrested using SIPS

4.2 System Integrity Protection Schemes

System Integrity Protection Schemes (SIPS) are utilized to provide increased power transfer capacity and improved system security. SIPS activation may be either event-based or response-based, meaning that the SIPS may be activated by, for example frequency measurements or trip signals from protection relays. The SIPS may for the Norwegian system be classified into four separate categories: generation tripping, HVDC Emergency Power, system separation and load shedding [28]. SIPS are *armed* when they are activated by the TSO; that is, they are set to automatically perform mitigating actions when activation criteria are fulfilled. In the following, HVDC Emergency Power and load shedding are presented as two types of SIPS, along with a third, less explored type of potential future SIPS, Demand-Side Response (DSR). These SIPS all relate to the active power balance of the system and thus also to the frequency dynamics of the power system.

4.2.1 HVDC Emergency Power

HVDC Emergency Power (HEP) enables HVDC links to increase power import in operating conditions when the frequency is low or increase export when the frequency is high and is

considered as part of corrective controls. The frequency activation thresholds are staggered to avoid all HVDC emergency power in a system to activate simultaneously[29]. An example of use is found in [30], where the Skagerak and Kontiskan links increased their power import by 50 and 150 MW respectively in response to a long lasting frequency deviation below 50 Hz. The emergency power did not cause power ratings of the HVDC links to be exceeded.

As HVDC is based on power electronics, power output can be changed rapidly, in the order of milliseconds. This allows for fast response to measured frequency deviations. The power output may be time-limited if the converter or cable are already operating at maximum capacity and the emergency power causes power ratings to be exceeded. Increased power import due to emergency power is taken from the stored energy in the DC-side capacitance [31] or from the exporting system on the other end of the HVDC link.

4.2.2 Load Shedding

Load shedding is an emergency control action and may be activated depending on frequency or voltage thresholds. If the latter, it is called Under-Voltage Load Shedding (UVLS) and if based on frequency Under-Frequency Load Shedding (UFLS). When there is a large frequency fall, there is insufficient generation in the system. By shedding connected load, the load demand of the system is reduced and generators may be able to regain kinetic energy after the inertial response following a generation loss. Load shedding may be necessary due to a lack of power reserves [32] and to maintain the system power balance. Load shedding serves as a barrier to hinder further system deterioration when subjected to disturbances and is typically initiated due to local frequency or voltage measurements.

To shed load, local measurements are taken of frequency or voltage and compared with pre-defined thresholds. For UFLS, the load will be shed if frequency drops below a predetermined frequency. If the threshold is exceeded the load is shed. The frequency is measured locally at the load where the decision to shed load is also made. The frequency threshold is decided by the TSO. To set the frequency thresholds around the system, the TSO collects projected maximum loads from the DSOs and perform calculations to decide which loads and thus which size of loads should be disconnected for each frequency level [33]. Despite the progressive nature of the system wide load shedding, individual loads are typically not configured to shed load in several steps. Rather, the load shedding thresholds are

staggered: different loads are configured to entirely disconnect at a specified frequency, as specified by the TSO. Entire substations are typically shed at a time. For the load shedding there is typically also a small time-delay as equipment such as circuit breakers do not operate instantaneously. The percentages of total system loads shed for different system frequencies are shown in tab. 4.1.

Table 4.1: Amount of load disconnected for frequency drops in the Norwegian power system [33]

Frequency [Hz]	Load shed, % of max load	Load shed, % of total UFLS
48.7	1.25	4.01
48.5	5.82	18.69
48.3	5.83	18.71
48.1	8.98	28.83
48.0	0.74	2.38
47.9	5.71	18.34
47.75	0.08	0.25
47.7	2.35	7.55
47.5	0.13	0.41
47.25	0.26	0.83
Total	**31.15**	**100**

Load shedding at low voltages is done by UVLS. UVLS seeks to avoid voltage collapse in the system when reactive power consumption exceeds the locally available reactive power reserves. UVLS will shed the load as the voltage drops to a sufficiently low level, seeking to reverse the frequency decline and bring the system back to a secure state. As reported by [33], UVLS is not common in the Norwegian grid but is used in for example the Bergen-region. Further details on implementation in the Nordic grid were not given due to confidentiality.

4.2.3 Demand-Side Response

While describing frequency dynamics in chapter 3, load demand was seen as constant following a generation loss. Using Demand-Side Response (DSR), this does not have to be true.

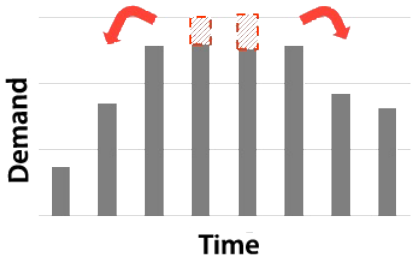

Figure 4.3: Static Demand-Side response by shifting power demand in time to reduce peak power consumption [36]

Demand-Side Response (DSR) is typically related to that of shifting power consumption in time to reduce peak power consumption and thus the need for investments in strengthening of the power grid. DSR is then thought of as a tool in the static power considerations. In order to reduce peak power consumption, demand-side response allows delayed use of power in certain situations and for certain equipment: thermal capacitance in power to heat (P2H) applications allows for shifting of consumption for water heating, air-conditioning, refrigerators and other heating or cooling systems. The ability to postpone load consumption serves as flexibility for the DSO or TSO operating the grid. Increased flexibility allows the power system to potentially be operated closer to maximum capacity, which may lead to lower costs in the long run due to increased utilization of present equipment. A small scale DSR test project has been done in Norway for static load flow considerations with great success [34], and a larger one is underway. In Europe, the same trend of increased DSR focus is observed in response to the Demand Connection Codes [35].

While power consumption shifting to reduce load at peak hours is one option of DSR, it may also be used for immediate and short term [1] load reduction. The same equipment that are good candidates for shifting longer term consumption may also be good candidates for short term load reduction by DSR. Equipment mentioned in the previous paragraph thus apply as potential candidates for DSR based on frequency response. Equipment such as electric cars with batteries may be especially good candidates; in [37] the possibility of cars connected to chargers to adjust power drawn from or supplied to the grid is is quantified to be able to supply 0-300 MW of DSR by 2030 with a total energy capacity of 6 TWh. The article continues that other types of consumer flexibility such as ventilation, heating and cooling of industrial

[1] Short term in the context of this thesis being the first tens of seconds or a few minutes after large outages, on the time-scale of the frequency responses

buildings as well as homes will offer significant potential for DSR.

Today, there are some large centralized applications for frequency stabilization around the world. One such example is a Battery Energy Storage Systems (BESS) in Zürich with 1 MW for extremely quick primary response and smoothing of small, local frequency fluctuations [38]. In Australia, a 100 MW Tesla battery supplies a much larger amount of power with a greater energy capacity and has been used to aid in stabilizing the grid after coal plant outages [39] and with great success [40]. Smaller batteries distributed around the grid may possibly be scaled to serve similar functionality, for which the aggregated effect of smaller batteries and other power electronic interfaces may serve the same effect as the aforementioned centralized batteries.

Before using DSR for frequency response, analyses must be performed. In [41], potential benefits for the Great Britain power grid are given and quantified in terms of system operation cost, amount of wind curtailment as well as carbon emissions. Rapid delivery of frequency response from DSR is found to be possibly extremely valuable, for which up to 5% of total system DSR-enabled load could effectively replace all other primary frequency response schemes. This thesis is concerned with time-domain simulations or dynamic analyses of the ability of DSR to impact grid frequency transients. In dynamic analyses, the time-delay for activation of DSR serves as a perhaps key constraint for using DSR during transients and in dynamic simulations: DSR needs to activate sufficiently fast in order to serve as a barrier to avoiding critical consequences after large grid outages or extraordinary events; the time-delay of DSR must be low. Too slow activation may be considered a failure of the corrective action scheme and may even be detrimental to the system response.

4.2.4 Time-delay of DSR

As time-delay is identified as a potential constraints for use of DSR as a corrective action, factors affecting time delay must be identified. The response of the DSR-compatible equipment would depend on a) the time-delay for the deactivation control signal to reach the equipment and b) the time delay for the equipment to reduce load demand after receiving the control signal. The control signals may be sent from a central processing unit in the grid, or the control signals could be sent from nearby the DSR-enabled equipment by decisions based on local measurements. Time delays may thus be sensor delays, processing time and

transfer time of the measurement data and control signals. Quantitative estimates of such time delays are omitted as they would be highly speculative. A hierarchical approach could be implemented, where for example substation level measurements can process measurement data and decide on response for a medium or small-size area. An example implementation of a substation level measurements is shown in fig. 4.4

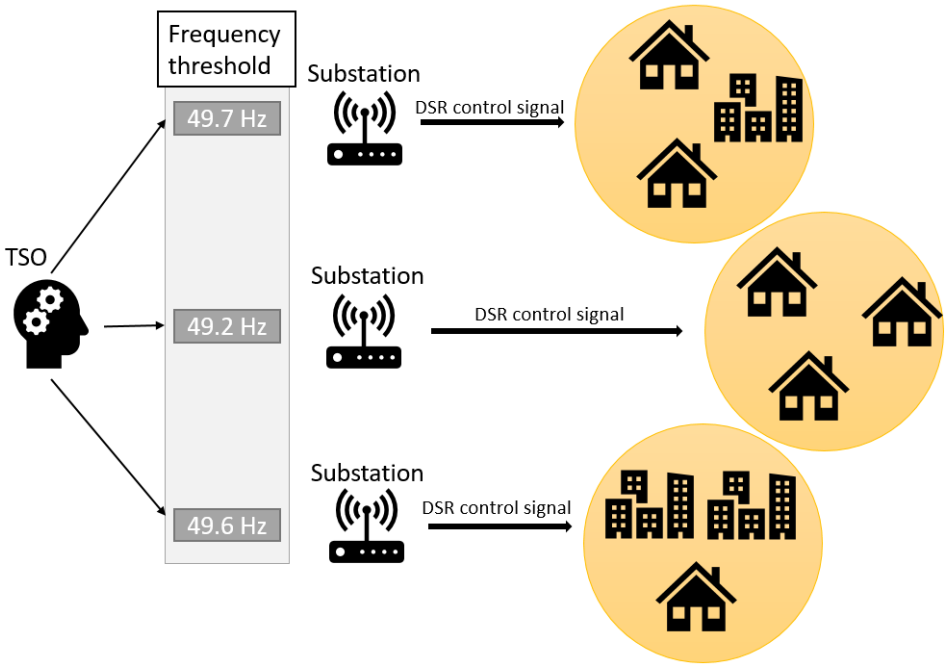

Figure 4.4: One possible approach for frequency-based DSR. DSR setpoints may be set at substations which independently monitor frequencies and send control signals to all DSR-enabled equipment to reduce load

The substations in fig. 4.4 have different frequency thresholds. When an individual substation detects a frequency below the set frequency threshold, it would send a control signal to connected consumers to would either cut their power consumption or even supply power in the case of batteries. In Norway, the control signal may be sent to the AMS unit in each home, as in [34]. The frequency thresholds at different substations are staggered in order to avoid sudden load steps as the system frequency reaches a certain value. The setting of frequency thresholds could be similar to that of setting frequency thresholds for UFLS, which in section 4.2.2 were described to be based on DSO maximum projected load sent to the TSO. The setpoints could then be changed after certain time intervals and varied stochastically to ensure that no single customers are repeatedly disconnected (activated DSR) at the same frequencies.

DSR differs significantly from load shedding in that the impact on the user experiences is little to none for DSR while large for load shedding; DSR only reduces the total power consumption by shifting or postponing power consumption for appliances that are largely not in active use, while load shedding disconnects *all* appliances causing possibly reduced quality of life. The distinction DSR frequency response and load shedding should be maintained by securing the advantage of DSR in terms of user experience; no single users should more frequently see DSR enabled due to a DSR frequency threshold set near the nominal frequency, for which frequency deviations more frequently exceed the frequency threshold. The frequency thresholds should because of this be frequently varied by TSOs and DSOs to ensure that no users are more unfortunate in the frequency threshold setpoints.

The effects of DSR for frequency response will be studied. For simulations of DSR in this thesis the time-delay of DSR is considered as well as the amount of load reduction that is available at each bus.

Chapter 5

Modelling, case studies and methodology

In the following chapter the software, modelling and implementation choices are covered along with motivations and reasoning for each choice.

5.1 Modelling and software

5.1.1 PSS®E

The software used in this thesis is PSS®E, referred to as PSS/E. It is software developed and maintained by Siemens and is widely in use all across the world. Features of PSS/E are a graphical interface which can be used for load flow computations, fault analysis, optimal power flow, dynamic analysis and much more [11]. The Psspy API [42] allows for interfacing between Python and PSS/E enabling extended automation and program control for advanced users.

5.1.2 Psspy Python framework

Python is used for interacting with the PSS/E software in favour of PSS/E graphical interface. A Python-class was written for using simple scripts to run case studies. The Python-class

controls PSS/E through the use of Psspy. This allows for initializing the model, changing parameters and running several simulations and automatically saving desired plots for use in this thesis. Example code is shown in appendix D, where a case study is explained step-by-step. The full code is also uploaded online.

5.1.3 Nordic 44

In order to simulate the Nordic power system, the Nordic 44 (N44) aggregated network model is used. N44 represents the Nordic system in lower detail than the detailed models of the Nordic TSOs, meaning fewer buses, generators, loads and branches: N44 has 44 buses of which 18 contain generators, 43 loads and 67 branches, a considerably reduced amount from the thousands of buses and branches in the Nordic system. This leads to reduced computation costs and increased manageability due to the reduced number of components. The model is implemented in both Siemens PSS/E and DIgSILENT PowerFactory. Different variants of the N44 model have been used for different purposes, and in this thesis the model in [43] is used. Further background and model details for N44 are given in appendix B.

As we will be simulating simultaneous HVDC outages, N44 needs to include HVDC links in the Nordic system. The HVDC links in N44 are shown in tab. 5.1 along with the corresponding bus numbers in N44 and maximum transfer capacity of the respective links. The cable transfer capacities do not have any inherent meaning in N44 as the HVDC links are modelled as PV and PQ loads. However, for contingency simulations the import is initially set to the rated power of the HVDC link to maximize the effect of simultaneous outages in the context of extraordinary events.

5.1.3.1 Addition of North Sea Link and NordLink

Two HVDC links under construction in the Nordic power grid are North Sea Link (NSL) and NordLink (NL). They are estimated to be completed in 2019 and 2020 respectively. Neither link is implemented in the N44 model but are added using Psspy to allow for contingency studies of simultaneous outages of both links. In order to use them for contingency simulations, both were added to N44 by creating new buses connected to the geographically closest bus in the N44 model. Bus numbers and connections are specified in tab. 5.2

Table 5.1: HVDC connections to external grids in Nordic44

Cable name	Bus number N44	Maximum transfer capacity [MW]
KontiSkan 1	3360	380
KontiSkan 2	3360	360
Skagerak 1	5610	250
Skagerak 2	5610	250
Skagerak 3	5610	500
Skagerak 4	5610	700
NorNed	5620	700
Vyborg Link	7010	1420
Estlink 1	7020	350
Estlink 2	7020	650
FennoSkan	Not modelled	500
Baltic Cable	8600	600
SwePol	8700	600
Nordbalt	Not modelled	700
NordLink (2019)	5630	1400
North Sea Link (2020)	6010	1400

Table 5.2: HVDC buses added to the N44 model [2]

HVDC Link	Bus number	Bus type static load flow	Connected to bus number	Area
NordLink	5630	PV	5600	NO3
North Sea Link	6010	PV	6000	NO4

Both HVDC links NSL and NL are modelled as simple PV-buses as shown in tab. 5.2 as both are based on Voltage Source Converter (VSC) technology [5], [6]. The branches connecting the buses for NSL and NL to the rest of the system are modelled in the same manner as existing branches connected to HVDC links in the N44 model with an impedance Z of $Z = 0.0 + j0.006$ and zero charging susceptance $B = 0.0$.

5.1.4 Model tuning

The N44 model was in [43] tuned towards an outage of 1110 MW at Ringhals Block 4 the 5th of March 2015, 11:00-12:00. The tuning towards a large outage is selected as the simultaneous HVDC contingencies will be very large. The tuning was shown to be accurate with regards to frequency response when ZIP load models were set to 10/10/80, with a significant 80% active power load component and ZIP load of 10/10/80 is therefore used in this thesis. The operating state of the grid at the given time and date can be described to have medium-high production and consumption, and, assuming a majority of generation is supplied by generation units based on rotating mass, that the system inertia is also medium-high. Higher or lower amounts of production or consumption may be seen by sorting historical data on the Nord Pool webpage [44], which may help find operating states with higher or lower inertia.

Table 5.3: Case data hour 11-12

Region	Consumption [MW]	Production
NO1	5561	2104
NO2	4899	8884
NO3	3039	2443
NO4	2489	3506
NO5	2651	6151
SE1	1242	3748
SE2	2265	6599
SE3	12540	9622
SE4	3720	754
FI	10831	8 659
Total	**49238**	**52471**

5.2 Static load flow modifications

To set the HVDC links to maximum import and to reduce system inertia, an algorithmic approach was undertaken to alter the tuned N44 model while attempting to retain the validity

of the results. The lack of historical data on HVDC link outages operating at high import motivated the choice of an algorithmic approach rather than tuning against specific historical events. Generation redistribution and load reduction functions were written, and in some case studies outages are scaled using outage scaling factors in order to test the maximum size of the outages that the system is able to withstand.

5.2.1 Generation redistribution

As the HVDC links in the tuned N44 model scenario are not operating at maximum transfer capacity, the import must be set to maximum in order to achieve the most critical simultaneous HVDC outages. Changing the import will affect the power flow of the system, which may negatively impact the tuning that was done by [43] and thus the results of the dynamic analyses. In order to attempt to maintain the power flow in N44 along with the dynamic properties resulting from tuning, generation redistribution is performed. Generation redistribution attempts to limit the changes in power flow that result from import adjustment at HVDC links. To do this, the generation in the area where import is increased, is reduced, in an attempt to maintain the inter-area power flows which were taking place before the HVDC import adjustment. Generation redistribution will ideally allow the slack bus (3300 Oskarshamn) to maintain the approximately same power output following the import adjustment, as the power flows in the system are similar.

Generation redistribution is described[1] in [2], for which the following is a slightly altered description:

1. Specify HVDC link to set to maximum import
2. Look up maximum transfer capacity of HVDC link P_{max}
3. Read and store current active power transfer of HVDC link $P_{current}$
4. Set load bus power consumption corresponding to HVDC link to $-P_{max}$
5. Read and store the generator active power generation in the market region where the HVDC link is located $P_{gen,area}$
6. Calculate the active power change from setting the HVDC link to maximum import

[1] Under the name *load* redistribution

as $P_{change} = P_{current} - P_{max}$ and distribute the active power change as a generation reduction for generators in the power system:

(a) Reduce the local generation if $P_{gen,area} > P_{change}$ (if local generation is sufficient to compensate the increased import):

i. Assess the number of generators in the local area N along with the total active power generation capacity in the area $P_{gen,cap,area}$.

ii. Reduce the generation in the area $P_{gen,area} = P_{gen,area} - P_{change}$, where the active power output of each generator is reduced by the same percentage of the generation

iii. Calculate the number of generators needed to supply $P_{gen,area}$ as $K = \lceil \frac{P_{gen,area}}{P_{gen,cap,area}/N} \rceil$

iv. Set generation of generators $1, \ldots, K$ to $P = \frac{P_{gen,area}}{K}$

v. Set remaining generators' generation to zero power output and disconnect from the grid

(b) Else if $P_{gen,area} < P_{change}$, set the generation in the local area to zero and reduce the generation in the remainder of the system (as local generation reduction is insufficient to compensate the increased import):

i. Calculate generation to reduce over the rest of the system as $P_{change} = P_{change} - P_{gen,area}$

ii. Set local generators' generation to zero

iii. Read total generation in the system $P_{gen,sys}$

iv. Calculate a generation change ratio $\rho = \frac{P_{slack}}{P_{gen,sys}}$

v. Set generation of each individual generator to $P_{gen,i} \cdot (1 - \rho)$

7. Perform a static load flow analysis

In the above, the local region refers to the market zone in which the generator is located. All generators in the same market zone are considered to be in a local region together in the above described algorithm. The validation of the algorithm in section 6.1 serves as an example.

5.2.2 Inertia reduction

To reduce the inertia, all load in the system is reduced by multiplying each load in N44 by $1-p$ where p is the percentage of load reduction. After reducing load, the system generation is reduced by the same amount to maintain power balance. To reduce the generation, parts of the generation redistribution algorithm in 5.2.1 is used. As load in one area is reduced, the generation redistribution algorithm tries to reduce generation in the same area by the same amount, and if not possible (due to total amount of generation in the area being lower than the amount of load reduction), will reduce the generation all across the system. This will also disconnect superfluous generators, that is, the generators that are not required to be online to supply the amount of active power that a lower number of online generators could also supply.

5.2.3 Outage scaling factor

In order to test the limits of what a given case is able to withstand before a system collapse occurs, an outage scaling factor ϕ is used. For outages at the rated transmission capacity of HVDC links $\phi = 1.0$ is used. Setting $\phi = 1.20$ means that each HVDC link considered in the case study has the active power import set to 120% of rated capacity. Similarly, $\phi = 0.8$ means that active power import is set to only 80% of rated capacity. An example is shown in tab. 5.4 for outage scaling factor applied to NL and NSL outages. Using ϕ for different case studies we are now able to scale the outage sizes so that the system is on the verge of collapsing, and so that outages are barely large enough to make the system collapse. This may lead to valuable information on weaknesses during extraordinary events for a system that is on the verge of collapse.

Table 5.4: Import at HVDC links is scaled by the outage scaling factor ϕ. The size of the outages that occur at the respective HVDC links is then also scaled

ϕ	NL import [MW]	NSL import [MW]	Total outage size [MW]
0.8	1120	1120	2240
1.0	1400	1400	2800
1.2	1680	1680	3360

5.3 Evaluation of consequences

In PSS/E, the system states that the user wishes to monitor must be specified before running a simulation. The specified system states are then written to a specified output file when the simulation runs. System states may be frequencies, voltages, angles or other quantities. The system states monitored in this thesis to see the effects of simultaneous HVDC contingencies are primarily generator states as generator dynamics significantly affect the simulation results. The default generator states monitored are, with descriptions from the Psspy API [42]:

ANGLE Machine relative rotor angle

PELEC Machine electrical power

ETERM Machine terminal voltage

SPEED Machine speed deviation from nominal

ANGLE is given in degrees, while PELEC, ETERM and SPEED are given in p.u. As p.u. speed deviation from nominal may be less intuitive than frequency, the frequency is calculated from the speed deviation by the formula $f = f_n + \Delta f_{p.u.} \cdot f_n$, where f is the frequency, f_n is the system nominal frequency (50 Hz) and $\Delta f_{p.u.}$. If there are no generators at a bus where voltage or frequency measurements are desirable, the bus frequency BSFREQ and bus voltage BSVOLT are monitored and BSFREQ is converted from p.u. deviation similar to that of SPEED. Additionally, branch active power flows are monitored in instances where power flows over certain branches are of interest, and bus load power is primarily monitored to illustrate that outages and load shedding occurs as specified, as well as for debugging purposes.

Heavy emphasis is placed on the system frequency response and the ability of corrective actions to improve the frequency response. Frequency based measurement criteria are frequency nadir, steady-state frequency and RoCoF. In the case studies frequency nadir is the lowest frequency achieved for the initial frequency dip, steady-state frequency is after some time when oscillations are sufficiently damped and RoCoF is the rate of change of frequency $\frac{df}{dt}$ and the calculation of RoCoF is given in section 5.3.3. As inertia is given for case studies, RoCoF is not listed in each case study as it can be calculated when both outage size and

inertia are given.

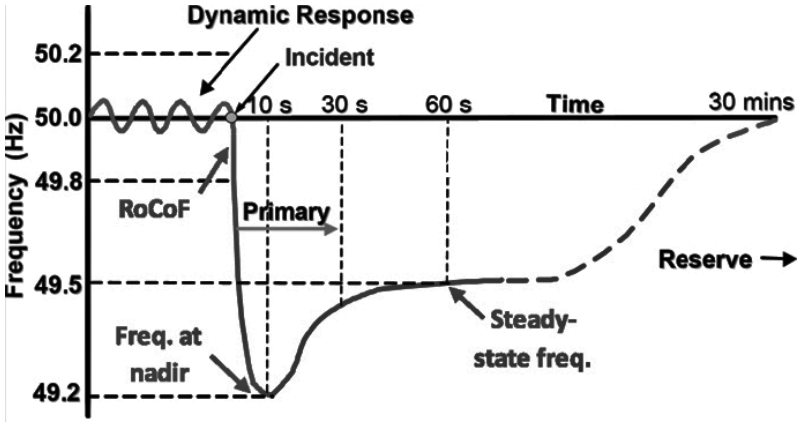

Figure 5.1: Frequency-based performance indicators are frequency nadir, steady-state frequency and RoCoF [45]

5.3.1 Calculation of frequency bias

In the simulations there are two types of frequency response that may be considered as primary response. The first is the classical primary response of generators, which adjust the mechanical power input setpoint in response to decreasing frequency, as explained by droop in section 3.3. The second is DSR frequency response.

5.3.1.1 Primary response frequency bias

Calculation of frequency bias due to generators primary response may be done by the governors' droop settings as in eq. 5.1 (taken from [20]) where the subscript i denotes the i-th generator unit, Δf is frequency change [Hz], f_n is the nominal system frequency [Hz], S_i is the droop in p.u. (as in section 3.3), P_{mi} is the generator mechanical power change, P_{ni} is the generator nominal power and K_i is the frequency bias. The aggregate frequency bias of the system is given in eq. 5.2, where R is the system frequency bias [MW/Hz], ΔP_T is the change in power supplied by turbines and N_G is the number of generators in the system.

The primary response may be saturated, but this is not visible directly from the equation and depends on the setpoint of the generator at the time instance when it is required to respond; the mechanical power input from the turbine may be close to rated power, leaving very little

reserves available for primary response. Eqs. 5.1 and 5.2 are not concerned with possibly limited amounts of reserves.

$$\frac{\Delta f}{f_n} = -S_i \frac{\Delta P_{mi}}{P_{ni}}, \qquad \frac{\Delta P_{mi}}{P_{ni}} = -K_i \frac{\Delta f}{f_n} \tag{5.1}$$

$$R = \frac{\Delta P_T}{\Delta f} = \frac{1}{\Delta f} \sum_{i=1}^{N_G} \Delta P_{mi} = -\sum_{i=1}^{N_G} \frac{K_i P_{ni}}{f_n} \tag{5.2}$$

An even simpler way to find the frequency bias of the system is to use eq. 5.3, where ΔP is simply the total outage size [MW] and Δf is the resulting steady-state frequency after the frequency has been contained. This method has the advantage that it will properly represent the frequency bias of the system even when some generators are configured to give primary response but have no operational reserve at the time of the outage; that is, the mechanical power input is already at its maximum. A disadvantage is that it does not necessarily represent the innate frequency bias resulting from the system's governor settings alone.

$$R = \frac{\Delta P}{\Delta f} \tag{5.3}$$

5.3.1.2 DSR frequency bias

The frequency bias of the DSR varies depending on how much of the load in the system is DSR-enabled. Assuming the initial activation threshold for the first DSR to activate is 49.9 Hz and that all DSR is enabled at 49.0 Hz, the frequency bias due to DSR response may be calculated as in eq. 5.4, where δ is the percentage of DSR-enabled load [Hz], Δf is the frequency deviation [Hz] below the activation threshold of 49.9 Hz, K is the number of loads and P_{Li} is load i in the power system model at the start of the dynamic simulation.

$$\frac{dP_{DSR}}{df} = \delta \Delta f \sum_{i=1}^{K} P_{Li}, \qquad 0\% \leq \delta \leq 100\%, \qquad 0 \leq \Delta f \leq 0.9 \tag{5.4}$$

The total load of the tuned N44 model is 52250 MW. 5% DSR-enabled load in the system will then, for DSR alone, allow a frequency bias of $\frac{52250 \cdot 0.05}{0.9} = 2903$ MW/Hz in the region 49.9 - 49.0 Hz, which is significant. Similar calculations for increased % of DSR-enabled load as well as reduced amount of total load in the Nordic system is shown in tab. 5.5. The arbitrarily

set DSR activation region of 49.9 - 49.0 Hz could be changed to alter the frequency bias but this is not further considered.

Table 5.5: Frequncy bias for DSR

Case	DSR-enabled load	Frequency bias [MW/Hz]
Normal load	5%	2903
Normal load	25%	14514
30% reduced load	5%	2032
30% reduced load	25%	10160

5.3.2 Calculation and estimation of system inertia

System inertia was in section 3.2.3 described as a critical system quantity. In order to measure the inertia of the system during case studies, two separate approaches are taken. The first approach gathers all inertia constants directly from the N44 .dyr-file describing the input parameters to the PSS/E dynamic models and aggregates them using eq. 3.4. The second approach estimates the system inertia constant using eq. 3.3 solving for H, where the outage size is known and RoCoF is calculated from the frequency response of the system. Using the COI-frequency to estimate system inertia has been shown [22] to be preferable with regards to accuracy over the use of arbitrary bus frequencies and RoCoF is therefore calculated based on COI-frequency. The inertia is then converted from seconds [s] to megawattseconds [MWs] by the use of eq. 3.5. Calculating system inertia using *both* approaches has the advantage of being useful for debugging; if results from the two approaches significantly differ, there may be some unintended effect occurring.

5.3.3 Calculation of RoCoF

RoCoF is used to estimate system inertia. The RoCoF varies depending on when it is calculated. This is evident from eq. 5.5. In order to capture the effects of the simultaneous HVDC outage at $t = 1.0$ seconds, the frequency is sampled at monitored at $t_1 = 1.0$ and $t_2 = 2.0$ seconds for f_1 and f_2 respectively. RoCoF is most steep immediately after outages have occurred as the system has not yet been allowed to respond. The time between two frequency

measurements for RoCoF calculations should be small to avoid filtering large RoCoF values [46]. The COI-frequency is relatively steadily decreasing after an outage occurs, as in fig. 3.4. A steadier frequency decrease allows for a larger time gap between measurements. If bus frequencies were to be used, however, the frequency typically contains several modes, causing greater variation of RoCoF depending on time instance and bus selected.

$$RoCoF = \frac{f_2 - f_1}{t_2 - t_1} \tag{5.5}$$

5.4 Implementation of System Integrity Protection Schemes

Several SIPS are implemented, including UFLS, UVLS, HVDC Emergency Power and DSR. In PSS/E, UFLS and UVLS are implemented by the use of the Protection Relay models DLSHBL and LVSHBL. HVDC Emergency Power and DSR are implemented by the use of PGU Python-based emulation which is explained in 5.4.3. An overview of the implementation of SIPS is seen in fig. 5.2.

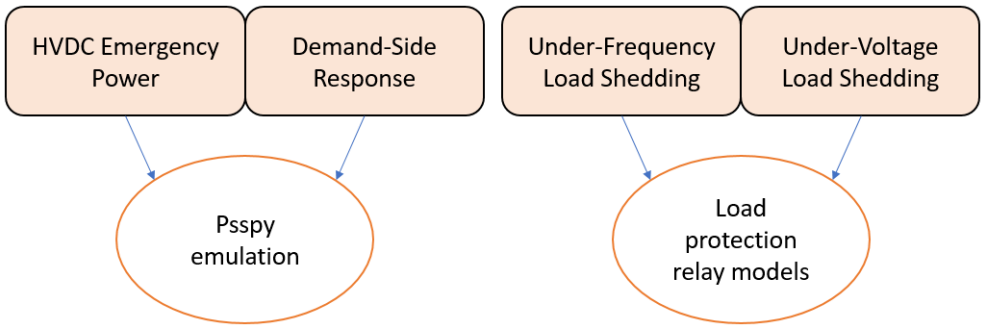

Figure 5.2: Overview of implementation of SIPS

5.4.1 Under-Frequency Load Shedding

Under-Frequency Load Shedding is implemented by adding the Protection Relay model DLSHBL to loads. For case studies in this thesis where the effect of UFLS is considered, the DLSHBL model is placed at each load at every load bus in the N44 system. The model parameters are shown in appendix A. 6 key settings are configured for the DLSHBL load shedding model, as seen in tab. 5.6. These settings are based on the previously presented tab. 4.1, but

with only 3 different frequency levels in contrast to the 10 different levels configured in UFLS protection relays in the present Norwegian system. The frequency thresholds must thus be aggregated and are decided by (very) simple averaging; the first load shedding threshold is set by averaging the 20% of total UFLS to 48.6 Hz, a threshold in the midst of the two highest frequency thresholds in tab. 4.1. As 20% of the total UFLS is $0.2 * 31.15 = 0.0623$, the fraction is rounded to 0.062 or 6.2%. The two other frequency thresholds were averaged similarly. The DLSHBL model also supports RoCoF-thresholds, but these thresholds do not seem to be in use in the Norwegian system [33] and the model parameters for RoCoF thresholds are thus left blank.

Table 5.6: Settings for protection relay model DLSHBL

Load shedding threshold [Hz]	Percentage of load shed [%]
48.6	6.2
48.2	15.6
47.9	9.3

5.4.2 Under-Voltage Load Shedding

Under-Voltage Load Shedding is implemented by adding the Protection Relay model LVSHBL to loads. For case studies in this thesis where UVLS is used, the LVSHBL model is only placed at loads at buses in the Swedish part of the N44 model, as voltage issues primarily occur in Sweden. The settings are as shown in tab. 5.7. Due to confidentiality of real-life UVLS settings [33], the given settings may not be indicative of real-life UVLS settings. The results of simulations with the selected UVLS settings may still be able to illustrate possible benefits of UVLS.

Table 5.7: Settings for protection relay model LVSHBL

Load shedding threshold [p.u.]	Percentage of load shed [%]
0.9	10.0
0.8	10.0
0.7	10.0

5.4.3 Programmable Generation Units

DSR and HVDC Emergency Power is implemented using the Psspy API and Python. From a Python class, objects are instantiated. For each of these objects, a bus number is given upon initialization. During simulations, the object then retrieves the bus frequency at the given bus from PSS/E in short, discrete intervals and adjusts the load at the bus based on the retrieved frequency. To simplify discussion, this Python class and corresponding objects are referred to as Programmable generation units[2] (PGU). The PGUs attempt to approximate power system security schemes using simple step-based responses. When designing a scenario in Psspy, the user can decide to add PGUs to the simulation prior to initiating dynamic simulations. If one or more PGUs are added, the PSS/E simulation will periodically stop every 50 milliseconds (default value; may be modified) to scan frequencies to initiate desired active power output modification at the bus where the PGU is placed. When a lower frequency threshold is exceeded, the PGU active power output is increased by decreasing the load at the bus according to specification. The PGUs also include the option to add a time delay the response to the given criteria, the option to only be activated for a limited amount of time (to for example emulate energy limits of a BESS) as well as an option to specify whether the response should cease (return load to pre-PGU response) as frequency activation thresholds are no longer exceeded due to frequency restoring back to nominal. An overview of PGU settings is given in tab. 5.8. The implementation is verified in section 6.3, and verification also serves the purpose of giving examples and clearing possible confusion as to how the PGUs are implemented. The activation of PGUs is *cumulative*, which means that at each frequency threshold in LIMITS, the additional MW PGU output in LIM_ACTIVATION will be added to the power output.

Table 5.8: Explanation of PGU settings

Lower frequency thresholds for the PGU object	LIMITS	[Hz]
Active power response at each threshold	LIM_ACTIVATION	[MW]
Maximum time available for each step	MAX_TIME	[s]
Time delay for each step response	TIME_DELAY	[s]

[2]The name is due to the user's ability to manually program the frequency response using simple vectors

5.4.3.1 Implementation of Demand-Side Response

Emulation of DSR is done by calling a function which reads all system load and instantiates PGUs at each load bus with a total power output based on a percentage of the load at the bus which it is placed. The percentage of load that is DSR-enabled is input by the user to determine how much of the load in the simulation is enabled for DSR. The DSR frequency response is linear with initial activation at 49.9 Hz and full activation at 49.0 Hz. For example, at 49.5 Hz, $\frac{49.5-49.0}{49.9-49.0} = 55.6\%$ of the DSR-enabled response is utilized. If the DSR-enabled load in the system was initially set 20% of all load, then 11.1% of the total system load has been reduced or removed by PGUs. In the example PGU settings for DSR in 5.9, the PGU power output at each threshold LIM_ACTIVATION is very small. With cumulative activation of PGUs, the maximum response is reached at 49.0 Hz despite the small power increments.

Table 5.9: Example PGU settings for Demand-Side Response

LIMITS	[Hz]	[49.90, 49.89, ..., 49.01, 49.00]
LIM_ACTIVATION	[MW]	[1, 1, ..., 1, 1]
MAX_TIME	[s]	[100, 100, ..., 100, 100]
TIME_DELAY	[s]	[0.5, 0.5, ..., 0.5, 0.5]

A limitation is imposed on the simulations for running DSR: placement of PGU on load bus 3000 causes the system to not converge due to improper behaviour of the PGU, increasing the load instead of decreasing the load. The author's best efforts were insufficient to locate the cause of this error and a simple fix was applied by excluding bus 3000 from the PGU unit list.

5.4.3.1.1 Sensitivity analyses

To calculate the effects of DSR upon system frequency, the amount of DSR available in the system is varied along with the time-delay for DSR activation. In all cases with DSR the load response will remain active as the frequency recovers from the initial large frequency dip (as in section 6.3.4). The percentage of system load which is available for DSR is iterated from 0% to 50% in 5% increments as shown in tab. 5.10. The time-delay for the DSR to activate is similarly iterated from 0.0 seconds to 5.0 seconds in 0.5 seconds increments as given in tab.

5.11. A sensitivity analysis is then performed using these increments to show the potential of DSR-enabled load to aid the frequency response of a future power system depending on how much load is used for DSR and how rapid it is to respond.

Table 5.10: Percentage of system load which is DSR-enabled

DSR-enabled load [%]
0
5
10
15
20
25
30
35
40
45
50

Table 5.11: DSR time-delay for given frequency thresholds.

Time-delay [s]
0.0
0.5
1.0
1.5
2.0
2.5
3.0
3.5
4.0
4.5
5.0

5.4.3.2 Implementation of HVDC Emergency Power

The PGUs emulate HVDC Emergency Power by adding a PGU to HVDC buses, where the PGUs have a single frequency threshold which activates the Emergency Power. The step response of the PGUs is an approximation to the quick response of HVDC converters.

Table 5.12: Example PGU settings for HVDC Emergency Power

LIMITS	[Hz]	[49.5]
LIM_ACTIVATION	[MW]	[200]
MAX_TIME	[s]	[20]
TIME_DELAY	[s]	[0.5]

Settings of PGUs for HVDC Emergency Power are difficult to set as there is a lack of publicly available information on the capabilities of HVDC Emergency Power and real-life settings

of HVDC links in operation in the Nordic system. As previously mentioned, an example of activation is found in [30] where Skagerak responded with 50 MW and KontiSkan with 150 MW. This constitutes approximately 3% and 20% of the maximum transfer capacity of each link. A possibly generous presumption is then made that all HVDC links may be able to supply up to 20% rated capacity as HVDC Emergency Power. For example, North Sea Link will then be able to supply 280 MW emergency power, while SwePol may supply up to 120 MW. The time-delay for response is set to 0.5 seconds as to not be instantaneous, but still fast. Frequency activation thresholds are staggered and vary between 49.7 Hz and 49.3 Hz. Initially all were set to 49.5 Hz, but this was avoided due to large load steps as the frequency reached 49.5 Hz.

A summary and overview of factors affecting the results of the dynamic simulations is given in fig. 5.3.

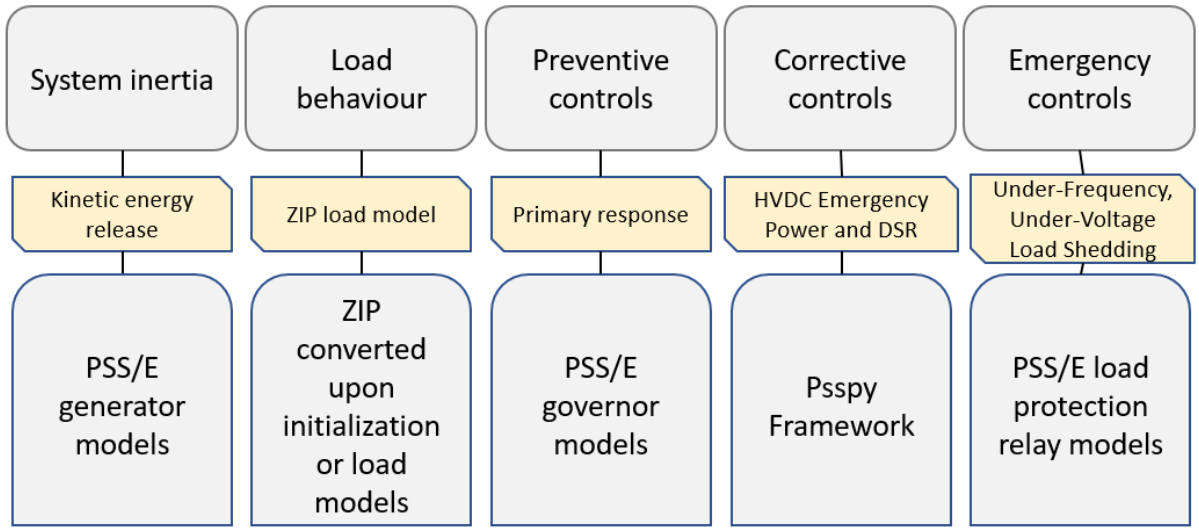

Figure 5.3: Factors and modelling that influence dynamic simulation results

5.5 Case studies

Case studies are ordered in four groups. It is assumed that the pre-contingency frequency is 50 Hz. Group one and two are focused on the ability of SIPS to aid the system frequency for large frequency excursions. Group three and four are focused on locations of outages and the maximum size of outages that may occur until the power system is no longer able to withstand the outages and collapses.

5.5.1 Case studies - Group one

This group of case studies is concerned with the simultaneous outage of HVDC links North Sea Link and NordLink in a higher inertia scenario. The simultaneous outages are simulated with successful activation of different SIPS to illustrate the effect SIPS may have on the frequency response and the general system response. Frequency response is in focus. Simultaneous outages of NL and NSL are the only outages studied in order to limit the number of case studies and to better be able to see the effect of different corrective measures. The case studies in this group, for a high inertia system, are:

- No successful activation of SIPS
- Successful activation of UFLS
- Successful activation of HVDC Emergency Power
- Successful activation of DSR
- Successful activation of DSR with saturated primary response
- Successful activation of DSR, HVDC Emergency Power and UFLS (unsaturated primary response)

The possible combinations of SIPS for considered events is shown as an event tree in fig. 5.4. The illustration of corrective actions shown in the event tree is not entirely accurate, as the DSR will continuously adjust power output, and may thus respond for example both before and after HVDC Emergency Power. Each case study in chapters 7 and 8 will include a supporting figure based on fig. 5.4 for keeping track of which branches are selected in the event tree for the case study.

5.5.2 Case studies - Group two

The second group of case studies is similar to the first group, but with lower inertia instead of higher inertia. The case studies are the same as in group one and are based on the same event tree in fig. 5.4 but following the low inertia branch instead of the high inertia branch.

The case studies in group two may be inaccurate in that, after reducing the load and generation of the system by 30% using load reduction as described in 5.2.2, the slack bus is operat-

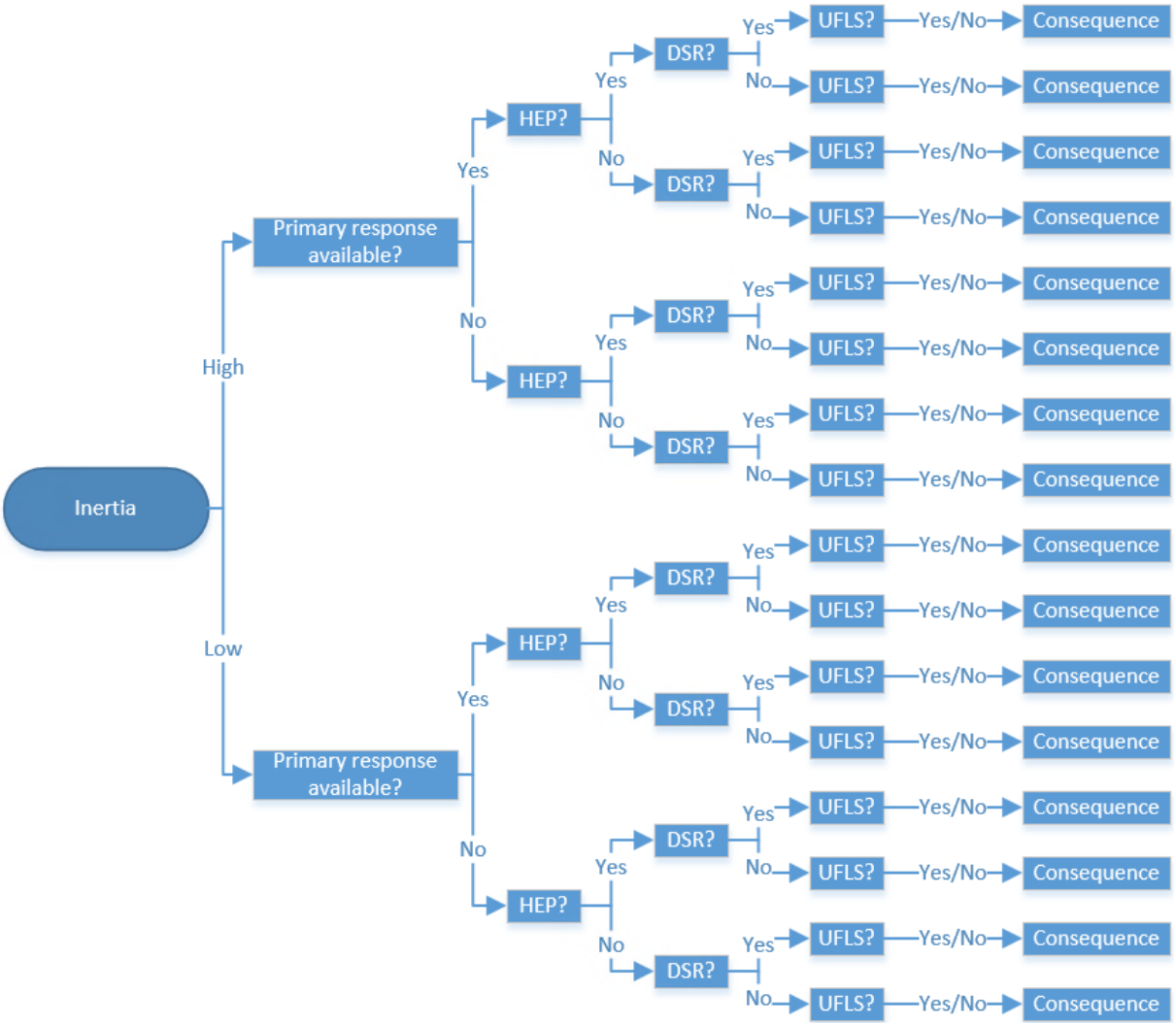

Figure 5.4: Event tree for inertia, primary response and SIPS

ing with a power output higher than that of the generator ratings. To reduce slack bus power output below the ratings in the model, a script is run to increase the power output at other generators in the power system. Running this script increased the estimated system inertia, as many generators can then no longer be disconnected to remove rotating mass from the system. The inertia of the system does then not become as low as desired for the case studies. The high power output at the slack bus is thus kept, but, as this may lead to strange behaviour in power system dynamics, only the frequency response is plotted and studied in this group to inspect system power balance instead of detailed system responses.

5.5.3 Case studies - Group three

In the third group of case studies, the possibility of differing consequences depending on *where* the simultaneous outages occur is inspected. The ability of the Nordic system to cope with large simultaneous outages in Norway, Sweden as well as Finland are inspected for cases with varying amounts of inertia. In addition, the outages are scaled using the outage scaling factor ϕ described in 5.2.3. The ability of frequency-based corrective actions to influence the system disturbance coping ability is inspected. Preliminary studies in [2] seemed to indicate large voltage issues in Sweden. The ability of UVLS in Sweden to influence the system's ability to withstand simultaneous outages is tested by excluding all other corrective or emergency actions and testing UVLS separately. For each case study using UVLS, there are thus no other corrective actions or protection mechanisms armed. In cases with corrective actions, UFLS, HVDC Emergency Power and DSR are armed at the same time, where DSR consists of 10% of the load with a 1.0 seconds activation delay.

In this case group, emphasis is placed on more detailed system response and explaining the sequence of events that occurs rather than the frequency response as in previous case groups.

Chapter 6

Validation of implementation

In this chapter it is verified that the implementation of generation redistribution algorithm and corrective actions is correct and that they work as intended.

6.1 Validation of generation redistribution

Generation redistribution is shown in tab. 6.1 to successfully distribute generation changes as intended and specified in section 5.2.1. As HVDC-links NL and NSL are added to the N44 model, the load of both HVDC buses is initially set to 0 MW. The links have a maximum transfer capacity of 1400 MW each as in tab. 5.1 and the load at the respective PV buses is set to -1400 MW for each bus to constitute an import of 1400 MW. Area NO3 only has one power plant in N44 which then sees a reduced generation of 1400 MW as intended. The total active power export of region NO3 will thus remain approximately the same as before the link load was changed. NO4 has two power plants. The total reduction of generation in NO4 is 1400 MW as intended, but divided over two power plants. The total generation in area NO4 is $735 + 6645 = 7380$ MW. The plant at bus 6100 supplies $\frac{6645}{7380} \approx 90\%$ of the generation in NO4 and when the link at bus 6030 is increased to import 1400 MW, the generation at plant 6100 is reduced by $\frac{1261}{1400} \approx 90\%$. The 73 MW generation change at plant 3300, the slack bus, is not due to generation distribution but due to static load flow calculations. Such a generation change shows that there is a difference in losses in the system and thus also in power flows which implies that retaining the original power flows is not entirely successful.

Table 6.1: Plant generation changes due to generation distribution

Bus Number	Area Name	$P_{Gen,before}$ (MW) Before	$P_{Gen,after}$ [MW]	Generation decrease
3000	SE3	2200	2200	0
3115	SE1	3525	3525	0
3245	SE2	1000	1000	0
3249	SE1	7294	7294	0
3300	SE3	2996	2923	73
3359	SE3	3310	3310	0
5100	NO6	972	972	0
5300	NO5	2551	2551	0
5400	NO2	2610	2610	0
5500	NO1	1131	1131	0
5600	NO3	2492	1092	1400
6000	NO4	735	596	139
6100	NO4	6645	5384	1261
6500	NO7	2443	2443	0
6700	NO8	3506	3506	0
7000	FI2	6513	6513	0
7100	FI1	2146	2146	0
8500	SE4	994	994	0

The machine generation redistribution shown in tab. 6.2 paints a similar picture as that described by the power plant generation, but is slightly harder to read. At plant 3249, the generation is redistributed among the inidividual machines. The total generation is the same, but as 6 machines are sufficient[1] to supply the plant's active power output, machine 7 is set to 0 MW output, which lets it be disconnected to reduce inertia. Plant 3300 is, again, the slack bus, and the generation change is here divided over the 3 machines. Plant 3359 also maintains the same power generation, but each machine is set to the same power output so machine 1 sees reduced output and machines 2 and 3 see increased output. At plant 5600, the output is reduced by 1400 MW by setting machine 2 to 0 MW output and setting machine 2 to 1092 MW output. Lastly, there is only one machine at plant 6000 so it is reduced by 139

[1]The maximum generation of each machine is not shown in tab. 6.2 but the reader is referred to appendix B for further model details.

MW, while at plant 6100 the output reduction is done by setting machine 5 to 0 MW output, while slightly increasing output of machines 1-4.

Table 6.2: Machine generation changes due to generation redistribution

Bus Number	Machine ID	Area Name	$P_{Gen,before}$ [MW]	$P_{Gen,after}$ [MW]	Generation decrease
3000	1	SE3	1100	1100	0
3000	2	SE3	1100	1100	0
3000	3	SE3	0	0	0
3115	1	SE1	1175	1175	0
3115	2	SE1	1175	1175	0
3115	3	SE1	1175	1175	0
3245	1	SE2	1000	1000	0
3249	1	SE1	1042	1216	-174
3249	2	SE1	1042	1216	-174
3249	3	SE1	1042	1216	-174
3249	4	SE1	1042	1216	-174
3249	5	SE1	1042	1216	-174
3249	6	SE1	1042	1216	-174
3249	7	SE1	1042	0	1042
3300	1	SE3	998.73	974.62	24.10
3300	2	SE3	998.73	974.62	24.10
3300	3	SE3	998.73	974.62	24.10
3359	1	SE3	1110	1103.33	6.66
3359	2	SE3	1100	1103.33	-3.33
3359	3	SE3	1100	1103.33	-3.33
3359	4	SE3	0	0	0
3359	5	SE3	0	0	0
3359	6	SE3	0	0	0
5100	1	NO6	972.43	972.43	0
5300	1	NO5	1275.66	1275.66	0
5300	2	NO5	1275.66	1275.66	0
5400	1	NO2	1305.32	1305.32	0
5400	2	NO2	1305.32	1305.32	0
5500	1	NO1	1131.56	1131.56	0
5600	1	NO3	1245.99	1091.99	154.00
5600	2	NO3	1245.99	0	1245.99
6000	1	NO4	735.73	596.18	139.54
6100	1	NO4	1329.06	1346.21	-17.15
6100	2	NO4	1329.06	1346.21	-17.15
6100	3	NO4	1329.06	1346.21	-17.15
6100	4	NO4	1329.06	1346.21	-17.15
6100	5	NO4	1329.06	0	1329.06
6500	1	NO7	814.33	814.33	0
6500	2	NO7	814.33	814.33	0
6500	3	NO7	814.33	814.33	0
6500	4	NO7	0	0	0
6700	1	NO8	1753	1753	0
6700	2	NO8	1753	1753	0
7000	1	FI2	1085.5	1085.5	0
7000	2	FI2	1085.5	1085.5	0
7000	3	FI2	1085.5	1085.5	0
7000	4	FI2	1085.5	1085.5	0
7000	5	FI2	1085.5	1085.5	0
7000	6	FI2	1085.5	1085.5	0
7000	7	FI2	0	0	0
7000	8	FI2	0	0	0
7000	9	FI2	0	0	0
7100	1	FI1	715.33	715.33	0
7100	2	FI1	715.33	715.33	0
7100	3	FI1	715.33	715.33	0
8500	1	SE4	994	994	0
8500	2	SE4	0	0	0
8500	3	SE4	0	0	0
8500	4	SE4	0	0	0
8500	5	SE4	0	0	0
8500	6	SE4	0	0	0

6.2 Validation of UFLS

To verify that the UFLS acts predictably, a simultaneous outage of EstLink 1-2 and Vyborg Link is simulated for a total import loss of 2420 MW. The UFLS protection relay model "DLSHBL" is placed on bus 7000 with settings as in tab. 6.3.

Table 6.3: UFLS settings

Load shedding threshold [Hz]	Amount of load shed
49.8	10%
49.6	10%
49.4	10%

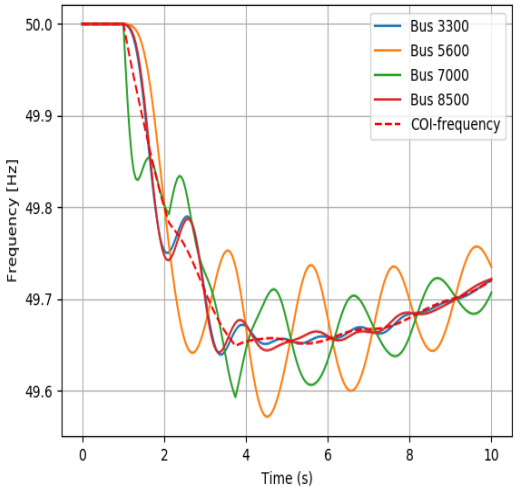

Figure 6.1: Bus frequencies and COI-frequency

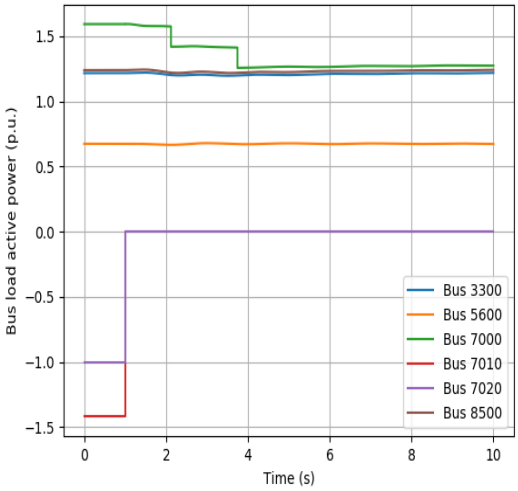

Figure 6.2: Bus loads showing load shedding

From figs. 6.1 and 6.2 it is clear that the UFLS operates as intended; As the frequency falls below 49.8 Hz at approximately t = 2s, the first 10% of load is shed at bus 7000. The second load shedding occurs at approximately t = 3.7s as the frequency falls below 49.6 Hz. The frequency then never falls below 49.4 Hz and the third load shedding specified by the protection relay model never occurs.

It is assumed that the UVLS protection relay model LVSHBL sheds load in the same manner as the UFLS protection relay model DLSHBL but for voltage thresholds instead. Load

shedding is thus not validated for UVLS.

6.3 Validation of PGU

The PGUs have been coded from scratch and are reliant on pausing the PSS/E simulations to perform checks in Python. In order to verify that the behaviour of the PGUs is as intended, this section ensures that the power in PSS/E is adjusted as specified by the Python-script.

6.3.1 Activation at given frequency limits

To test whether the PGU reduces the load as specified when the frequency drops to specified values, a simultaneous outage of EstLink 1-2 and Vyborg Link is simulated for a total import loss of 2420 MW. To counteract this, a PGU is placed at bus 7000 Helsinki. The specifications for the PGU are as in tab. 6.4. The power change is large in order to be observable in the change of p.u. load in the output plots.

Table 6.4: PGU settings for verifying activation at correct frequency thresholds

Frequency [Hz]	49.9	49.8	49.7	49.6	49.5
Step load [MW]	300	300	300	300	300
Delay [s]	0	0	0	0	0
Time available [s]	100	100	100	100	100

As seen from figs. 6.3 and 6.4, the PGU adjusts load as intended when the frequency falls. The interaction with PSSE load demand plot is seen as there are several load steps at bus 7000 in conjunction with the PGU output adjustments. As S_{base} in the N44 model is 1000 MVAr, the 300 MW load steps may appear too small in the load plot; the steps seem to be less than 0.1 p.u. In fact, they are 0.06 p.u. as there are 5 loads at bus 7000 and the PGU load change is divided equally among them.

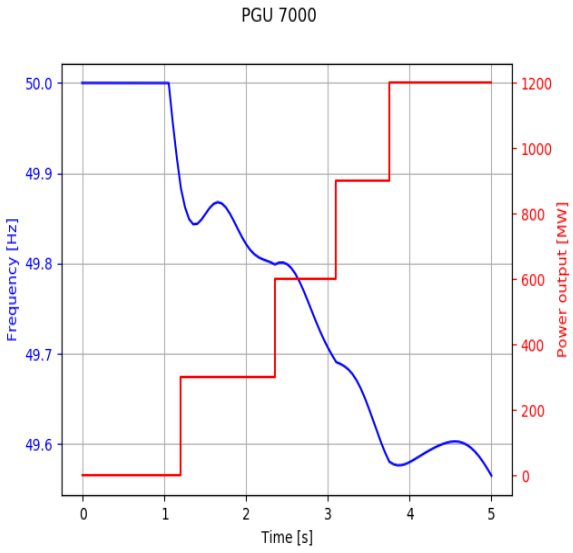

Figure 6.3: PGU frequency response for verifying activation at correct frequency thresholds

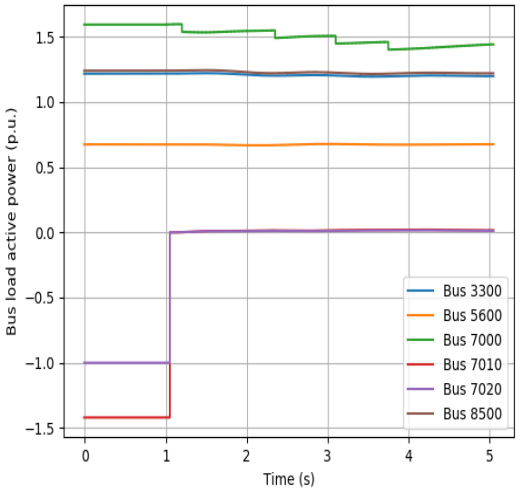

Figure 6.4: Load adjusted for verifying activation at correct frequency thresholds

6.3.2 Time delay to activate

To test whether the PGU responds with load change after the specified amount of time, the same case as in the previous subsection is run. Now, however, the delay-parameter of the PGU has been adjusted to 1.0 seconds for all steps, as shown in tab. 6.5.

Table 6.5: PGU settings with time-delay of 1 second

Frequency [Hz]	49.9	49.8	49.7	49.6	49.5
Step load [MW]	300	300	300	300	300
Delay [s]	1	1	1	1	1
Time available [s]	100	100	100	100	100

Figs. 6.5 and 6.6 show that the time-delay is working as intended. As the frequency drops below the first threshold 49.9 Hz, it takes approximately 1 second for the first load step of the PGU to kick in. The delay is not exactly 1 second. This is due to the Python interface pausing the simulation every 25-50 milliseconds to scan for exceeded frequency thresholds, and then only reacting thereafter.

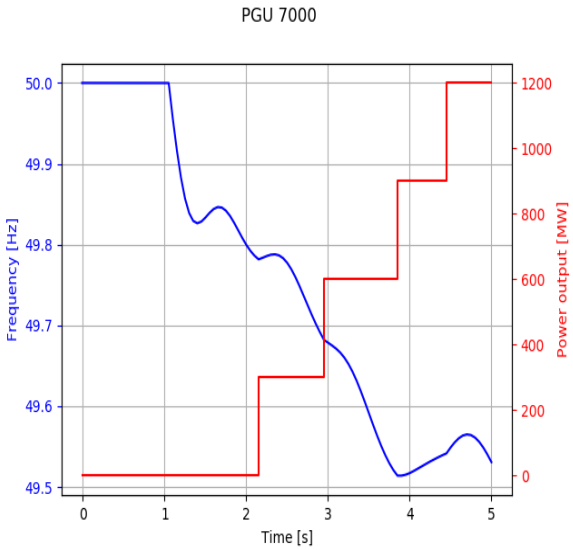

Figure 6.5: PGU frequency response with time-delay of 1 second

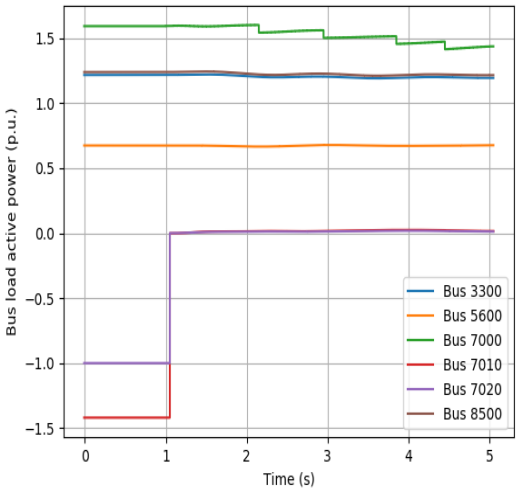

Figure 6.6: Load adjusted with time-delay of 1 second

6.3.3 Time available

To test whether the PGU power output only is allowed for the specified time available, a single load step of 500 MW is specified to last for an arbitrary selected length of 3 seconds, as seen in tab. 6.6.

Table 6.6: PGU settings for testing time-limited activation

Frequency [Hz]	49.5
Step load [MW]	500
Delay [s]	0
Time available [s]	3.0

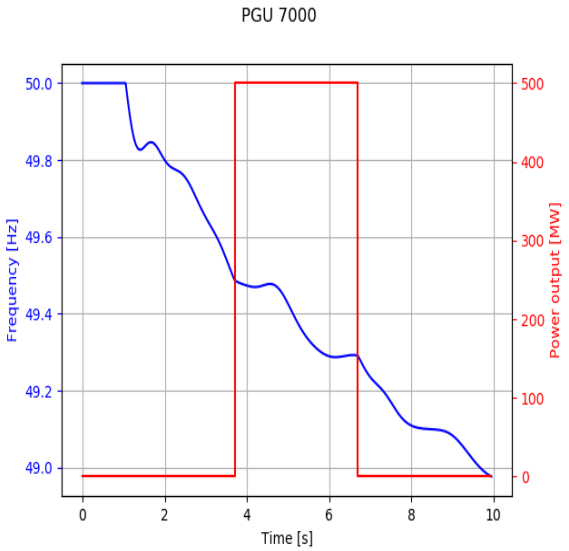

Figure 6.7: PGU frequency response with 3 seconds availability

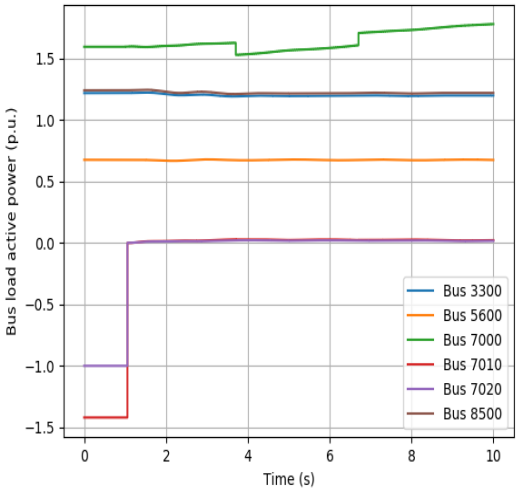

Figure 6.8: Load adjusted with 3 seconds availability

Figs. 6.7 and 6.8 show that the PGU reduces the load for only 3 seconds, before returning to the original load. It is thus working as intended. In fig. 6.8 the Z- and I-components of the ZIP load model at bus 7000 cause the load to continuously increase over the shown timespan. These effects are not considered as they are unrelated to the PGU.

6.3.4 Remains active

The previous runs of PGUs have all had active power responses that deactivate when the frequency starts rising and thresholds are no longer exceeded. As this is not always desirable, a PGU option (which is activated by default) is included to cause the PGU to not decrease active power output (increase load) after it first has been increased. In order to verify that this option works as intended, a test-case is run. The settings for the PGU at bus 7000 are seen in tab. 6.7.

Table 6.7: Settings for testing of option "Remains active"

Frequency [Hz]	49.5
Step load [MW]	1500
Delay [s]	1
Time available [s]	3.0

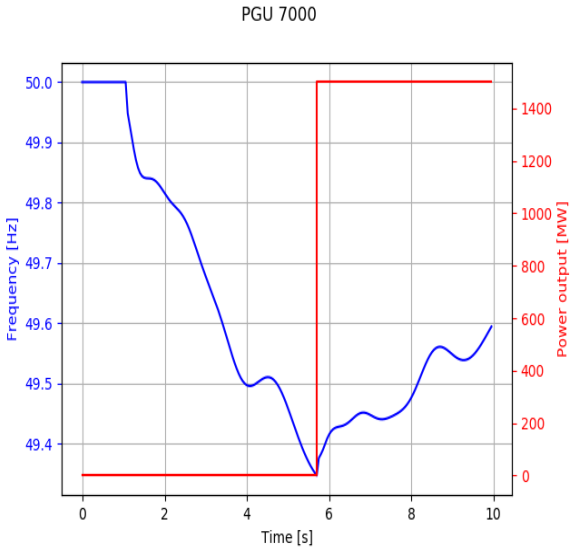

Figure 6.9: PGU response remaining active when frequency thresholds are no longer exceeded

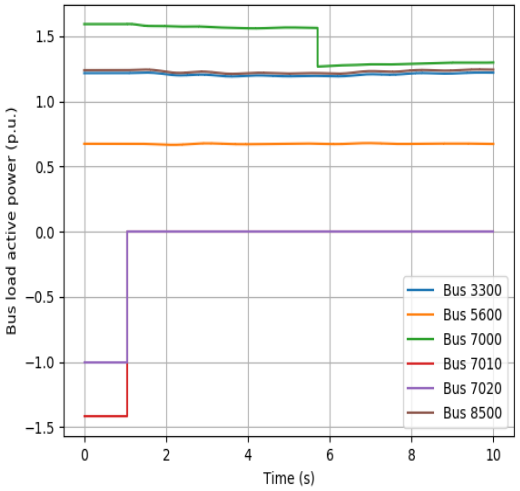

Figure 6.10: Load remain adjusted when frequency thresholds are no longer exceeded

As intended, the large step load of 1500 MW at 49.5 Hz causes the frequency to start increasing. Different from previous cases is that even after the frequency rises above 49.5 Hz, the PGU power output is not decreased back to 0 MW. The "remains active" option is successful.

6.3.5 PGU for use in simulations and interaction with UFLS

During work with the PGU significant compatibility issues were encountered for the PGU interacting with UFLS; the PGU would cancel the load shedding og UFLS. This subsection aims to verify that no such cancellation takes place and that the different settings for PGU can be used simultaneously.

Figs. 6.11 and 6.12 show that there is no detrimental interaction between the PGU and UFLS

Table 6.8: PGU settings for studying interaction with UFLS

Frequency [Hz]	49.9	49.8	49.7	49.6	49.5
Step load [MW]	150	150	150	150	150
Delay [s]	1	1	1	1	1
Time available [s]	3	3	3	3	3

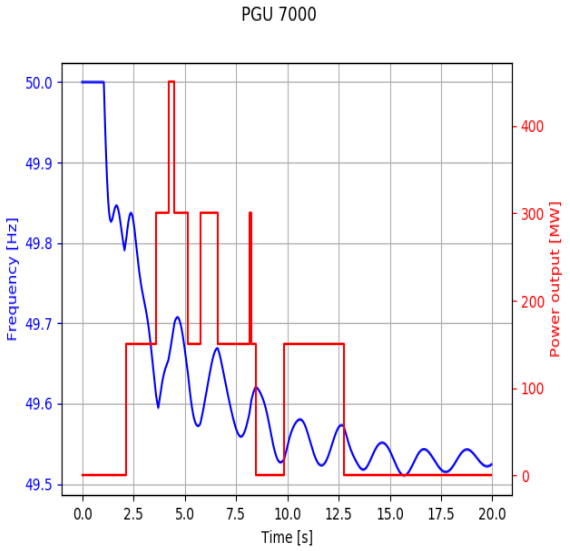

Figure 6.11: PGU frequency response interacting with UFLS

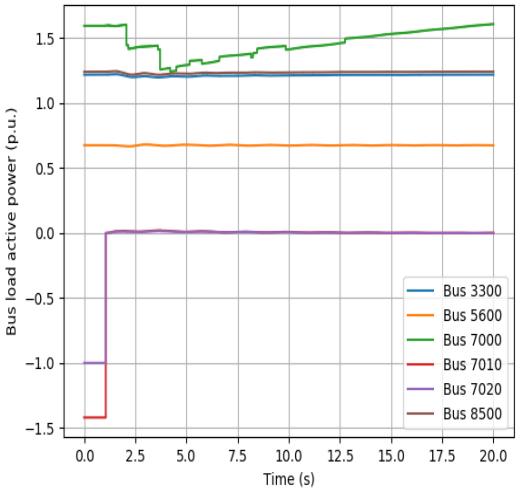

Figure 6.12: Load adjusted as seen in PSS®E plots by both PGU and UFLS

and that both function as intended. To see this, a step-by-step explanation of the sequence of events is necessary. At t = 1s, the frequency drops below 49.9 Hz. This causes the first load step at t = 2s which should reduce the load at bus 7000 by a total of 150 MW, or 30 MW at each of the five loads. However, we see that the frequency falls to 49.8 Hz also at approximately t = 2s, which causes UFLS to also shed 10% load. In the load response there is thus a large step and a smaller step at approximately t = 2s. Further, the frequency rises again, which causes the activation of the 49.8 Hz step of the PGU; it is only activated after approximately 3.5 seconds, at which point the frequency has been below 49.8 Hz continuously for 1 second. Shortly thereafter, at t = 4.0 seconds, the frequency has been below 49.7 Hz for 1 second and the third step activates; however, the frequency rises above 49.7 Hz shortly after activation and the third step is deactivated again before again being activated at approximately t = 5.5 seconds. Further details are omitted in favour of fig. 6.13

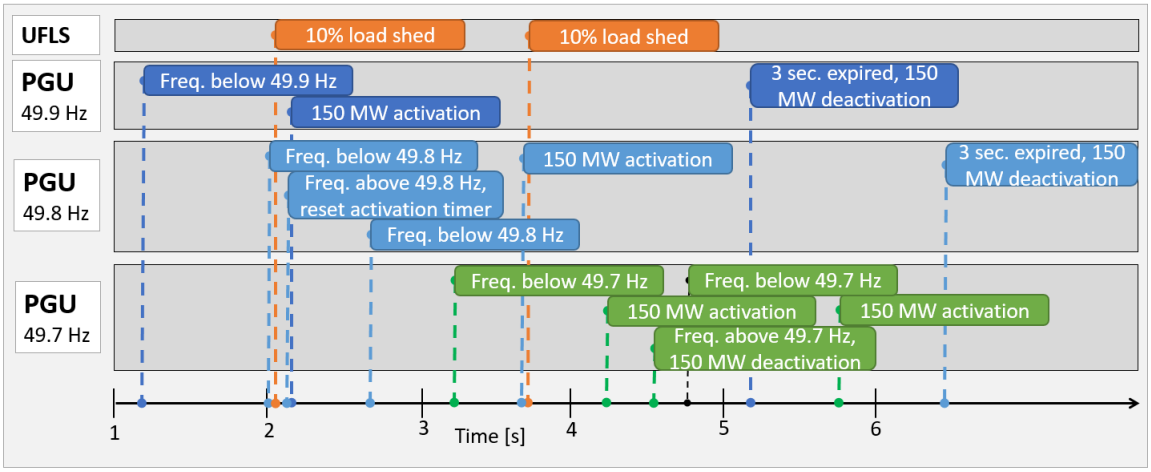

Figure 6.13: PGU and UFLS behaviour

Chapter 7

Results - Case group 1: High inertia frequency response

In this section, there is a simultaneous outage of NordLink and North Sea Link which prior to outages are all importing power at HVDC link maximum transmission capacity. The inertia of the system is approximately 290 GWs and the generators' total frequency bias for the Nordic power system (excluding DSR) is 8400 MW/Hz. The simultaneous outage of NordLink and North Sea Link leads to an outage of 2800 MW. See section 5.5.1 for further details on this group of cases.

Figure 7.1: Event tree for case without corrective actions

7.1 No corrective actions

The loss of power import is shown by the loads moving from a negative consumption of 1.4 p.u. equivalent to 1400 MW to 0 p.u. in fig. 7.7. The loss of import causes an initially steep frequency drop as seen in fig. 7.2, where the frequency in close proximity to the outages (bus 5600 connects to NordLink at bus 5610) falls very rapidly but all generators still manage to remain in synchronism with the rest of the grid as shown by the angles in fig. 7.3. The frequency reaches its nadir after approximately 10 seconds at 49.1 Hz for the COI-frequency, and at approximately 49.0 Hz for frequencies at bus 5600 and 7000. As expected, the electrical power output at bus 5600 increases drastically (bus 5600 is in close proximity to the NSL outage as seen by tab. 5.2) at the time of the outages due to the inertial response and starts oscillating, as shown in fig. 7.4. The electrical power output reaches a steady-state output at a higher p.u. output than prior to the outage as the governor primary response has caused generators at bus 5600 to increase the power output in response to the frequency drop. As the plot of generator mechanical powers in fig. 7.6 shows, primary response is not modelled for all N44 generators; only the hydro generators will adjust the power output (bus 5600 in the figure), leaving a constant mechanical power input at thermal and nuclear power plants. Of the shown generators, the voltages in Sweden and Finland dip especially low while the voltage at bus 5600 seems relatively unaffected, as seen in fig. 7.5.

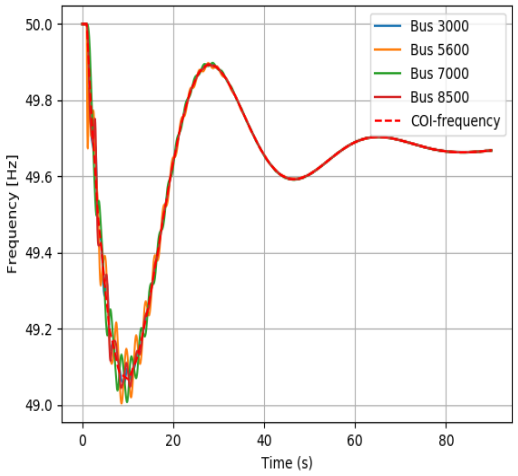

Figure 7.2: Generator frequencies

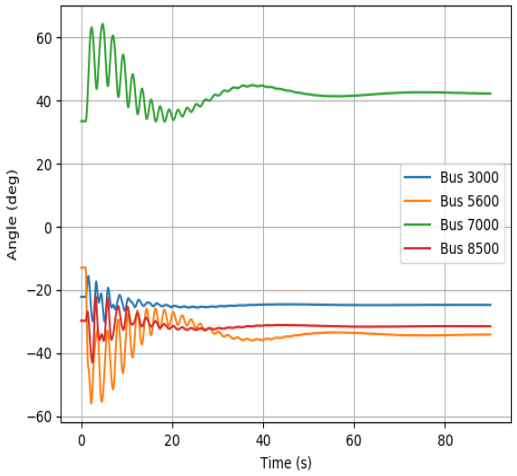

Figure 7.3: Generator angles

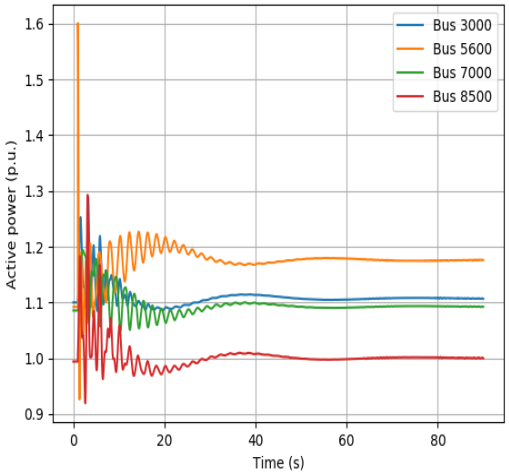

Figure 7.4: Generator active powers

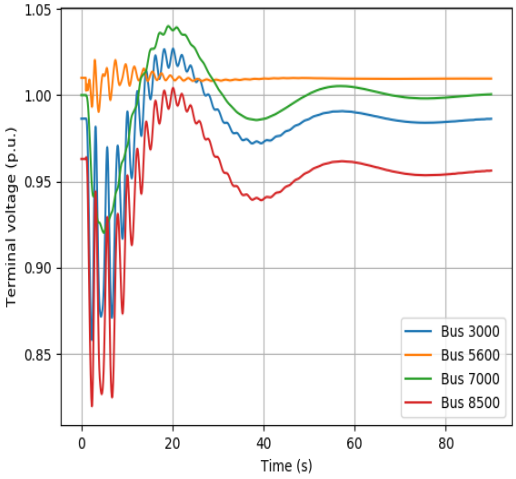

Figure 7.5: Generator terminal voltages

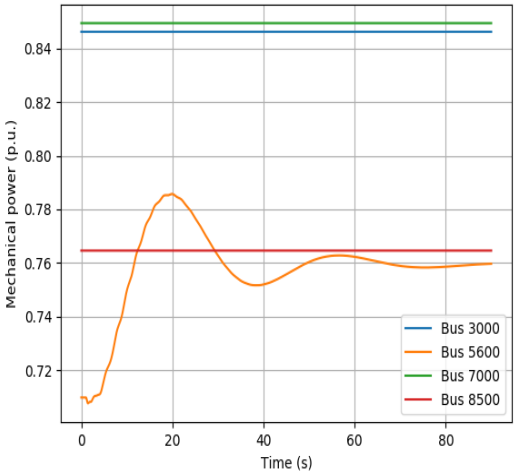

Figure 7.6: Generator mechanical power input

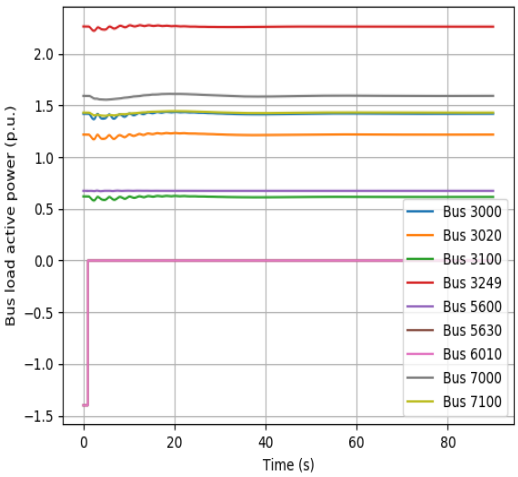

Figure 7.7: Load power demand

Figure 7.8: Event tree for case HVDC Emergency Power

7.2 Under-Frequency Load Shedding

In this case, UFLS is armed with settings as shown in tab. 4.1. As the frequency is never low enough for the first frequency threshold, no load shedding occurs and the simulation results are the same as shown in section 7.1.

7.3 HVDC Emergency Power

The system response when HVDC Emergency Power is armed is initially the same as that of section 7.1. As the HVDC Emergency Power frequency thresholds for activation are staggered around 49.5 Hz, the response will start to differ from previous cases only as the frequency falls to approximately 49.5 Hz. As shown in figs. 7.9 to 7.12, the system response is very similar and hard to distinguish from the case in section 7.1, apart from a higher frequency nadir and steady-state frequency due to the HVDC Emergency Power supplying extra active power to the system. The frequency nadir and steady-state frequency are approximately 49.3 Hz and 49.8 Hz. A slightly lower generation increase due to primary response is observed in fig. 7.11 as the primary response is aided by HVDC Emergency Power to contain the frequency and primary response thus causes a lower mechanical power setpoint change. The effect of HVDC Emergency Power activation is illustrated in fig. 7.13. As shown, the HVDC Emergency Power at bus 5610 Skagerak activates at 49.6 Hz[1] and contributes to reducing the generation deficit in the system. Other activations of HVDC Emergency Power are not shown in order to limit the number of plots.

[1]There is a 0.5 seconds delay between detected frequency and activation of PGU response; as the response is activated at t=4 seconds, the activation threshold is at t=3.5 seconds or 49.6 Hz

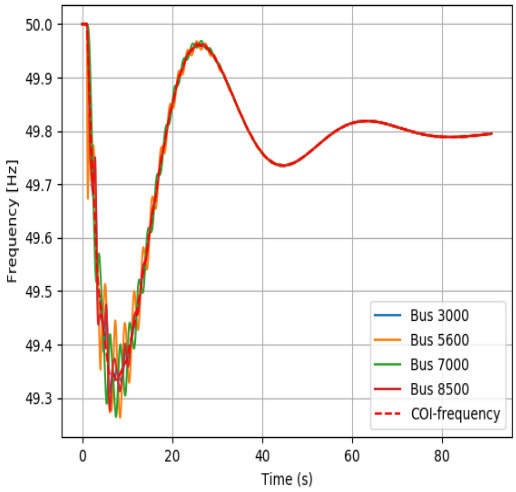

Figure 7.9: Generator frequencies

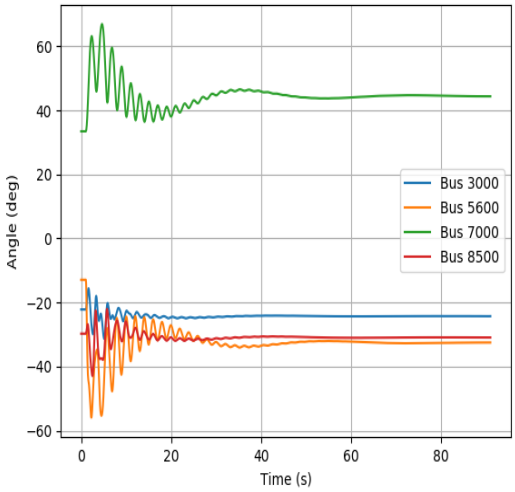

Figure 7.10: Generator angles

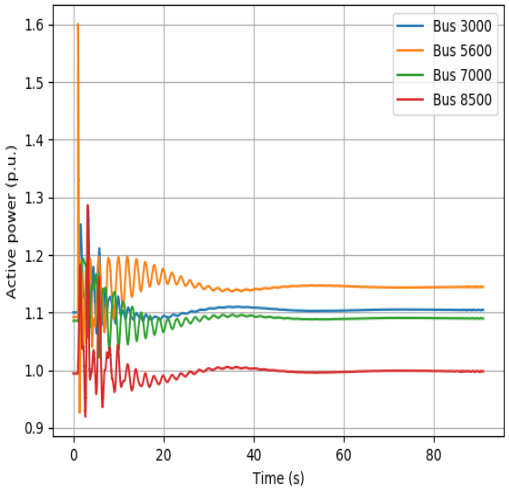

Figure 7.11: Generator active powers

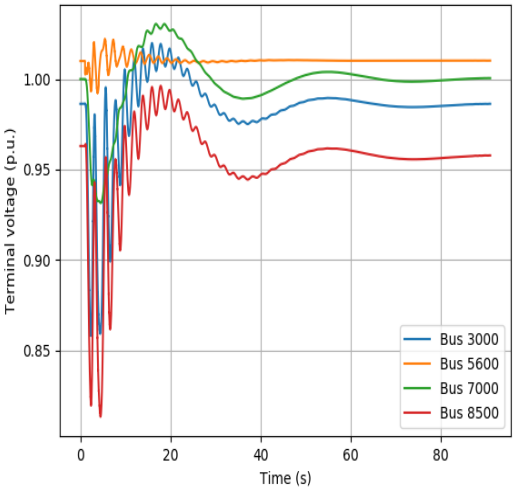

Figure 7.12: Generator terminal voltages

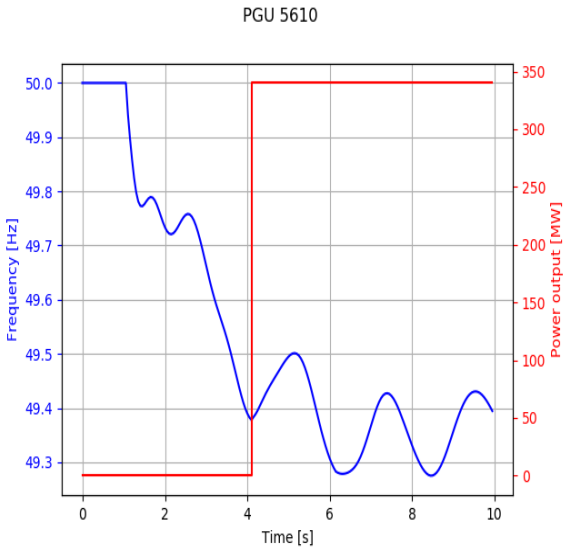

Figure 7.13: HVDC Emergency Power activation at bus 5610 Skagerak

Figure 7.14: Event tree for case Demand-Side Response

7.4 Demand-Side Response

Figure 7.15 shows that DSR with low time-delay has positive effects on the frequency nadir. The frequency nadir is significantly improved with increasing amounts of DSR-enabled load if the time-delay is low. As the time-delay increases, the effect of increasing the % of DSR-enabled load decreases. This is due to the system frequency falling too far before the DSR is able to respond and contribute to containing the frequency drop.

Low activation time-delay of DSR-enabled load also has a positive effect on the steady-state response of the system as shown in fig. 7.16. The steady-state frequency slightly increases with increasing % of DSR-enabled load for low time-delays. As the time-delay is increased, however, the achieved steady-state frequency exceeds the nominal frequency of 50 Hz. This may or may not be intuitive. An explanation is given below.

To illustrate the DSR response for low and high time-delays, the DSR due to the PGU at an arbitrary bus is selected which is bus 7000 in figs. 7.18 and 7.20. When the DSR time-delay is low, as in fig. 7.18, the DSR response improves the frequency response by almost immediately reducing the power deficit in the system as the frequency drops, thus aiding in containing the frequency drop. When the time-delay is high, as in fig. 7.20, the frequency falls to approximately 49.2 Hz before there is any response at all from the DSR, as seen in fig. 7.20. 49.2 Hz is very close to the frequency nadir of the base case without any SIPS as seen in section 7.1. After the 5 second delay, the PGU now has to respond to a much larger frequency drop than if the time-delay was short. The PGU thus suddenly ramps up production (decreases load) and the total DSR active power response is far higher than the power import lost in the simultaneous HVDC-outage; at bus 7000, the response with short time-delay is less than 140 MW, while a longer time-delay approaches 300 MW. If all buses with DSR were to be considered, the aggregated response will be very large.

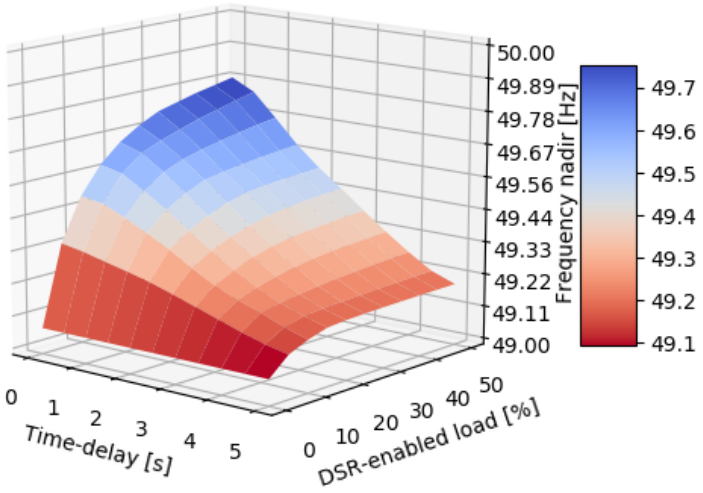

Figure 7.15: Surface plot of frequency nadir as function of time-delay and percentage DSR

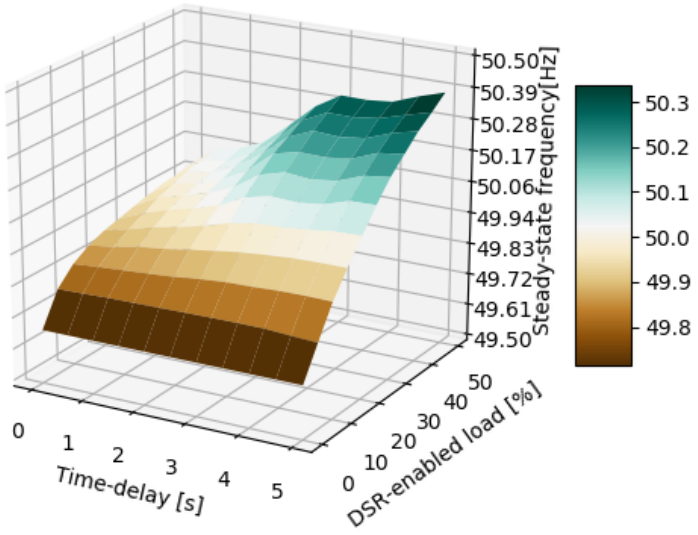

Figure 7.16: Surface plot of steady-state frequency as function of time-delay and percentage DSR

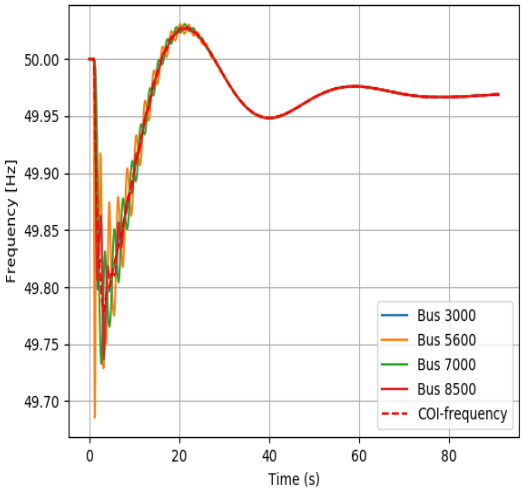

Figure 7.17

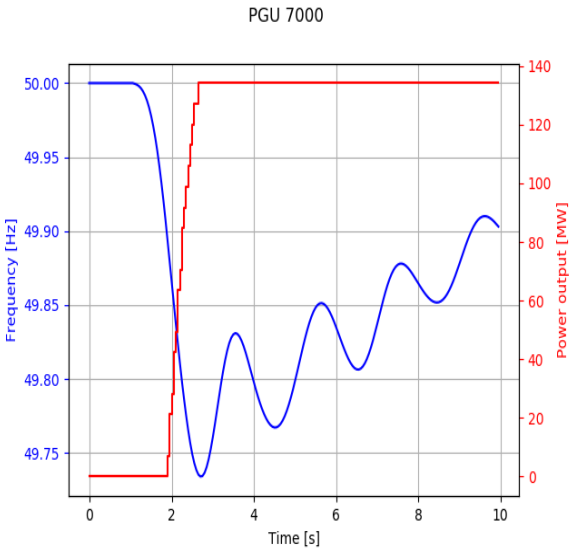

Figure 7.18

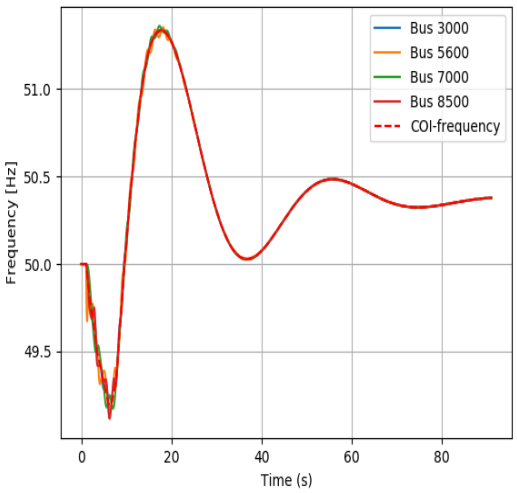

Figure 7.19

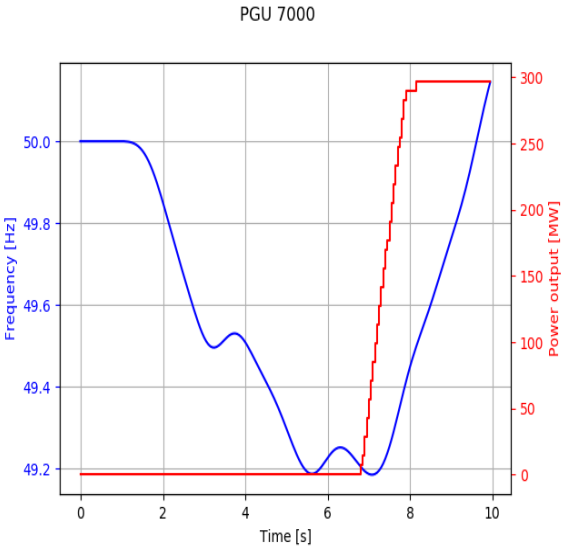

Figure 7.20

Figure 7.21: Event tree for Demand-Side Response with no reserves for primary response

7.5 Demand-Side Response with saturated primary response

Sensitivity analyses for DSR is shown by frequency nadir and steady-state frequency for cases with saturated primary response are in figs. 7.22 and 7.23 respectively. It is seen from fig. 7.22 that the nadir is greatly improved by adding up to 10% DSR-enabled load. The steady-state frequency achieved if the time-delay is too large is extremely high as seen from fig. 7.23, again due to the frequency reaching low values before DSR is able to activate as in section 7.4. A weakness of this analysis may be that, if the primary reserves are saturated in terms of ability to increase power output, a frequency increase would demand that primary response *decreases* power output of generators, which means the generators can no longer be considered saturated. This is not accounted for in the surface plots in figs. 7.22 and 7.23 and may cause higher steady-state frequencies than would have been when the frequency exceeds 50 Hz. There are extreme frequencies achieved with lows and highs approximating 47.0 and 54 Hz respectively, for which the extremity of system states make the results more imprecise than other cases.

The frequency response is illustrated in figs. 7.24 and 7.26 for a low and high time-delay respectively. As there is no primary response, the frequency response is much larger than that of section 7.4. The frequency response of the fast and slow DSR differ considerably. When DSR is quick to react as in fig. 7.24, the frequency is continuously falling as the DSR is simply a proportional response and there is no PI-controller causing primary response to contain the frequency further frequency decline. With a longer time-delay as in fig. 7.26, the frequency is dropping continuously until it abruptly starts shoots upwards as the initial activation delay is over. The low frequencies achieved during the wait for activation of DSR again cause the PGU power output to be higher than with a low time-delay, but the effect is less pronounced than in section 7.4.

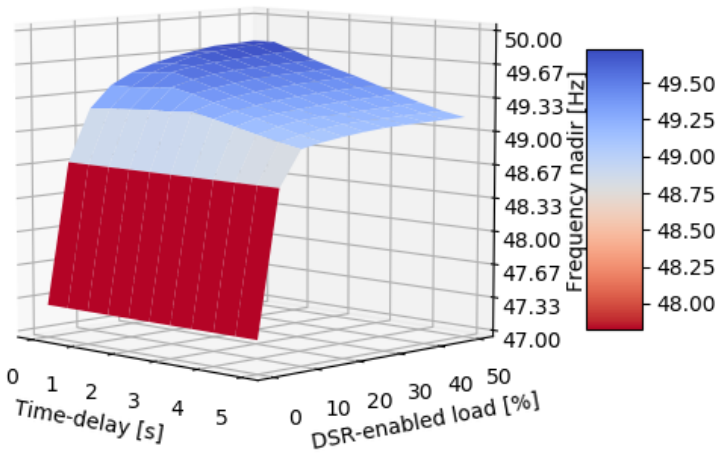

Figure 7.22: Surface plot of frequency nadir as function of time-delay and percentage DSR

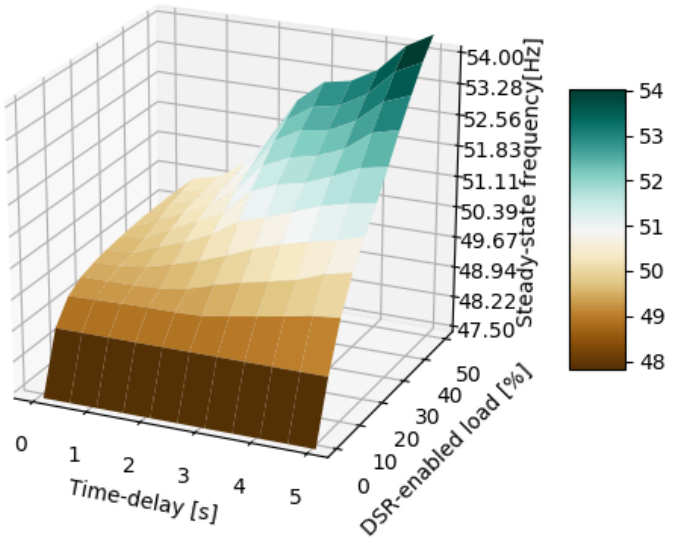

Figure 7.23: Surface plot of steady-state frequency as function of time-delay and percentage DSR

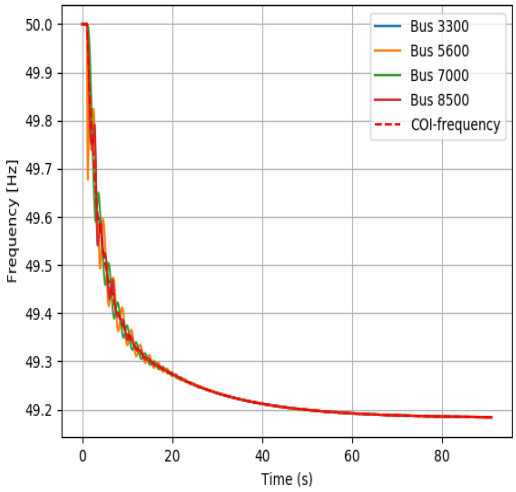

Figure 7.24

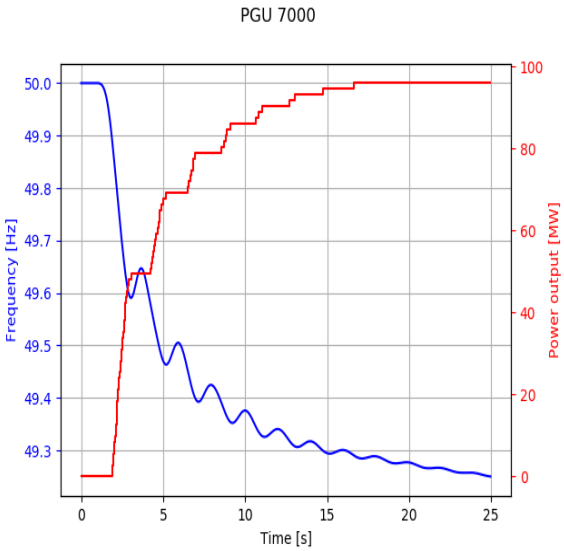

Figure 7.25

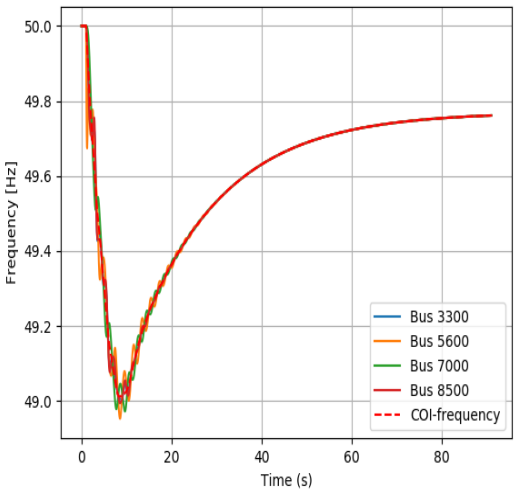

Figure 7.26

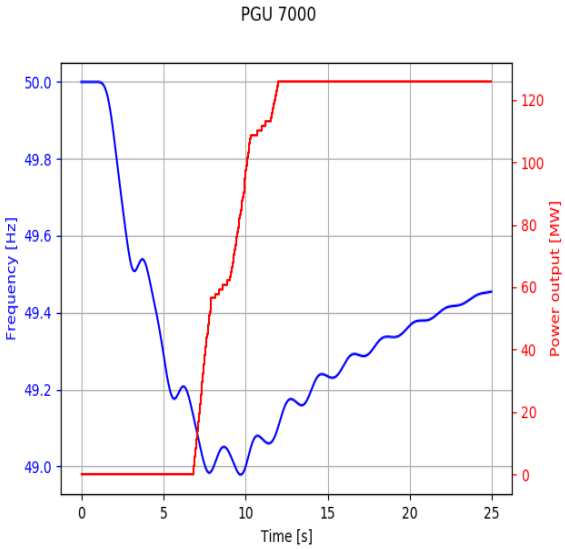

Figure 7.27

Figure 7.28: Event tree for case with DSR, HVDC Emergency Power and UFLS

7.6 Demand-Side Response, HVDC Emergency Power and UFLS

The frequency nadir for varied time-delay and % DSR-enabled load is shown in fig. 7.29 and the corresponding steady-state frequency achieved is shown in fig. 7.30. The impact of DSR on system frequency is lessened as the system power balance is aided by HVDC Emergency Power. UFLS does again not affect the results due to load shedding frequency thresholds not being met.

Plots of frequency response for % DSR-enabled load at 10% and a 1.0 seconds time-delay is shown in fig. 7.31. There are large oscillations in the frequency at approximately t = 5 seconds as the HVDC Emergency Power starts to initiate and the frequency starts rising. The frequency slightly overshoots the nominal frequency before settling at just above 49.9 Hz. The generator angles, active powers and voltages are all very similar to the base case without protective schemes in section 7.1 and are thus not shown.

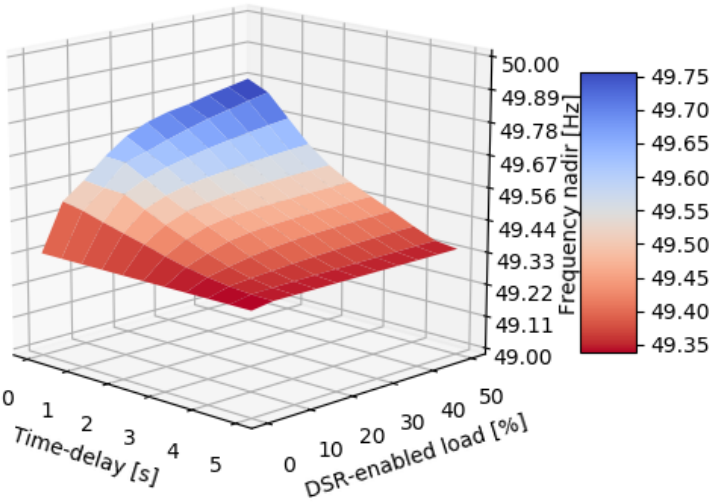

Figure 7.29: Surface plot of frequency nadir as function of time-delay and percentage DSR

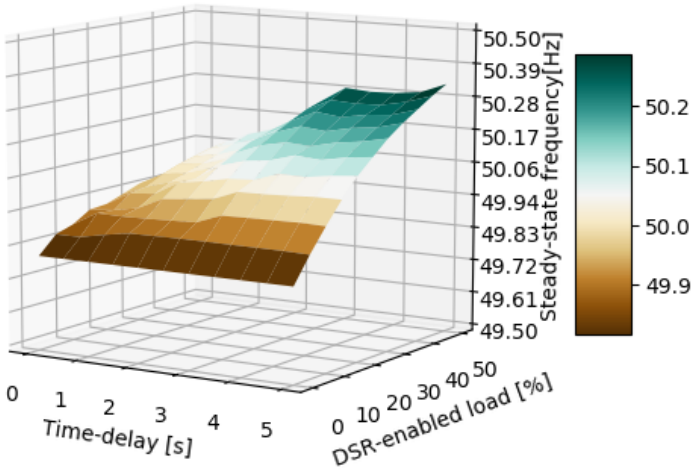

Figure 7.30: Surface plot of steady-state frequency as function of time-delay and percentage DSR

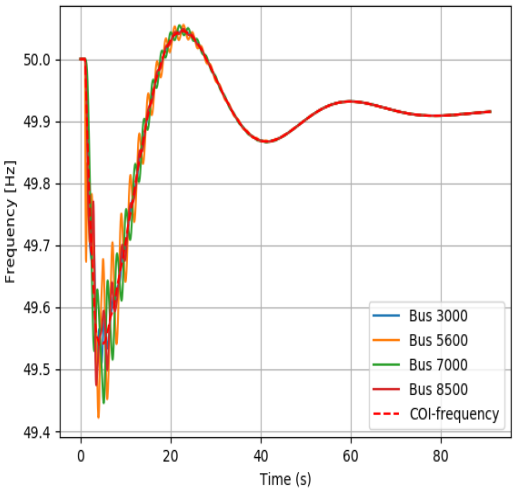

Figure 7.31: Generator frequencies

7.7 Summary of case 1

The frequency response in terms of nadir and steady-state frequency is summarized here for the case studies in this group. Cases with 10% DSR-enabled load is selected for cases where DSR is applied, as 10% is perhaps not an excessive amount of DSR-enabled load yet shows large improvements over the results without DSR, but where the results largely depend on the DSR time-delay.

Table 7.1: Frequency nadir of cases in group 1

Protective schemes	**Nadir frequency [Hz]**
No protective schemes	49.08
Only UFLS	49.08
Only HVDC Emergency Power	49.35
Only 10% DSR, 0.0 seconds delay	49.49
Only 10% DSR, 5.0 seconds delay	49.16
Only 10% DSR, 0.0 seconds delay, no primary reserves	49.18
Only 10% DSR, 5.0 seconds delay, no primary reserves	49.01
All corrective actions, only 10% DSR, 0.0 seconds delay	49.55
All corrective actions, only 10% DSR, 5.0 seconds delay	49.35

Table 7.2: Steady-state frequency of cases in group 1

Protective schemes	**Steady-state [Hz]**
No protective schemes	49.67
Only UFLS	49.67
Only HVDC Emergency Power	49.80
Only 10% DSR, 0.0 seconds delay	49.84
Only 10% DSR, 5.0 seconds delay	49.89
Only 10% DSR, 0.0 seconds delay, no primary reserves	49.18
Only 10% DSR, 5.0 seconds delay, no primary reserves	49.76
All corrective actions, only 10% DSR, 0.0 seconds delay	49.87
All corrective actions, only 10% DSR, 5.0 seconds delay	49.95

Figure 8.1: Event tree for case without corrective actions

Chapter 8

Results - Case group 2: Low inertia frequency response

In this section, there is a simultaneous outage of NordLink and North Sea Link which prior to outages are all importing power at HVDC link maximum transmission capacity. The inertia of the system is approximately 200 GWs and the generators' total frequency bias for the Nordic power system (excluding DSR) is 3500 MW/Hz. The simultaneous outage of NordLink and North Sea Link leads to an outage of 2800 MW. See section 5.5.2 for details on this group of cases.

8.1 No corrective actions

Low inertia and no protective schemes leads to extreme frequency drops. The COI-frequency in fig. 8.2 falls to approximately 48.1 Hz 8 seconds after the outage while some generator frequencies even fall to 48.0 Hz, before swinging back up to 49.5 Hz and moving to a steady-state frequency of approximately 49.2 Hz.

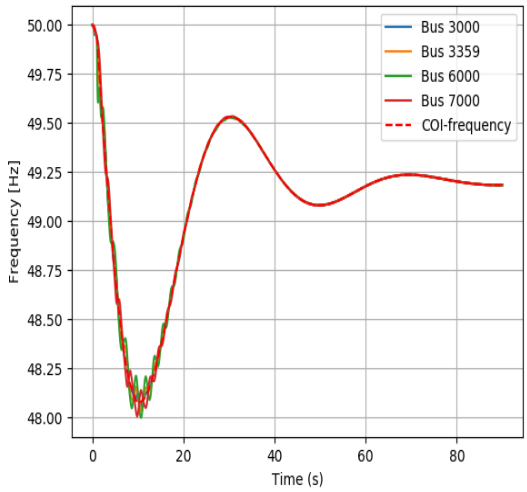

Figure 8.2: Generator frequencies

Figure 8.3: Event tree when for case UFLS

8.2 UFLS

Contrary to the case in section 7.2, the low inertia now causes the frequency to fall sufficiently that UFLS activation is possible. The frequency response of the system in fig. 8.4 shows that the first load shedding threshold at 48.6 Hz is sufficient to stop further frequency dips and allow the frequency to recover.

The total load shed is 2187.18 MW and and the sequence of load shedding that occurs in the system is shown in tab. 8.1. The sequence of where load is shed may be inaccurate due to insufficient model tuning for low inertia scenario. All the load shedding occurs after approximately 5-6 seconds, so further precision on the sequence of events may not be unnecessary.

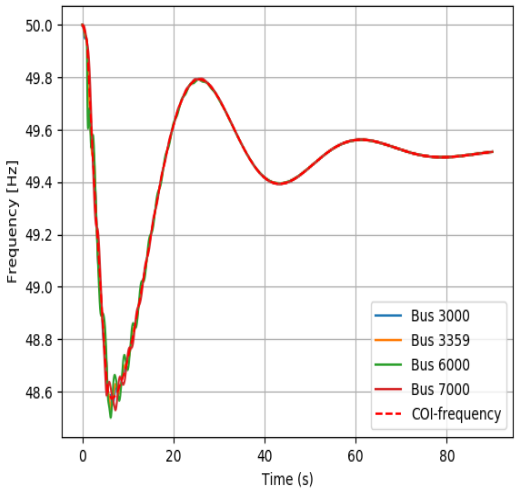

Figure 8.4: Generator frequencies

Table 8.1: Overview of load shed after outage

Bus number	Area	Time [s]	Frequency [Hz]	Load shed [MW]
7000	FI1	5.325	48.60	345.80
8500	SE4	5.575	48.60	164.55
3300	SE3	5.580	48.60	105.66
3000	SE3	5.585	48.60	185.40
3359	SE3	5.585	48.60	254.92
6500	NO3	5.600	48.60	131.88
5100	NO1	5.610	48.60	50.09
5400	NO1	5.610	48.60	95.47
5500	NO1	5.610	48.60	190.94
5600	NO2	5.610	48.60	59.32
5300	NO5	5.630	48.60	115.05
6100	NO4	5.640	48.60	104.14
3100	SE2	5.665	48.60	27.04
6700	NO4	5.780	48.60	107.39
3115	SE1	6.405	48.60	26.95
7100	FI2	6.420	48.60	124.28
3249	SE2	6.435	48.60	98.30

Figure 8.5: Event tree for case HVDC Emergency Power

8.3 HVDC Emergency Power

Use of HVDC Emergency Power in a low inertia scenario leads to a frequency nadir of approximately 48.6 Hz and a steady-state frequency of approximately 49.4 Hz, as shown in fig. 8.6. The frequency nadir is the same as that of UFLS in section 8.2, but with a slightly lower steady-state frequency as the total contributed HVDC Emergency Power is lesser than the load shed in the UFLS case; total HVDC Emergency Power activated is X MW.

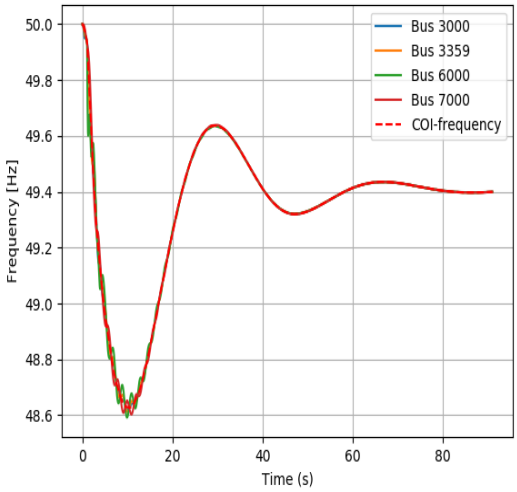

Figure 8.6: Generator frequencies

Figure 8.7: Event tree for case Demand-Side Response

8.4 Demand-Side Response

Due to low inertia, the impact of DSR is larger in this case compared to the higher inertia in section 7.4. The frequency nadir is again shown to be highly sensitive to the time-delay, as shown in fig. 8.8 shown to be especially critical for the ability of DSR to hinder low frequency nadirs. As the time-delay increases, increased amounts of DSR cause a lower impact on the frequency nadir but an increasing steady-state frequency which at some points exceeds the nominal frequency as shown in fig. 8.9, due to the effects with increased DSR response when there is large time-delay, as explained in section 7.4.

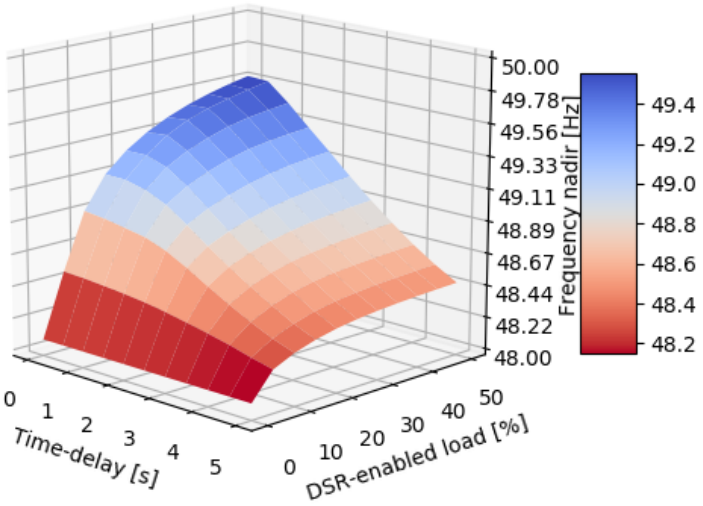

Figure 8.8: Surface plot of frequency nadir as function of time-delay and percentage DSR

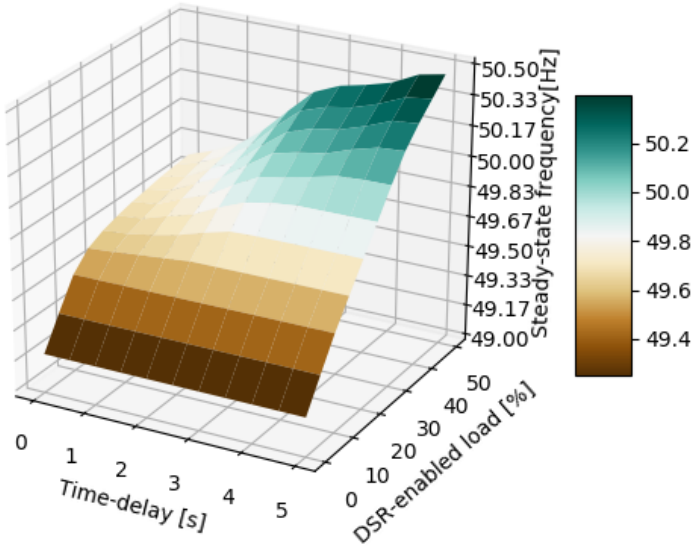

Figure 8.9: Surface plot of steady-state frequency as function of time-delay and percentage DSR

Figure 8.10: Event tree for Demand-Side Response with no reserves for primary response

8.5 Demand-Side Response with saturated primary response

With frequency nadirs reaching lows of almost 42.0 Hz in fig. 8.11 and steady-state frequencies ranging from 42.0 Hz to 57.5 Hz in fig. 8.12, the validity of the results achieved must immediately be questioned. The system would likely have collapsed far before achieving such states.

The results with less extreme frequencies seem to show that if DSR is to be sufficient to contain the frequency in a low inertia case with saturated primary response, there needs to be 25% DSR-enabled load or more to avoid extremely low frequency nadirs as illustrated by the large dependency on % DSR-enabled load when there is a low % in fig. 8.11. When there is a sufficiently large amount of DSR-enabled load, very short time-delay or very long time-delay leads to a lower frequency nadir than something in between; At a time-delay of 1.5 seconds and 50% DSR-enabled load, both an increase or decrease in time-delay or a decrease in % DSR-enabled load lead to lower frequency nadir. It is similar for, for example, 2.5 seconds time-delay and 25% DSR-enabled load. Considering also the steady-state frequencies shown in fig. 8.12, a minimum of 25% DSR-enabled load is desirable to avoid the lowest steady-state frequencies. At a larger time-delay than approximately 2.5 seconds and with % DSR-enabled load surpassing 25%, the steady-state frequencies soon become too large. At very low time-delays, the steady-state frequencies are lower than at slightly higher time-delays; this is due to behaviour described in section 7.4. It is then desirable to find a point which achieves both reasonable frequency nadir and a steady-state frequency that is neither too high or too low. At for example 2.5 seconds time-delay and 25% DSR-enabled load this seems to be achieved. It is thus clear that some combinations that are not minimum or maximum time-delay or % DSR-enabled load will give the best results when the primary response is saturated.

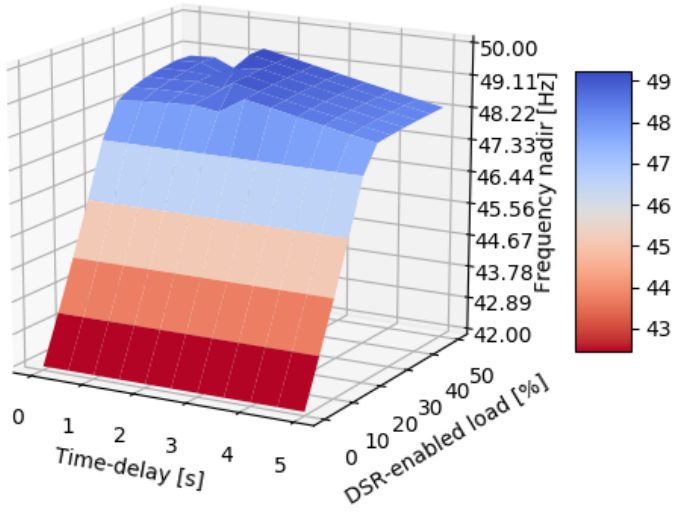

Figure 8.11: Surface plot of frequency nadir as function of time-delay and percentage DSR

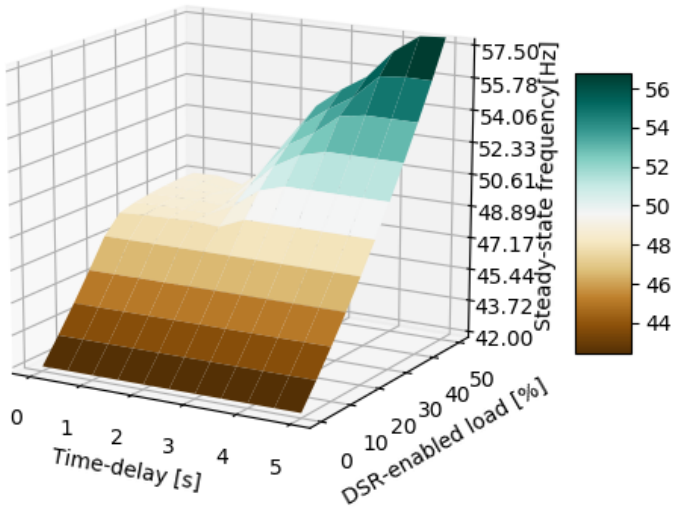

Figure 8.12: Surface plot of steady-state frequency as function of time-delay and percentage DSR

Figure 8.13: Event tree for case with DSR, HVDC Emergency Power and UFLS

8.6 Demand-Side Response, HVDC Emergency Power and UFLS

The frequency nadir in fig. 8.14 shows part of the dependency of the system frequency response on DSR parameters. The lowest frequency achieved is 48.60 Hz at 0% DSR-enabled due to UFLS as shown in section 8.2 or due to HVDC Emergency Power in section 8.3 which gave similar results in terms of frequency nadir. Low time-delay and high amount of DSR-enabled load leads to the best response in terms of frequency nadir, as has been observed in other cases. Steady-state frequency achieved is shown in fig. 8.15 varies greatly and is slightly below 49.5 Hz when there is no DSR is while achieving approximately 50.3 Hz for the cases with the longest time-delay and highest % DSR-enabled load. If it is desirable that steady-state frequency is approximately 50 Hz shortly after the simultaneous outages then a shorter time-delay with more DSR-enabled load or a longer time-delay with less DSR-enabled load is preferable. This is due to the same mechanisms as described in section 7.4. Finally, comparing this case to previous cases, it is clear that the effect of DSR-enabled load in a system with UFLS and HVDC Emergency Power is much less prominent than in case studies where UFLS and HVDC Emergency Power are nonexistent or fail to activate. The frequency response of the system with a 1.0 second time-delay and 10% DSR-enabled load is shown in fig. 8.16, where the COI-frequency nadir is approximately 49.2 Hz before the frequency recovers to slightly above 49.6 Hz.

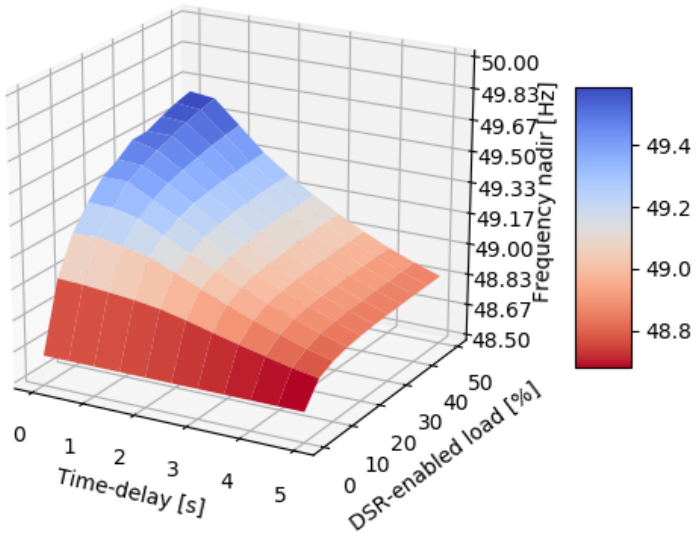

Figure 8.14: Surface plot of frequency nadir as function of time-delay and percentage DSR

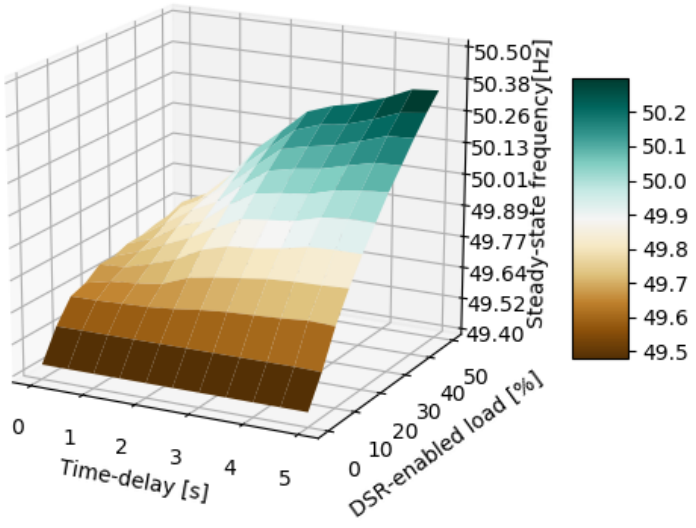

Figure 8.15: Surface plot of steady-state frequency as function of time-delay and percentage DSR

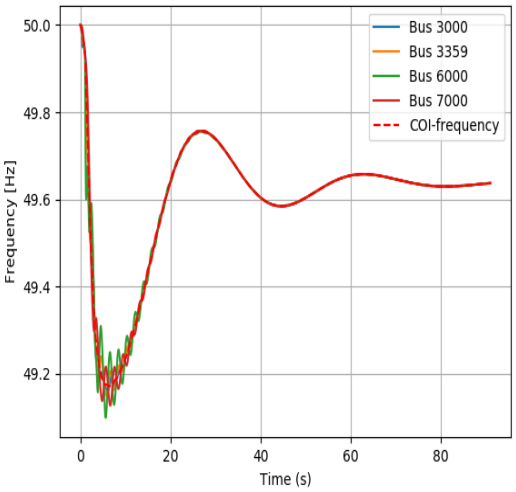

Figure 8.16: Generator frequencies

8.7 Summary of case 2

The frequency response in terms of nadir and steady-state frequency is summarized here for the case studies in this group. Cases with 10% DSR-enabled load is selected for cases where DSR is applied, as 10% is perhaps not an excessive amount of DSR-enabled load yet shows large improvements over the results without DSR, but where the results largely depend on the DSR time-delay.

Table 8.2: Frequency nadir of cases in group 2

Protective schemes	**Nadir frequency [Hz]**
No protective schemes	48.07
Only UFLS	48.60
Only HVDC Emergency Power	48.64
Only 10% DSR, 0.0 seconds delay	48.89
Only 10% DSR, 5.0 seconds delay	48.32
Only 10% DSR, 0.0 seconds delay, no primary reserves	44.55
Only 10% DSR, 5.0 seconds delay, no primary reserves	44.54
All corrective actions, 10% DSR, 0.0 seconds delay	49.19
All corrective actions, 10% DSR, 5.0 seconds delay	48.79

Table 8.3: Steady-state frequency of cases in group 2

Protective schemes	**Steady-state [Hz]**
No protective schemes	49.19
Only UFLS	49.53
Only HVDC Emergency Power	49.41
Only 10% DSR, 0.0 seconds delay	49.51
Only 10% DSR, 5.0 seconds delay	49.51
Only 10% DSR, 0.0 seconds delay, no primary reserves	44.55
Only 10% DSR, 5.0 seconds delay, no primary reserves	44.55
All corrective actions, Only 10% DSR, 0.0 seconds delay	49.63
All corrective actions, Only 10% DSR, 0.0 seconds delay	49.68

Chapter 9

Results - Case group 3: Effect of location of outage of HVDC links

See section 5.5.3 for further details on this group of cases.

9.1 Outages of KontiSkan, Baltic Cable and SwePol

In this section, there is a simultaneous outage of KontiSkan, Baltic Cable and SwePol which prior to outages are all importing power at HVDC link maximum transmission capacity. The inertia of the system is approximately 240 GWs and the generators' total frequency bias for the Nordic power system (excluding DSR) is 6700 MW/Hz. The simultaneous outage of KontiSkan, Baltic Cable and SwePol leads to an outage of 1940 MW if the outage size is not scaled.

9.1.1 Outages without corrective actions

For an outage scaling factor ϕ=1.0, the simultaneous outages do not lead to simulation divergence or system collapse. However, voltages are immediately after the outages very low in the South and in the middle of Sweden. Bus 3100 sees the lowest voltages and is in N44 one of the few buses in the area without any generator. The plots for this are not shown as the plots for an outage scaling factor ϕ = 1.33 show the same behaviour, only more extreme:

when the outages are scaled using $\phi = 1.33$ we find the maximum outage size of 2580 MW before the system will collapse. This implies that $\phi = 1.34$ will lead to system collapse. The plots of the response of the N44 system with $\phi = 1.33$ and $\phi = 1.34$ are shown in figs. 9.1 to 9.4. We see that even when the voltages do not collapse in fig. 9.1, they reach a low of approximately 0.70 p.u. in southern Sweden. It is also seen that the change of the angles in fig. 9.3 is varying; some angles decrease while others are increased, which if pushed further may lead to system separation. The rapid voltage drop in fig. 9.2 for $\phi = 1.33$ shows a voltage collapse a few seconds after the initial outage. The generator angles in fig. 9.4 show that the low voltages lead to loss of synchronism for generators at bus 3300, 3359 and 8500, all in the south of Sweden. This is likely due to low power transfer capabilities resulting from low voltages in Sweden. The voltage collapse and low power transfer capabilities leads to generators in the South of Sweden separating from the remainder of the power grid.

9.1.2 Outages with frequency-based corrective actions

Applying UFLS, HVDC Emergency Power and DSR, the response of these corrective actions cause no visible difference in system response compared to that of cases in section 9.1 and the maximum outage scaling factors are identical. Plots of system response for this case are thus not shown due to the extensive similarity to what has already been shown.

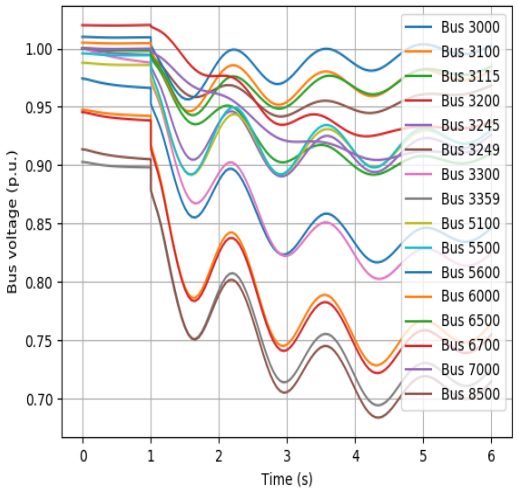

Figure 9.1: Bus voltages, $\phi = 1.33$

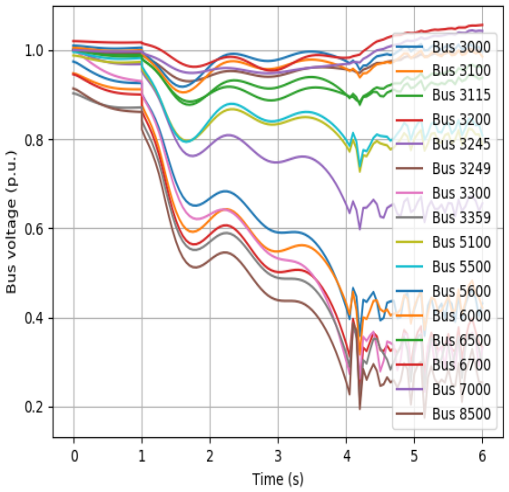

Figure 9.2: Bus voltages, $\phi = 1.34$

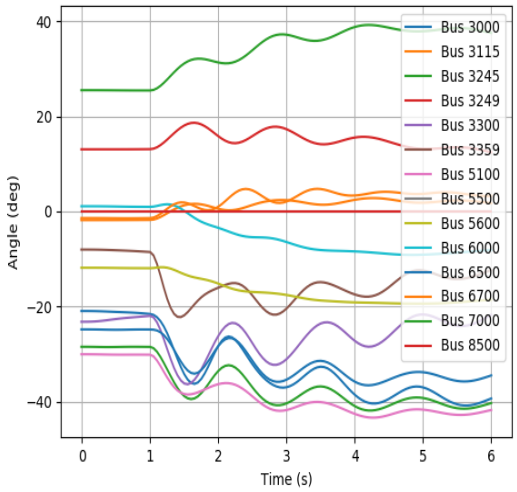

Figure 9.3: Generator angles, $\phi = 1.33$

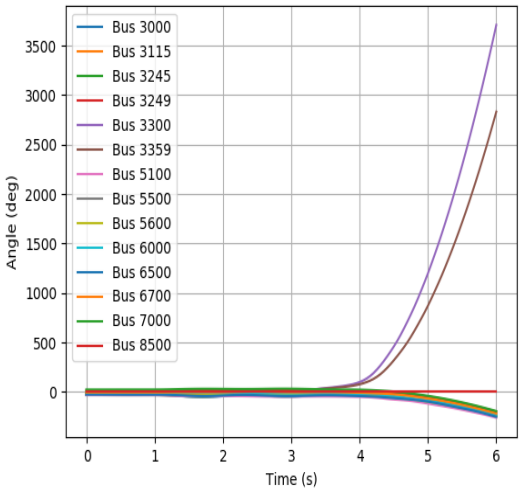

Figure 9.4: Generator angles, $\phi = 1.34$

9.1.3 Outages with UVLS

When UVLS protection relays are enabled in Sweden, the system is capable of surviving much higher outages than in the previous sections with or without frequency-based corrective actions. The figs. 9.5 to 9.8 show the response of the system for an outage scaling factor $\phi = 2.0$ or outages *twice*[1] the size of the maximum transmission capacity of KontiSkan, Baltic cable and Swepol for a total of 3880 MW loss. Load is in the first half second after the simultaneous outages shed at buses in southern Sweden, as well as further north at, for example,

[1] Larger outages were not tested

3100 Hjalta. 8500 Malmö, 3359 Ringhals and 3100 Hjalta reach the second voltage shedding threshold at 0.8 p.u., where the former two buses perform second stage load shedding a few hundred milliseconds after the first stage load shedding. The latter bus only reaches 0.8 p.u. voltage after approximately 1.5 seconds. This may be an indication that these three buses are especially vulnerable to rapid voltage collapse following large outages. It is nevertheless clear that voltage-based load shedding as a response to rapidly declining voltage in Sweden allows the system or N44 model to cope with much larger outages.

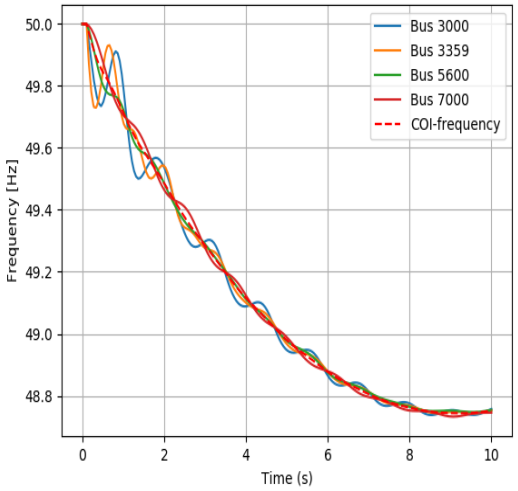

Figure 9.5: Generator frequencies, $\phi = 2.0$, with UVLS

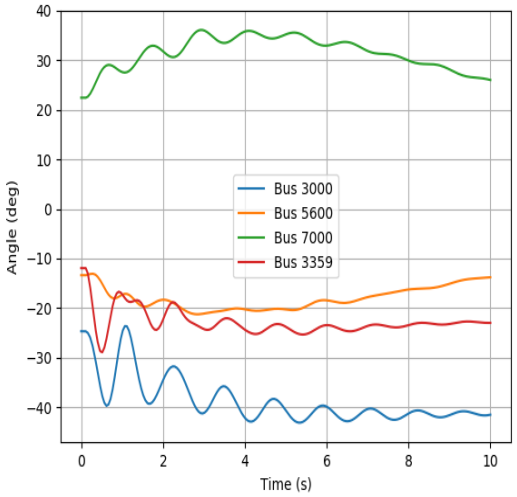

Figure 9.6: Generator angles, $\phi = 2.0$, with UVLS

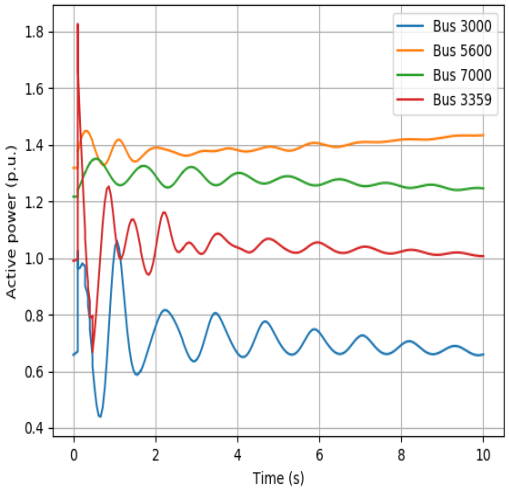

Figure 9.7: Generator active powers, $\phi = 2.0$, with UVLS

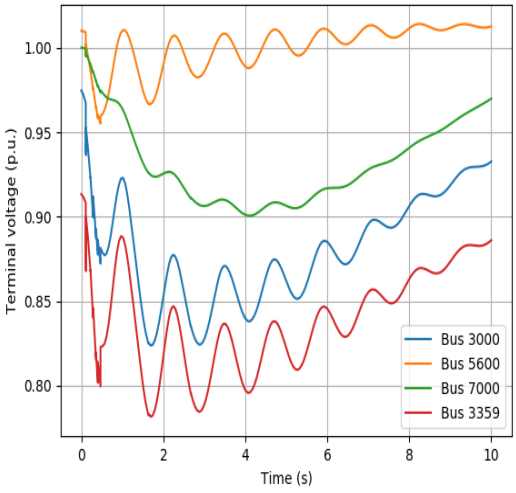

Figure 9.8: Generator terminal voltages, $\phi = 2.0$, with UVLS

9.2 Outages of Vyborg Link and EstLink

In this section, there is a simultaneous outage of Vyborg Link and EstLink which prior to outages are all importing power at HVDC link maximum transmission capacity. The inertia of the system is approximately 200 GWs and the generators' total frequency bias for the Nordic power system (excluding DSR) is 5150 MW/Hz. The simultaneous outage of Vyborg Link and EstLink leads to an outage of 2420 MW if the outage size is not scaled.

9.2.1 Outages without corrective actions

Simultaneous outages of Vyborg and EstLink lead to rapid[2] oscillations at around 0.8 Hz with low damping. These oscillations are shown in plots of generator frequencies and angles in figs. 9.9 and 9.10 respectively. Low voltages in southern Sweden is also observed. The rapid oscillations seem to be fading after approximately one minute. Zoomed in plots of generator electric power output and terminal voltages are shown in figs. 9.11 and 9.12 respectively, from which it is visible that the oscillations are at approximately 0.8 Hz. The generators in Finland are swinging approximately 180 degrees phase-shifted relative to many of the other generators in the system, as is visible from for example generator 5600 (West Norway) and generator 7000 (Finland) swinging in fig. 9.11. The oscillations with low damping occurring are shown to lead to large oscillations in inter-area power flows by the branch flows in fig. 9.13. Branches 5101 Hasle to 3359 Ringhals show large oscillations in power flows between Norway and Sweden while the branches 3249 Grundfors to 7100 Ouli as well as 3115 Porjus to 7100 Oulu show large oscillations between Sweden and Finland.

If the outages are increased in size, the damping of rapid oscillations decreases as seen and an amplitude decrease is barely observable for each period in figs. 9.14 and 9.16 where $\phi = 1.30$. By then slightly increasing the outage scaling factor to $\phi = 1.31$, the system is no longer able to withstand the simultaneous outage and the response is seen in figs. 9.15 and 9.17. Again, the voltage collapses in southern Sweden and the system simulations no longer converge after around 6 seconds when the generators in southern Sweden lose synchronism with the rest of the grid as observed by generator angles in fig. 9.17. For $\phi = 1.30$, it is in fig.

[2] 0.8 Hz is fast compared to the large power system frequency excursions occurring with a time period of approximately 40 seconds or frequency of 25 mHz

9.16 observed that the angles of generators at bus 5600 and 6000 in the south and west of Norway are seemingly phase shifted approximately 180 degrees from the rest of the grid and a large angular difference occurs between these two generators versus the remainder of the system.

9.2.2 Outages with frequency-based corrective actions

Applying the corrective actions previously described being UFLS, HVDC Emergency Power and DSR, there is no visible response compared to that of cases in section 9.2.1 and the maximum outage scaling factors are identical. Plots of system response for this case are thus not shown due to the extensive similarity to what has already been shown.

9.2.3 Outages with UVLS

The results of simultaneous outages with $\phi = 1.5$ with UVLS are shown in figs. 9.18 to 9.21. It is seen that the damping is significantly improved for the Nordic system and that the system is able to cope with a much larger outage than without UVLS, as the voltage-based load shedding hinders the voltage in Sweden from falling too low immediately after the simultaneous outages. Higher voltages allow better power transfer capabilities and possibly also power system stabilizers to perform their intended function as different regions of the grid are able to stay synchronized due to increased power transfer.

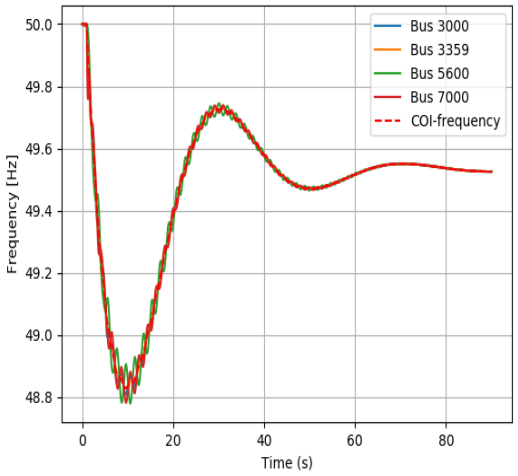

Figure 9.9: Generator frequencies, $\phi = 1.0$

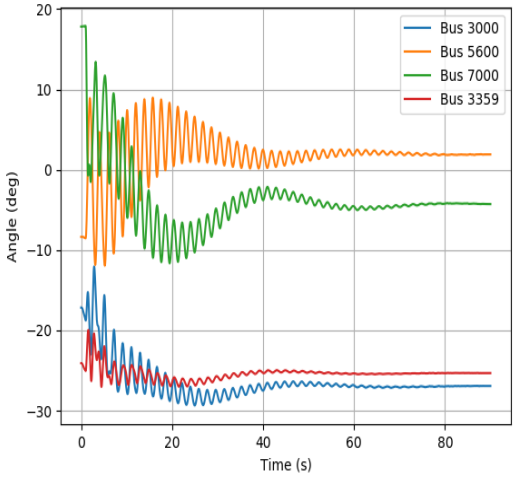

Figure 9.10: Generator angles, $\phi = 1.0$

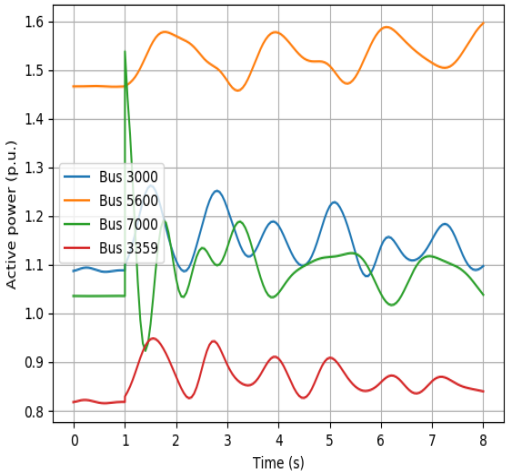

Figure 9.11: Generators electric power output, $\phi = 1.0$

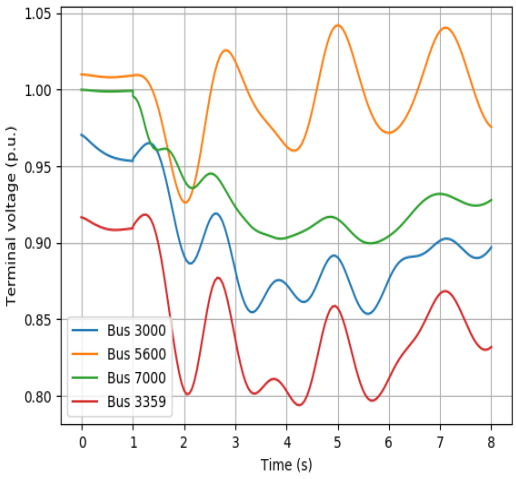

Figure 9.12: Terminal voltages, $\phi = 1.0$

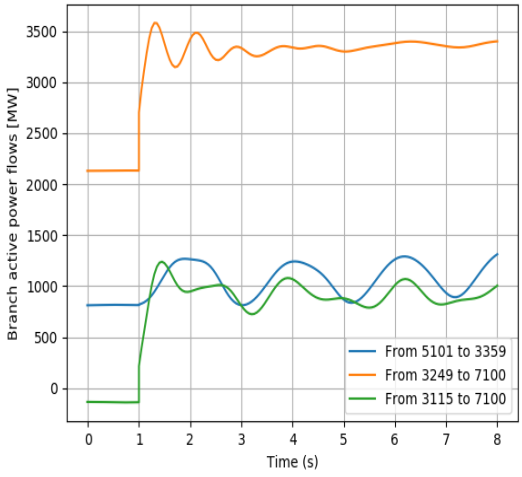

Figure 9.13: Branch flows, $\phi = 1.0$

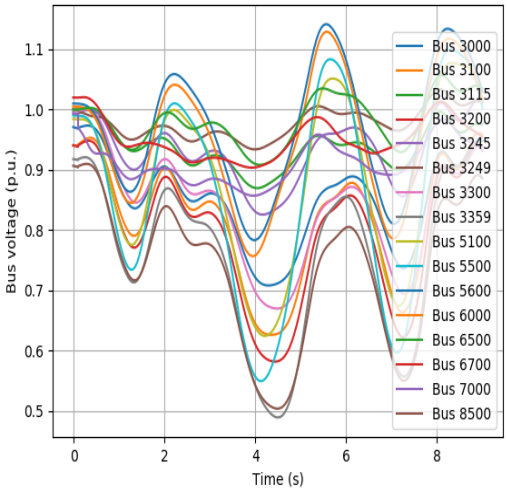

Figure 9.14: Bus voltages, $\phi = 1.30$

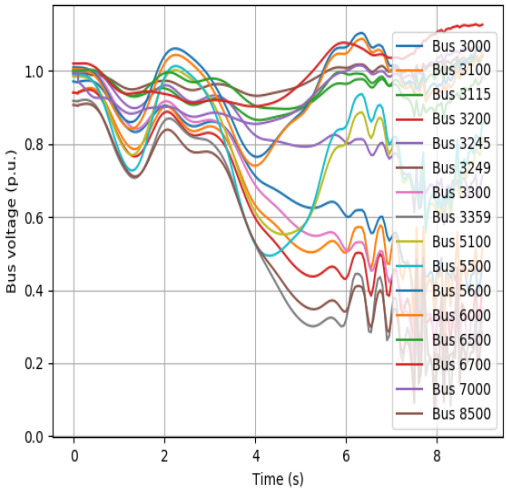

Figure 9.15: Bus voltages, $\phi = 1.31$

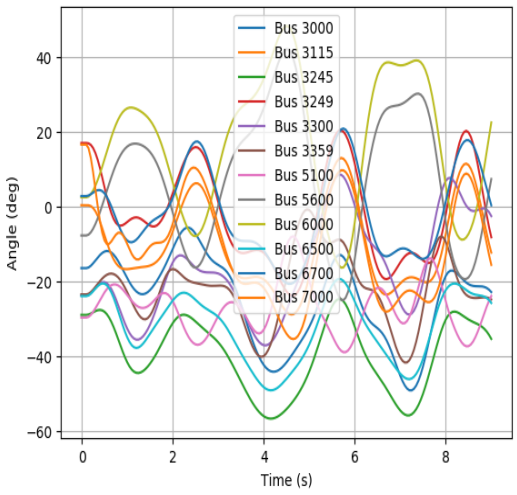

Figure 9.16: Generator angles, $\phi = 1.30$

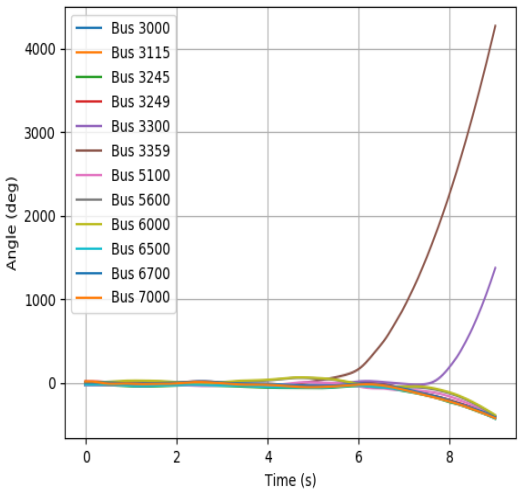

Figure 9.17: Generator angles, $\phi = 1.31$

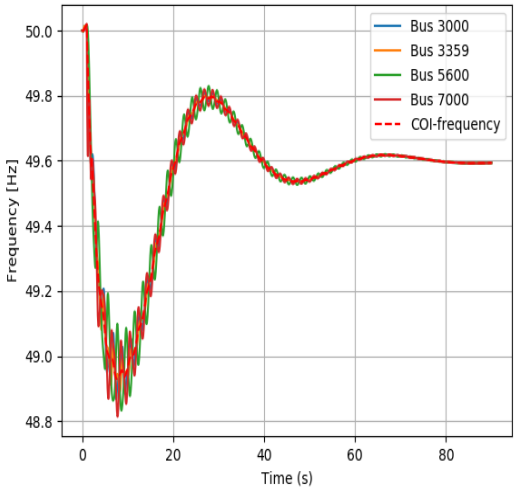

Figure 9.18: Generator frequencies, ϕ = 1.50, with UVLS

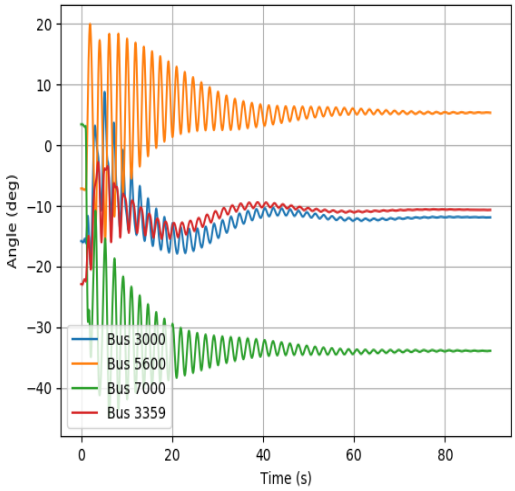

Figure 9.19: Generator angles, $\phi = 1.50$, with UVLS

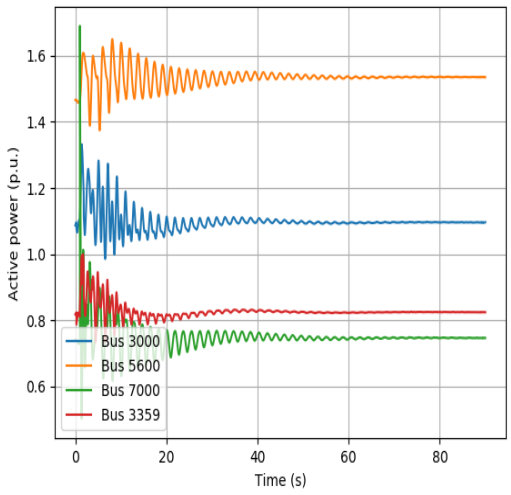

Figure 9.20: Generator active powers, ϕ = 1.50, with UVLS

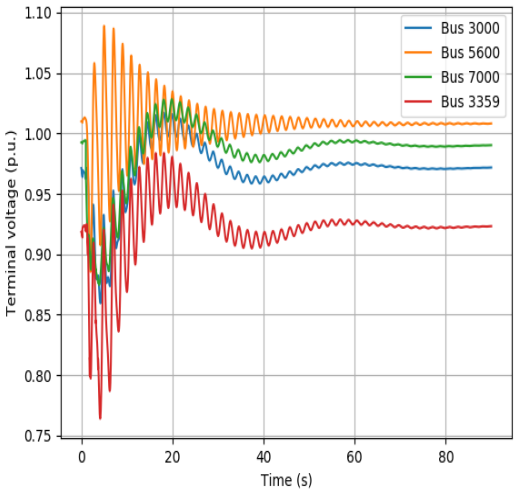

Figure 9.21: Generator terminal voltages, $\phi = 1.50$, with UVLS

9.3 Outages of NordLink and North Sea Link

In this section, there is a simultaneous outage of NordLink and North Sea Link which prior to outages are all importing power at HVDC link maximum transmission capacity. The inertia of the system is approximately 240 GWs and the generators' total frequency bias for the Nordic power system (excluding DSR) is 8400 MW/Hz. The simultaneous outage of NordLink and North Sea Link leads to an outage of 2800 MW if the outage size is not scaled.

9.3.1 Outages without corrective actions

The simultaneous outages of North Sea Link and NordLink without corrective actions have been shown the case in section 7.1, but for slightly higher inertia. The system response plots are not included for this case due to extensive similarities with the aforementioned case, with some numerical differences in terms of frequency nadir due to lower inertia of this case.

Applying the outage scaling factors $\phi = 1.15$ and $\phi = 1.16$ to see how the system responds when it does not collapse and how it responds when it collapses, we get system response as in figs. 9.22 to 9.25. For $\phi = 1.15$ the voltage at bus 3100 reaches the extremely low value of approximately 0.5 p.u. before it recovers, while other buses in Sweden such as bus 3000 and 3020 reach the voltage nadir of approximately 0.73 p.u. As was seen in the case with outages in Finland in section 9.2, the angles of Norwegian and Finnish generators seem to be swinging approximately 180 degrees phase shifted relative to one another; in fig. 9.24, we see that Finland and the north of Sweden swing approximately 180 degrees phase-shifted relative to the rest of the power system. The angular difference is also large, and the system thus seems to be on the verge of separation. For $\phi = 1.16$, when the system does collapse, the voltage at bus 3100 falls as low as 0.2 p.u. as the simulation starts to diverge, and buses such as 3000 and 3020 approach 0.45 p.u. voltage. This is shown in fig. 9.23. The low voltage levels are reached after approximately 4 seconds, which is similar to previously described cases. At this point in time, generator angles start separating. The angles separating is shown in fig. 9.25, where the large amount of monitored generator angles comes to use; we clearly see clustering of generator angles, which may be grouped by location in the Nordic power region, where the clusters represent southern Norway (the bottom cluster), southern Sweden (the

middle cluster) as well as northern Sweden and Norway with Finland (the top cluster). It is seen that after approximately 4-0 - 4.5 seconds the angular difference between the clusters starts becoming significant and that, for example, generators at bus 3359 even separate from its own cluster and loses synchronism with the grid.

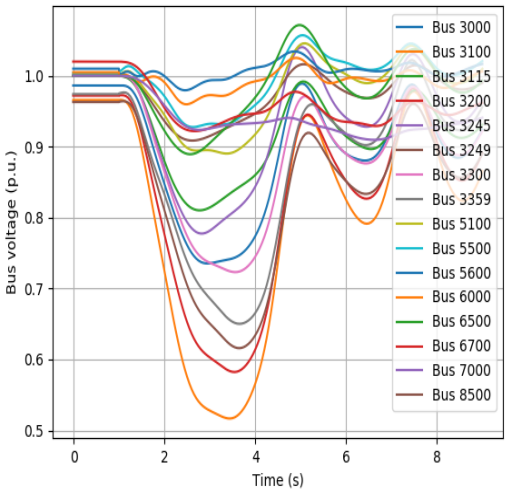

Figure 9.22: Bus voltages, $\phi = 1.15$

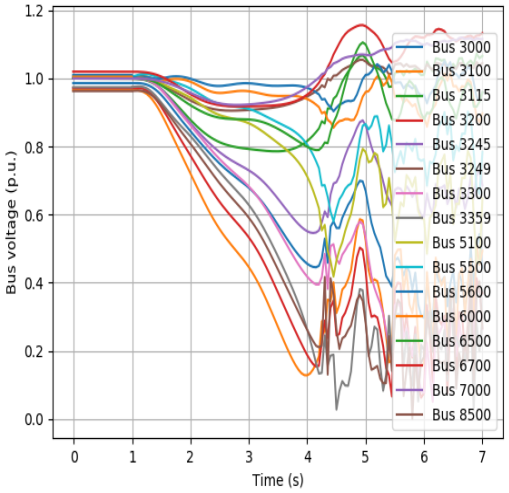

Figure 9.23: Bus voltages, $\phi = 1.16$

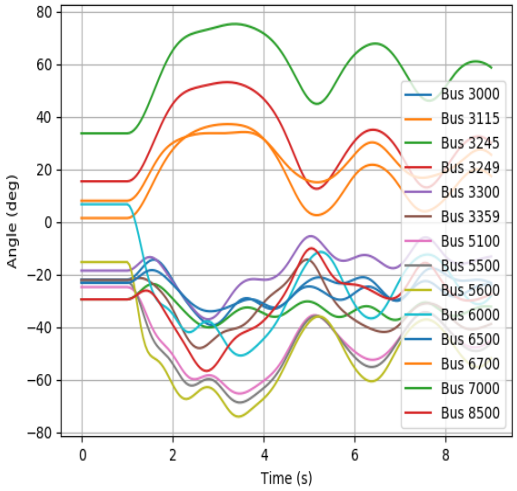

Figure 9.24: Generator angles, $\phi = 1.15$

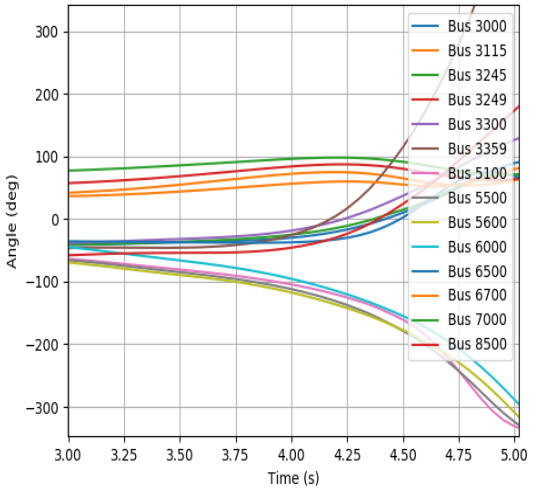

Figure 9.25: Generator angles, $\phi = 1.16$

9.3.2 Outages with frequency-based corrective actions

Using both HVDC Emergency Power, DSR and UFLS with the outage scaling factor $\phi = 1.16$ the voltage does not collapse, but it collapses at $\phi = 1.17$ instead. This is a marginal in-

crease and the system response is very similar to that of section 9.3.1 and plots are thus not shown.

9.3.3 Outages with UVLS

UVLS in Sweden greatly improves the ability of the Nordic system to cope with simultaneous outages of HVDC-links as shown in figs. 9.26 and 9.27 where the system is able to withstand an outage with scaling factor $\phi = 1.75$. For $\phi = 1.75$, the bus voltages drop very rapidly following the simultaneous outages as shown in fig. 9.26, where, as in section 9.3.1, bus 3100 reaches voltage values sub 0.5 p.u. while bus 3000 and 3020 approach 0.75 p.u., but now for a significantly higher outage size of 4900 MW at $\phi = 1.75$ versus an outage of $\phi = 1.15$ for an outage of 3220 MW. Even after voltage-based load shedding in Sweden, the behaviour is the same, the voltage starts dropping as the system approaches its limits. It may thus seem that voltage collapse in Sweden is one of the primary challenges following large outages in Norway.

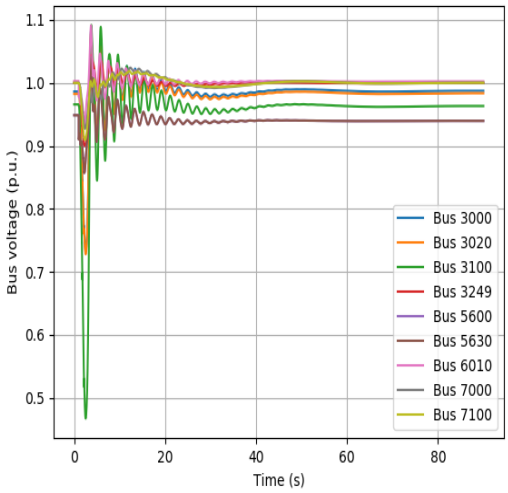

Figure 9.26: Bus voltages, with UVLS in Sweden, $\phi = 1.75$

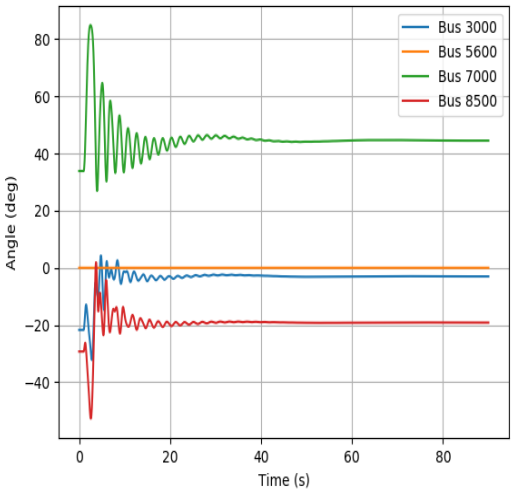

Figure 9.27: Generator angles, with UVLS in Sweden, $\phi = 1.75$

Chapter 10

Results, discussion and conclusion

10.1 Results

A summary of frequency response results from case groups 1 and 2 are shown in figs. 10.1 and 10.2 for frequency nadir and steady-state frequency results respectively. The corresponding case descriptions are shown in tab 10.1 for each of the column pairs shown. The results using DSR only show 10% DSR-enabled load.

From figs. 10.1 and 10.2 it is indicated that outages of NL and NSL will lead to severe frequency drops despite frequency-based corrective controls acting on the power system. As the inertia of the system decreases, frequency issues following such large outages are exacerbated. The system is especially vulnerable when there are no primary reserves. DSR shows strong potential to improve the frequency response, even with only 10% DSR-enabled load, but the system response is then critically dependent on the time-delay of DSR.

For case group 3, outages in the range of 2500 - 3500 MW in Norway, Sweden and Finland have all caused major voltage issues in southern Sweden leading to generators losing synchronism or separation of the grid. Frequency-based corrective did not improve the ability of the system to withstand such large outages. UVLS in Sweden was the only option attempted which improved the system response and allowed the Nordic power system to withstand even larger outages.

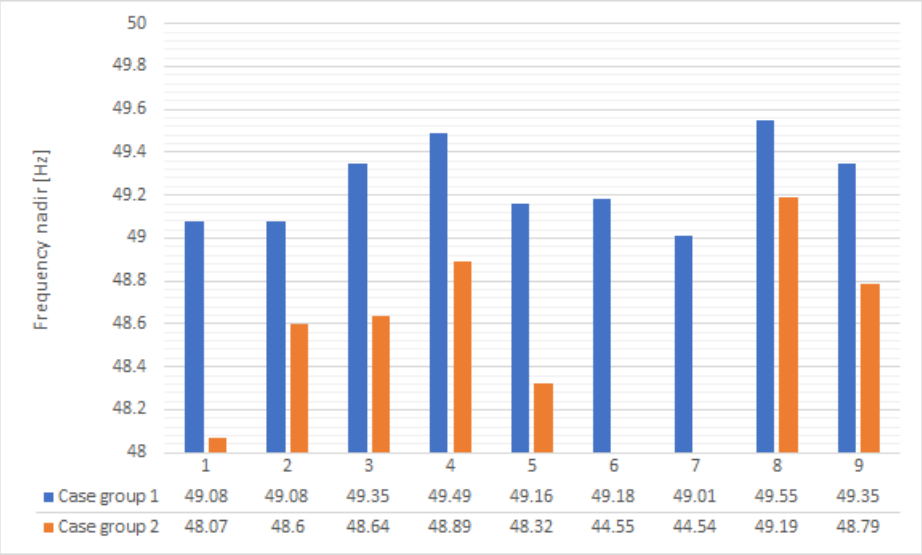

Figure 10.1: A selection of frequency nadir results from case studies

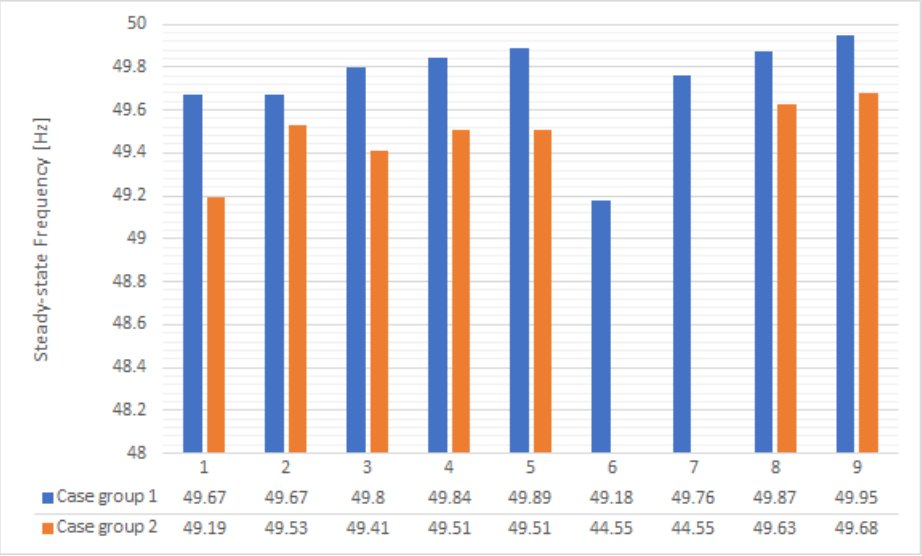

Figure 10.2: A selection of steady-state frequency results from case studies

Table 10.1: The corrective actions applied to the cases illustrated in figs. 10.1 and 10.2

Nr.	Corrective actions
1	No corrective actions
2	Only UFLS
3	Only HVDC Emergency Power
4	Only 10% DSR, 0.0 seconds delay
5	Only 10% DSR, 5.0 seconds delay
6	Only 10% DSR, 0.0 seconds delay, no primary reserves
7	Only 10% DSR, 5.0 seconds delay, no primary reserves
8	All corrective actions, 10% DSR, 0.0 seconds delay
9	All corrective actions, 10% DSR, 5.0 seconds delay

10.2 Discussion

Simulations in N44 using PSS/E and an extensive Python interface for modifying system generation and controlling system load has enabled us to study the consequences of simultaneous outages of multiple importing HVDC links for outages that far exceed the dimensioning fault of the Nordic power system. The consequences of such outages, especially for the power system with low inertia, is large frequency drops, generators losing synchronism and low voltages.

The modelling of UFLS, HVDC Emergency Power, DSR and even UVLS in some cases, allowed us to see the effect of barriers in the power system after a simultaneous HVDC contingency. While the effect of these corrective actions greatly improve the system frequency response, especially for DSR with low time-delay, an unexpected vulnerability is identified as the voltage response of the southern Swedish power grid.

10.2.1 Low voltage in southern Sweden

Large voltage dips in the Swedish power system seems to be a major issue for the simultaneous outages that have been studied. This may be behaviour caused by inaccuracy in the N44 model or it may be the actual response that would occur for such simultaneous outages in the real power grid. In [43] the voltage in Sweden has been an issue using the N44 model, but the voltage in the Swedish system has also been an issue in real-life, such as in the 2003 blackout [47]. There may thus be some semblance of truth in the results encountered and that a voltage collapse represents a critical consequence in the extraordinary event of a simultaneous outage. While aggressive UVLS may not be an option, measures to improve the voltage response for the Swedish power system may be beneficial for the system's ability to cope with large simultaneous outages in Norway, Sweden or Finland. From a Norwegian perspective, our TSO, Statnett, may then possibly reduce the consequences of simultaneous outages of HVDC links in Norway by investing in STATCOMs or similar means for voltage stability in Sweden, which is an interesting result.

10.2.2 Verification of results

The tuning of the N44 model in [43] was for an outage very different to the outages studied in this thesis. No real life data of detailed system response has been found for simultaneous outages of HVDC-links, let alone detailed responses of outages of HVDC-links at high import, and it is thus difficult, if not impossible, to properly verify that the results in this thesis are accurate. The model tuning in this thesis is largely performed by changing active powers in different regions of the grid to attempt to limit the change of power flows when import of HVDC-links is set to a high value. The load reduction and generation redistribution functions are simple and static load flow calculations prior to dynamic simulations do not always lead to well-initialized operating states for dynamic simulations as mentioned in sections 5.5.2 and 5.5.3. This may be an indication that the algorithmic approach for changing active power flows is flawed. By making further adjustments (increasing or decreasing system generation slightly) to the cases, they do, however, become well initialized. Manual tweaking of a few specific case studies may seem a more surefire method to possibly acquiring more accurate results, but such cases would still be victim of large uncertainties due to manual tuning and manual tweaking of model parameters being highly speculative when there is no real-life data to compare with the simulation results. Manual tuning would then at best be based on guesses about the state of the future power grid. Manual tuning is also time consuming and would then be unviable for the many different case studies and outage sizes considered in this thesis.

10.2.3 Use of the Nordic 44 model

Using the N44 model for contingency simulations rather than a highly detailed model may be a strength in this thesis. Apart from the obvious lighter computational burden and increased manageability of a smaller model, the cascades and sequences of events for a detailed model may have led to widely different results for which the use of event trees to unravel the alternate event sequences would be an insurmountable task. By not considering many protection mechanisms that would no doubt activate for such large contingencies, and instead focusing on aggregate responses of generators and loads, a possible voltage vulnerability of the Swedish system has been revealed, one that would possibly otherwise remain hidden if all

system protection mechanisms were armed. Thus it seems that aggregated network models may serve as an important supplement to that of detailed network models.

A weakness of using N44 is that the low accuracy for load flow calculations limits the viability of studying the effect that branch protection relays such as overcurrent protection relays may have on the dynamic response of the system following simultaneous HVDC contingencies. Inaccurate branch flows could lead to protection relays tripping arbitrary power lines, which would further alter power flows and degrade the accuracy of the simulations. For this reason, overcurrent protection relays have not been included in any case studies in this thesis. Overcurrent protection relays would likely lead to more accurate results when using a more detailed model with higher accuracy for load flow, or simply a model designed for accurate power flows. The N44 model could possibly not be tuned for branch flows as is; the Norwegian system is represented by 25 buses, Sweden by 15 buses and Finland by 4 buses. The lower detail for Sweden and especially Finland would likely be unable to represent accurate system wide power flows.

Detailed grid models could also allow for study of lower grid levels such as the subtransmission or distribution levels. The lower voltage level grids near the HVDC link outages would see large transients and possibly also encounter large issues in the seconds following the contingencies. Depending on how much the distribution grid or subtransmission grid near the HVDC converter station has been strengthened in conjunction with the construction of HVDC links, the impact of the outages may be large or small. The aggregated nature of the N44 model is unable to capture the effects of the outages on the detailed grid, and, for example, cascading outages in the distribution grid may lead to more severe consequences than what is observed in N44. In N44, it is assumed that the subtransmission and distribution levels in the distribution grid are able to withstand the outages and that no criticalities in the form of further cascading outages or large disturbances occur.

10.2.4 System frequency response

All case studies have had an initial frequency of 50.0 Hz prior to outages. In a real system, the frequency might be higher or lower than 50 Hz when the outages occur. For frequencies starting at lower than 50 Hz, the consequences may then become more critical than the case studies in this thesis suggest. Further, synthetic inertia for converter interfaces or frequency

dependency of loads are among many elements that may improve the system frequency response but have not been included in the case studies in this thesis. The generators' primary response in the N44 system may also be too large in some case studies; while each generator in N44 may only supply power up to the maximum mechanical turbine input in the model, every generator that has some governor droop setting participates in the primary response response of generators in N44 model, and the 600 MW and 1200 MW requirements[23] for FCR-N and FCR-D respectively are not taken into account. A frequency deviation of 0.5 Hz with 8400 MW/Hz frequency bias may then cause a primary response that far exceeds the reserves that would be available in a given operating state in the real Nordic power system. Some of the results presented in this thesis may then be seen as optimistic with regards to primary response and reserves.

HVDC Emergency Power is modelled as an instantaneous load step occurring 0.5 seconds after the set frequency threshold is reached. The 0.5 seconds delay may be lower than the response time in a real life system, and without ramping it may seem unrealistic. Ramping is hard to model without sufficient data. As detailed responses of HVDC Emergency Power is not of interest, but rather the active power balance of the system, this is deemed an acceptable model for the purposes in this thesis. Longer time-delay or ramping would worsen the system frequency response for cases with HVDC Emergency Power. PGUs were implemented with the ability to set a maximum time available for HVDC Emergency Power, as increased power output of HVDC links might only be temporarily available due to thermal or other considerations. As no data was found on time-limits for HVDC Emergency Power, the response was set to remain active indefinitely (up to a maximum of 90 seconds, as that was the longest simulation time).

The possibly most interesting aspect of the system frequency response is the future potential for use of DSR against simultaneous HVDC contingencies. Some assumptions that have been made are that the % of DSR-enabled load and time-delay is assumed to be the same at each load in N44 for each case study. In real life, geographical and political differences may lead to individual countries and regions having different amounts of DSR-enabled load as well as time-delay. Predictions on how DSR may become more common in different regions in the next decades is out of scope for this thesis as we only seek to illuminate the potential of DSR for the Nordic system. A possibly larger weakness of the DSR modelled in this thesis is that the activation time-delay is given a single value for all loads. The lumped load

characteristic of N44 that each load bus represents large regions or entire distribution grids hides the underlying details in which different loads may have the same frequency activation threshold but different time-delays. Some loads in the system may be faster to shed, while others take longer, either due to different communication delay, measurement delay or response time of electronic equipment. This means that, at each load bus, some loads will respond very rapidly, while others may respond more slowly. The DSR activation time for longer time-delays are then perhaps overly pessimistic, as many loads will have had time to reduce power consumption before the 5.0 seconds have passed (but not all), while shortest time-delays may be overly optimistic as some individual loads in the lumped load will require more time to reduce power consumption. More detailed models for DSR should then perhaps be used. Nevertheless, the impact of increasing amounts of DSR and time-delay is illustrated.

A final point of concern for DSR; recall that DSR was in section 5.4.3.1 mentioned to be excluded at bus 3000 as DSR at bus 3000 caused the system to not converge due to improper behaviour. This leads to less DSR in Sweden where the system has been shown to be especially vulnerable. The exclusion of bus 3000 for DSR may thus seem unfortunate and likely impacts the effectiveness of DSR beyond what the impact of the load reduction has on frequency; the most critical location does not have load reduction by DSR. However, the voltage issues as illustrated by UVLS response improvement versus that of frequency-based corrective actions gives reason to believe that the effect of inclusion of DSR at bus 3000 would be small compared to voltage-based corrective actions.

10.3 Conclusion

The simultaneous outages of multiple HVDC links importing power in the Nordic power system leads to large frequency drops. The power system becomes especially vulnerable as the inertia of the power system decreases and when there are little or no primary reserves available. The addition of frequency response to Demand-Side Response shows great promise to hinder large frequency drops, but the time-delay for activation must be low to be able to hinder large frequency transients. A vulnerability of the Nordic power system is revealed in the form of voltage instability in southern Sweden following the studied contingencies; voltage

collapse leads to generators losing synchronism and separation of the grid. Construction of HVDC link such as NordLink and North Sea Link may thus increase the risk of blackouts in Sweden. From the results and discussion follows two recommendations for the Nordic TSOs:

- Emphasize achieving low time-delay for DSR activation in response to frequency decline in future projects on development and implementation of DSR in the Nordic system. DSR must be regarded as a tool in dynamic as well static analyses.
- Investments in voltage stabilizing equipment such as STATCOMs in southern Sweden to improve the ability of the Nordic system to withstand very large outages. Investments in voltage stabilizing measures should accompany investments in increased HVDC link capacity and interconnection with other synchronous systems.

The aggregated network model N44 has proven useful for the considerations in this thesis by possibly revealing a vulnerability in the Nordic system that, using more detailed models, might have been hidden by a variety of sequences of events.

Chapter 11

Further work

Demand-Side Response and HVDC Emergency Power should be modelled using PSS/E dynamic models instead of being reliant on the Python-framework written by the author for using Psspy for interfacing with PSS/E. This would allow for running case studies with DSR and HVDC Emergency Power in PSS/E directly. Both corrective schemes may possibly be implemented by adaptation of existing models or by writing Fortran models from scratch. The latter option was considered for this thesis but was discarded due to the safer and possibly less time-consuming option of using well-known and easily understandable Python code. Addition of such models in PSS/E dynamic models instead of using the Python framework could be a valuable addition to the N44 model.

Simultaneous HVDC outages should be studied using a highly detailed grid model. As mentioned in the discussion, the change of load flows following the studied outages were not considered as N44 was not built for such studies nor tuned for them. Overcurrent relays in a more detailed model could show the sequence of events for cascading outages in the sub-transmission grid or distribution grid and thus be able to show the impact that these parts of the grid may have on the total system response. Other dynamic of quasi-static events may then also be included. Event trees should then be used to be able to consider which cascades did not occur, as the consequences of what could have happened are easily concealed by the deterministic nature of PSS/E simulations. Alternatively, probabilistic simulations of cascading outages may be used.

The voltage issues of Southern Sweden in the simulations that have been performed may be

a weakness of the model. In order to figure out if the behaviour of the N44 model voltage response is realistic, historical data on Nordic system voltage response should be used to tune the N44 model towards the voltage response. As the model used in this thesis is tuned towards frequency response, the behaviour may be very different. If Swedish voltage issues still apply after tuning of voltage response, the plausibility of the results presented in this thesis will have been improved.

Incorporating modal analysis to study how the given contingencies affect the small-signal stability of the system may serve as a compliment to the large-signal stability in this thesis, as decreased damping was evident for HVDC contingencies occurring in Finland. Modal analysis may then be an aid to see the precise changes in stability and damping of the system. A prerequisite may then be that models of DSR and HVDC Emergency Power are implemented using transfer functions and block diagrams so that their effect on the power system stability may be observed. However, the results are likely to be meaningful even without the two aforementioned corrective actions, as decreased damping was visible even without corrective actions. Modal analysis may also be beneficial in observing the system voltage response.

Bibliography

[1] SINTEF. (Aug. 18, 2016). HILP - analysis of extraordinary events in power systems, SINTEF, [Online]. Available: https://www.sintef.no/en/projects/hilp/ (visited on 11/19/2017).

[2] E. H. Solvang, "Impact of simultaneous outages of HVDC-links on the nordic power system," NTNU, Trondheim, not available online, Dec. 21, 2017. (visited on 12/21/2017).

[3] Statnett, Fingrid, Svenska Kraftnät, and Energinet.dk. (2016). Challenges and opportunities for the nordic power system, Report Challenges and Opportunities for the Nordic Power System, [Online]. Available: http://www.fingrid.fi/fi/ajankohtaista/Ajankohtaista%20liitteet/Ajankohtaisten%20liitteet/2016/Report%20Challenges%20and%20Opportunities%20for%20the%20Nordic%20Power%20System.pdf.

[4] Statnett, Fingrid, Energinet.dk, and S. kraftnät. (2017). Nordic grid development plan 2017, [Online]. Available: http://www.svk.se/siteassets/om-oss/rapporter/2017/nordic-grid-development-plan-2017-eng.pdf.

[5] M. Callavik, P. Lundberg, and O. Hansson, *NORDLINK pioneering VSC-HVDC interconnector between norway and germany*, Mar. 2015. [Online]. Available: https://library.e.abb.com/public/aaa99cf7067cd258c1257e0d002c9a7b/Nordlink%20White%20Paper%20from%20ABB.pdf (visited on 11/16/2017).

[6] P. Technology. (). North sea link (NSL), Power Technology, [Online]. Available: http://www.power-technology.com/projects/north-sea-link-nsl/ (visited on 11/16/2017).

[7] Y. Li, X. Xu, S. Chen, and Z. Yan, "Determine the reliable generating capacity of power systems with high HVDC penetration considering both stability and ancillary service

requirements," *Transmission Distribution IET Generation*, vol. 12, no. 3, pp. 540–547, 2018, ISSN: 1751-8687. DOI: 10.1049/iet-gtd.2017.0425.

[8] I. B. Sperstad, G. Kjølle, S. H. Jakobsen, O. Gjerde, T. K. Vrana, L. Haarla, and J. Turunen, "Vulnerability analysis of HVDC contingencies in the nordic power system," presented at the CIGRE, Unpublished, Paris: SINTEF Energy Research, Unpublished, Aug. 2018.

[9] O. Gjerde, G. H. Kjølle, N. K. Detlefsen, and G. Brønmo, "Risk and vulnerability analysis of power systems including extraordinary events," in *2011 IEEE Trondheim PowerTech*, Jun. 2011, pp. 1–5. DOI: 10.1109/PTC.2011.6019251.

[10] S. H. Jakobsen and L. Kalemba, "The nordic44 test network," NTNU, Trondheim, Internal document (not available online), Sep. 28, 2017.

[11] Siemens. (). PSS®e - power transmission system planning software - digital grid - siemens, [Online]. Available: http://w3.siemens.com/smartgrid/global/en/products-systems-solutions/software-solutions/planning-data-management-software/planning-simulation/pages/pss-e.aspx (visited on 11/20/2017).

[12] N. N. Taleb, *The Black Swan - The Impact of the Highly Improbable*. Penguin Books, 2007, 444 pp., ISBN: 978-0-14-103459-1. (visited on 04/15/2018).

[13] D. Kahneman, *Thinking, Fast and Slow*, 1st ed. Farrar, Straus and Giroux, Apr. 2, 2013, 499 pp., ISBN: 978-0-374-53355-7.

[14] I. Dobson, B. A. Carreras, V. E. Lynch, and D. E. Newman, "Complex systems analysis of series of blackouts: Cascading failure, critical points, and self-organization," *Chaos: An Interdisciplinary Journal of Nonlinear Science*, vol. 17, no. 2, p. 026 103, Jun. 1, 2007, ISSN: 1054-1500. DOI: 10.1063/1.2737822. [Online]. Available: http://aip.scitation.org/doi/full/10.1063/1.2737822 (visited on 11/09/2017).

[15] Vaiman, Bell, Chen, Chowdhury, Dobson, Hines, Papic, Miller, and Zhang, "Risk assessment of cascading outages: Methodologies and challenges," *IEEE Transactions on Power Systems*, vol. 27, no. 2, pp. 631–641, May 2012, ISSN: 0885-8950. DOI: 10.1109/TPWRS.2011.2177868.

[16] G. H. Kjølle and O. Gjerde, "Vulnerability analysis related to extraordinary events in power systems," in *2015 IEEE Eindhoven PowerTech*, Jun. 2015, pp. 1–6. DOI: 10.1109/PTC.2015.7232388.

[17] J. Bialek, E. Ciapessoni, D. Cirio, E. Cotilla-Sanchez, C. Dent, I. Dobson, P. Henneaux, P. Hines, J. Jardim, S. Miller, M. Panteli, M. Papic, A. Pitto, J. Quiros-Tortos, and D. Wu, "Benchmarking and validation of cascading failure analysis tools," *IEEE Transactions on Power Systems*, vol. 31, no. 6, pp. 4887–4900, Nov. 2016, ISSN: 0885-8950. DOI: 10.1109/TPWRS.2016.2518660.

[18] V. V. Vadlamudi, C. Hamon, O. Gjerde, G. Kjølle, and S. Perkin, "On improving data and models on corrective control failures for use in probabilistic reliability management," in *2016 International Conference on Probabilistic Methods Applied to Power Systems (PMAPS)*, Oct. 2016, pp. 1–6. DOI: 10.1109/PMAPS.2016.7764089.

[19] G. Hug and A. Ulbig, *Power System Dynamics, Control and Operation*. Zürich: ETH Zürich, Feb. 2017, Course material not available online.

[20] J. Machowski, J. Bialek, and J. Bumby, *Power System Dynamics Stability and Control*, 2nd ed. Wiley, 2008, ISBN: 978-0-470-72558-0.

[21] ENTSO-E. (2017). EUR-lex - 32017r1485 - EN - EUR-lex, [Online]. Available: http://eur-lex.europa.eu/legal-content/EN/TXT/?toc=OJ%3AL%3A2017%3A220%3ATOC&uri=uriserv%3AOJ.L_.2017.220.01.0001.01.ENG (visited on 12/13/2017).

[22] E. Ørum, M. Kuivaniemi, M. Laasonen, A. I. Bruseth, E. A. Jansson, A. Danell, K. Elkington, and N. Modig, "Future system inertia," ENTSO-E. [Online]. Available: https://www.entsoe.eu/Documents/Publications/SOC/Nordic/Nordic_report_Future_System_Inertia.pdf (visited on 02/14/2018).

[23] Statnett. (2016). Dagens løsninger i systemdriften.pdf, [Online]. Available: http://www.statnett.no/Global/Drift%20og%20Marked/Systemansvaret/Dagens%20l%C3%B8sninger%20i%20systemdriften.pdf.

[24] ——, (Jan. 2012). Technical product specification for delivery of frequency restoration reserves to statnett, LFC Technical Product Specification, [Online]. Available: http://www.statnett.no/PageFiles/2581/LFC%20Technical%20Product%20Specification.pdf (visited on 02/15/2018).

[25] V. V. Vadlamudi, *ELK-16: Advanced Power System Analysis*. Trondheim: NTNU, Faculty of Information Technology and Electrical Engineering, Department of Electric Power Engineering, Power Systems Group, Aug. 29, 2017, Course material not available online. (visited on 12/12/2017).

[26] K. Hatipoglu, I. Fidan, and G. Radman, "Investigating effect of voltage changes on static ZIP load model in a microgrid environment," in *2012 North American Power Symposium (NAPS)*, Sep. 2012, pp. 1–5. DOI: 10.1109/NAPS.2012.6336407.

[27] M. A. Elizondo, Y. Chen, and Z. Huang, "Reliability value of fast state estimation on power systems," in *PES T D 2012*, May 2012, pp. 1–6. DOI: 10.1109/TDC.2012.6281657.

[28] E. Hillberg, F. Trengereid, Ø. Breidablik, K. Uhlen, G. Kjølle, S. Løvlund, and J. O. Gjerde, "System integrity protection schemes – increasing operational security and system capacity," presented at the CIGRE 2012, NTNU, 2012. [Online]. Available: https://www.sintef.no/globalassets/project/vulnerability-and-security/publications/papers/cigre-2012_sips-for-security-and-capacity---paper_revresubmitted.pdf (visited on 04/24/2018).

[29] E. Styvaktakis, "Current practices in europe on emergency and restoration," Brussels: ENTSO-E, May 27, 2014, p. 22.

[30] UCTE. (Jan. 30, 2007). Final report - system disturbance on 4 november 2006, [Online]. Available: https://www.entsoe.eu/fileadmin/user_upload/_library/publications/ce/otherreports/Final-Report-20070130.pdf (visited on 03/08/2018).

[31] Y. Liu, S. Yang, S. Zhang, and F. Z. Peng, "Comparison of synchronous condenser and STATCOM for inertial response support," in *2014 IEEE Energy Conversion Congress and Exposition (ECCE)*, Sep. 2014, pp. 2684–2690. DOI: 10.1109/ECCE.2014.6953761.

[32] NVE. (Oct. 2007). Endringer i forskrift om systemansvar i kraftsystemet, Leveringskvalitet i kraftsystemet, [Online]. Available: http://publikasjoner.nve.no/dokument/2007/dokument2007_10.pdf (visited on 01/16/2018).

[33] S. B. Skaatan and Statnett, *SV: Prosedyre for belastningsfrakobling (BFK) til bruk i masteroppgave NTNU*, E-mail, Jan. 29, 2018. (visited on 01/29/2018).

[34] K. S. Hornnes and Statnett, "Storskala laststyring," CenSES energi og klimakonferanse, 2015, [Online]. Available: https://www.ntnu.no/documents/7414984/1266492912/Presentasjon-+Knut+Styve+Hornnes.pdf/16886fb5-ab25-4a3e-a5eb-ca3975ed444e (visited on 03/15/2018).

[35] *Commission regulation (EU) 2016/1388 of 17 august 2016 establishing a network code on demand connection (text with EEA relevance)*, Aug. 18, 2016. [Online]. Available: http://data.europa.eu/eli/reg/2016/1388/oj/eng (visited on 05/23/2018).

[36] Energy Market Authority. (Sep. 3, 2018). Demand side management, [Online]. Available: https://www.ema.gov.sg/Demand_Side_Management.aspx (visited on 06/03/2018).

[37] A. Kringstad, V. Holmefjord, and J. Aarstad, "Fleksibilitet i det nordiske kraftmarkedet," Statnett, Oslo, Analysis, Nov. 1, 2018, p. 56.

[38] M. Koller, T. Borsche, A. Ulbig, and G. Andersson, "Review of grid applications with the zurich 1mw battery energy storage system," *Electric Power Systems Research*, vol. 120, pp. 128–135, Mar. 2015, ISSN: 03787796. DOI: 10.1016/j.epsr.2014.06.023. [Online]. Available: http://linkinghub.elsevier.com/retrieve/pii/S0378779614002326 (visited on 03/28/2018).

[39] F. Lambert. (Jan. 23, 2018). Tesla's giant battery in australia made around $1 million in just a few days, Electrek, [Online]. Available: https://electrek.co/2018/01/23/tesla-giant-battery-australia-1-million/ (visited on 03/28/2018).

[40] R. Ramsdal. (May 14, 2018). Teslas gigabatteri har kuttet 90 prosent av strømbrudd-kostnadene, Tu.no, [Online]. Available: https://www.tu.no/artikler/teslas-gigabatteri-har-kuttet-90-prosent-av-strombrudd-kostnadene/437408 (visited on 05/20/2018).

[41] F. Teng, M. Aunedi, D. Pudjianto, and G. Strbac, "Benefits of demand-side response in providing frequency response service in the future GB power system," *Frontiers in Energy Research*, vol. 3, 2015, ISSN: 2296-598X. DOI: 10.3389/fenrg.2015.00036. [Online]. Available: https://www.frontiersin.org/articles/10.3389/fenrg.2015.00036/full (visited on 03/28/2018).

[42] Siemens, *PSS e 33.5 application program interface*, 2015.

[43] S. M. Hamre, "Inertia and FCR in the present and future nordic power system - inertia compensation," Master thesis, NTNU, Trondheim, 2015. [Online]. Available: https://brage.bibsys.no/xmlui/handle/11250/2368231 (visited on 09/27/2017).

[44] Nordpool. (). Historical market data, [Online]. Available: http://www.nordpoolspot.com/historical-market-data/ (visited on 09/18/2017).

[45] F. Gonzalez-Longatt, E. Chikuni, and E. Rashayi, "Effects of the synthetic inertia from wind power on the total system inertia after a frequency disturbance," in *2013 IEEE International Conference on Industrial Technology (ICIT)*, Feb. 2013, pp. 826–832. DOI: 10.1109/ICIT.2013.6505779.

[46] ENTSO-E, "Rate of change of frequency (ROCOF) withstand capability," ENTSO-E, Brussels, Mar. 29, 2017. [Online]. Available: https://www.entsoe.eu/Documents/Network%20codes%20documents/Implementation/CNC/IGD-RoCoF_withstand_capability.pdf (visited on 11/23/2017).

[47] S. Larsson and E. Ek, "The black-out in southern sweden and eastern denmark, september 23, 2003," in *IEEE Power Engineering Society General Meeting, 2004.*, Jun. 2004, 1668–1672 Vol.2. DOI: 10.1109/PES.2004.1373158.

[48] L. Vanfretti, S. H. Olsen, V. S. N. Arava, G. Laera, A. Bidadfar, T. Rabuzin, S. H. Jakobsen, J. Lavenius, M. Baudette, and F. J. Gómez-López, "An open data repository and a data processing software toolset of an equivalent nordic grid model matched to historical electricity market data," *Data in Brief*, vol. 11, pp. 349–357, Supplement C Apr. 1, 2017, ISSN: 2352-3409. DOI: 10.1016/j.dib.2017.02.021. [Online]. Available: http://www.sciencedirect.com/science/article/pii/S2352340917300409 (visited on 10/03/2017).

[49] S. W. Nordhagen, "Reliability analysis of the nordic44 model and modelling of corrective actions in OPAL," Master thesis, NTNU, Trondheim, 2017. [Online]. Available: https://brage.bibsys.no/xmlui/handle/11250/2440582 (visited on 09/27/2017).

[50] K. Bjørsvik, "A scheme for creating an small-signal on-line dynamic security assessment tool - using PSS/e and PacDyn," Master thesis, NTNU, Trondheim, 2016. [Online]. Available: https://brage.bibsys.no/xmlui/handle/11250/2400486 (visited on 09/27/2017).

Appendix A

PSSE models

In the PSS®E documentation there is large amounts of documentation on the varied functionality and models included in the program. An extract of dynamic models' tables for load protection relays DLSHBL and LVSHBL are given in this appendix, where the models are used for UFLS and UVLS respectively. The parameters of the models are set to the values given in tabs. A.1 and A.2. Parameters set to 0.0 are not active.

A.1 DLSHBL

Rate of Frequency Load Shedding Model

Table A.1: DLSHBL CONs

CONs	Value	Description
J	48.6	f_1, first load shedding point (Hz)
J+1	0.0	t_1, first point pickup time (sec)
J+2	0.062	$frac_1$, first fraction of load to be shed
J+3	48.2	f_2, second load shedding point (Hz)
J+4	0.0	t_2, second point pickup time (sec)
J+5	0.156	$frac_2$, second fraction of load to be shed
J+6	47.9	f_3, third load shedding point (Hz)
J+7	0.0	t_3, third point pickup time (sec)
J+8	0.093	$frac_3$, third fraction of load to be shed
J+9	0.0	t_1, first point pickup time (sec)
J+10	0.0	df_1, first rate of frequency shedding point (Hz/sec)
J+11	0.0	df_2, second rate of frequency shedding point (Hz/sec)
J+12	0.0	df_3, third rate of frequency shedding point (Hz/sec)

A.2 LVSHBL

Undervoltage Load Shedding Model

Table A.2: LVSHBL CONs

CONs	Value	Description
J	0.9	V1, first load shedding point (pu)
J+1	0.0	T1, first point pickup time (sec)
J+2	0.1	F1, first fraction of load to be shed
J+3	0.8	V2, second load shedding point (pu)
J+4	0.0	T2, second point pickup time (sec)
J+5	0.1	F2, second fraction of load to be shed
J+6	0.7	V3, third load shedding point (pu)
J+7	0.0	T3, third point pickup time (sec)
J+8	0.1	F3, third fraction of load to be shed
J+9	0.0	TB, breaker time (sec)

Appendix B

Nordic 44

This appendix is based on a similar appendix in [2].

The Nordic44 (N44) model is an aggregated network model of the Nordic power system which was first presented in [48]. The model consists of 44 buses (thereby the name Nordic44), 79 branches, 80 generators and 28 loads. The model aims to achieve sufficiently accurate simulation results with lower computational time and costs than more detailed network models. A graphical illustration of the model is shown in fig. B.1. The buses are placed in equivalent market areas as in Nord Pool, giving 5 areas for Norway, 4 areas for Sweden and 1 area for Finland.

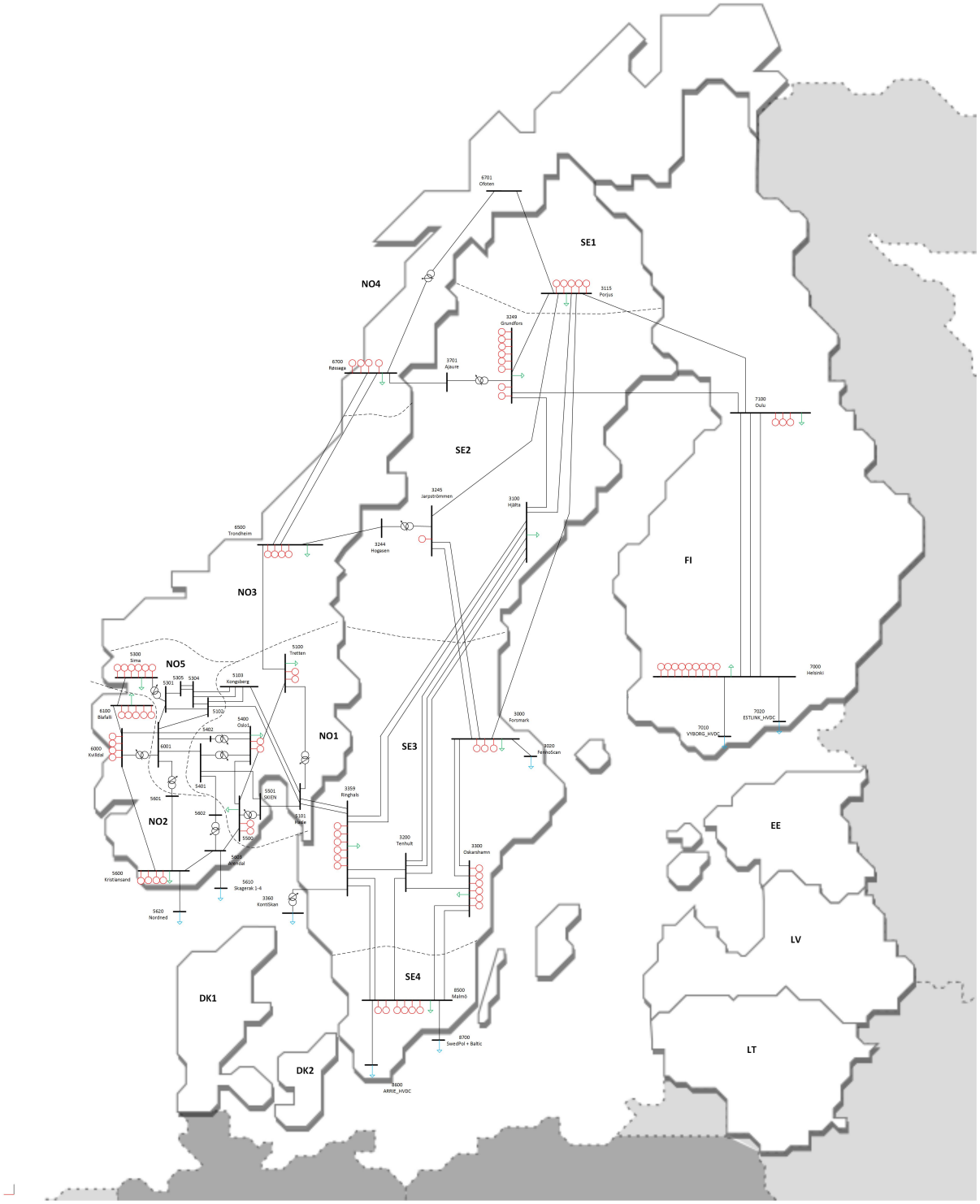

Figure B.1: The Nordic 44 aggregated network model from [49] with small modifications

Bus Number	Bus Name	Base kV	Area
3000	FORSMARK	420	SE3
3020	DANNEBO_HVDC	420	SE3
3100	HJALTA	420	SE2
3115	PORJUS	420	SE1
3200	TENHULT	420	SE3
3244	HOGASEN	300	SE2
3245	JARPSTROMMEN	420	SE2
3249	GRUNDFORS	420	SE2
3300	OSKARSHAMN	420	SE3
3359	RINGHALS	420	SE3
3360	STENKU_HVDC	135	SE3
3701	AJAURE	300	SE2
5100	TRETTEN	300	NO1
5101	HASLE	420	NO1
5102	DAGALI	420	NO5
5103	KONGSBERG	420	NO1
5300	SIMA	300	NO5
5301	AURLAND	420	NO5
5304	GEILO	420	NO5
5305	EIDFJORD	420	NO5
5400	OSLO1	300	NO1
5401	SYLLING	420	NO1
5402	KAGGEFOSS	420	NO1
5500	OSLO2	300	NO1
5501	SKIEN	420	NO1
5600	KRISTIANSAND	300	NO2
5601	STAVANGER	300	NO2
5602	SANDEFJORD	420	NO2
5603	ARENDAL	300	NO2
5610	KRISTIA_HVDC	300	NO2
5620	FEDA_HVDC	300	NO2
6000	KVILLDAL	300	NO2
6001	HAGAFOSS	420	NO5
6100	BLAFALLI	300	NO2
6500	TRONDHEIM	300	NO3
6700	ROSSAGA	300	NO4
6701	OFOTEN	420	NO4
7000	HELSINKI	420	FI1
7010	VYBORG_HVDC	420	FI1
7020	ESTLINK_HVDC	420	FI1
7100	OULU	420	FI1
8500	MALMO	420	SE4
8600	ARRIE_HVDC	420	SE4
8700	KARLSH_HVDC	420	SE4

Table B.1: Nordic 44 buses

B.1 N44 model history

There are several precursors to the N44 model. These include test networks Nordic 15, Nordic 18, Nordic 23 and Nordic 32, for which the details leading up to the Nordic 44 test network are described in [10]. N44 itself has several variations based on different theses, for which there are two primary model branches that are referred to as the *NTNU branch* and the *KTH branch*. The latter is based on work done at KTH [1] where effort was made to map Nord Pool historical data to the model and assigning geographical names and area data to buses. The thesis in [49] is based on the KTH-model because of its suitability for power system reliability studies, and the model was in [49] further modified by adding load buses 6702 and 7130 for internal power exchange between Norway and Finland, as well as the addition of 7130 Fenno-Skan for power transmission between Sweden and Finland.

The NTNU branch emphasises dynamic simulations instead of static load flow simulations and is tuned for time-domain studies. Tuning of N44 was performed in [43] to study synthetic inertia, and further used in [50] for small-signal analysis. The branches of the model are illustrated in fig. B.2, where this thesis' model adjustment is also placed into the order of models. As a majority of the changes to the model in this thesis are based on algorithms (for example creating multiple models with generation adjustments or primary reserves deactivated) and several frequency response mechanisms are emulated through Python, it may be difficult to continue development on this N44 branch or to consider the changes made as part of N44 rather than just adjustments for case studies. The only additions made directly to the N44 model in PSS/E, and which may be easily utilizied in future model development, are the dynamic load protection relay models for load shedding.

[1] The Royal Institute of Technology in Stockholm

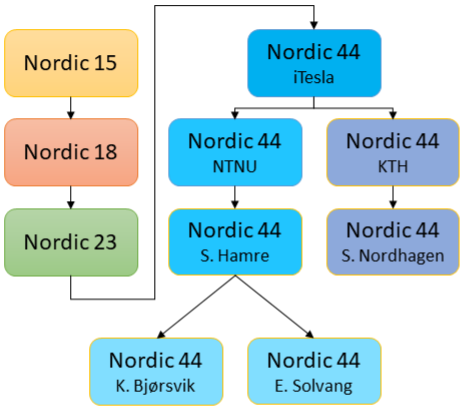

Figure B.2: The development and branches of N44

B.2 Tuning of model towards outages

The work in this thesis is based on tuning in [43] where N44 frequency response was tuned towards a scheduled outage of 1110 MW at Ringhals in Sweden at 5th of March 2015. Tuning was performed by altering the ZIP load to a 10% / 10% / 80% Z/I/P load composition and changing static power flows to match that of the Nord Pool data in hour 11:00 - 12:00 on the specified date. Altering of dynamic models' settings was also performed, such as changing governor settings. Further details are given in the respective thesis. After tuning, the frequency response of the N44 model was shown to be very close to that of the Nordic power grid. All simulations in this thesis are based on the tuning described as a starting point for generation redistribution algorithms that have been described in chapter 5.

Appendix C

PSSE case example

If the reader is interested in applying any of the code in the framework to future projects, a short introductory code explanation from one of the simpler cases is given below.

Line 1 Imports the author's Python framework, which loads the Psspy module as well as other modules

Line 4 Starts the case definition. This case is for the outages in section 7.1

Line 8 Sets variable for maximum transmission capacity of North Sea Link

Line 9 Sets variable for maximum transmission capacity of NordLink

Line 10 Loads the PSS/e and sets the name of the case. The name of the case is used for appending to plots and PSS/E .sav and .dyr files

Line 11 Sets options for the case to be run in PSS/E. For example, the simulation time is set to 90 seconds.

Line 14 Adds HVDC buses to the N44 model as described in section 5.1.3.1

Line 15 Sets the load power import at bus 6010 North Sea Link to maximum transmission capacity and redistributes generation in the area. Redistribution is done as in section 5.2.1

Line 16 Sets the load power consumption at bus 5630 NordLink to maximum transmission capacity and redistributes generation in the area

Line 17 Disconnects generators that have been set to 0 generation by the generation redistribution algorithm

Line 18 Runs a static load flow computation to initialize the model after the load and generation changes that have been made

Line 19 Saves PSS/E .sav and .dyr files to disk for the adjustments that have been made so that it is possible to inspect the adjusted case files in PSS/E GUI

Line 22 Sets the outage of North Sea Link to happen at $t = 1.0$ seconds

Line 23 Sets the outage of NordLink to happen at $t = 1.0$ seconds

Line 24 Prepares the PSS/E dynamic simulation by converting loads to ZIP-loads and initializing dynamic simulation

Line 25 Specifies which machines, buses and branches should be monitored, along with the respective system states such as voltages, angles and active power generation/-consumption/branch flows.

Line 28 Runs the dynamic simulation and executes outages as has been specified

Line 29 Reads datasets from output-files and stores it in the case object (PsspyObject is a class, where each object is a separate case)

Line 30 Calculates the COI-frequency using all machine inertia constants and frequency data as specified in section 3.2.2

Line 31 Plots the results that were specified that the user wishes to monitor, and saves all plots to Latex-folder with case name appended

```
1  import psspyObject
2
3
4  def run_case():
5      # Outage in Norway without any kind of SIPS
6
7  # CONFIGURE PSSPY VARIABLES AND MODELS
8      north_sea_link_load = -1400  # North Sea Link 1400 MW, minus sign means import
9      nord_link_load = -1400  # NordLink 1400 MW
10     current_case = psspyObject.PsspyCase("case1_outage_norway")
11     current_case.configure_case_options(False, 90.0, 0, 10, True, False)
12
13 # STATIC LOAD FLOW ADJUSTMENTS
```

```
    current_case.add_hvdc_buses()
    current_case.set_hvdc_active_power_and_redistribute(6010, north_sea_link_load)  # Set North Sea Link import to 1400 MW
    current_case.set_hvdc_active_power_and_redistribute(5630, nord_link_load)  # Set Nord Link import to 1400 MW
    current_case.disconnect_inactive_generators()
    current_case.run_static_load_flow()
    current_case.save_network_data()

# PREPARATION FOR DYNAMIC ANALYSIS
    current_case.add_event(1.0, 2, 6010, [-north_sea_link_load])  # Step active power to 0 and reactive power to 0
    current_case.add_event(1.0, 2, 5630, [-nord_link_load])
    current_case.prepare_dynamic_simulation(0.005)
    current_case.monitor_channels([3000, 5600, 7000, 8500], [1, 2, 4, 6, 7], (3000, 3020, 3100, 3249, 5600, 5630, 6010, 7000, 7100), (1,2,4), [[3359, 3359], [5101, 3100]])

# RUN SIMULATION AND POST-PROCESS
    current_case.run_dynamic_simulation()
    current_case.read_results()
    current_case.calculate_coi_frequency()
    current_case.plot_results_and_save()
```

Appendix D

Python PSS/E Framework

An excerpt of the code used for simulations is shown here. The code is for the PGUs. The remainder of Python code written for interfacing with this PGU code and used for the work in this thesis as well as in [2] is given in the files associated with the upload of the master thesis.

D.1 Programmable Generation Units

```
import os
import matplotlib.pyplot as plt
import numpy as np

# PSSPY-related packages
import psspy
import dyntools
import redirect

# Default variables for PSSPY
_i = psspy.getdefaultint()
_f = psspy.getdefaultreal()
_s = psspy.getdefaultchar()

class ProgrammableGenerationUnit(object):
    """Creates an object which monitors frequency, ROCOF and voltage to alter the load at a given bus in
     response to the
     local bus quantities, emulating increased generation by reducing load consumption."""
    def __init__(self, bus_number, monitor_type = "BSFREQ", d_write = 5, limits = [49.9, 49.8, 49.7],
     activation_at_limits = [20, 20, 20],
```

```
19                 time_to_activate = [5.0, 5.0, 5.0], max_time_available = [5.0, 5.0, 5.0], max_output =
    10000,
20                 response_remains_active = False):
21         # Variables required upon initialization
22         self.bus_number = bus_number  # Bus at which the PGU is placed
23         # self.load_id = load_id  # Don't have to use load_id, this line can be removed?
24         self.max_change = max_output  # Total max amount of power this unit can supply
25         self.d_write = d_write  # The amount of time-steps between each stop to manually check values and
    initiate control
26
27         # Storing the present load at the bus when PGU is initialized
28         numbers = np.array(psspy.alodbusint(-1, 1, "NUMBER")[1][0])
29         self.load_bus_index = np.where(numbers == bus_number)[0]
30         self.load_at_start = np.array(psspy.alodbusreal(-1, 1, "MVANOM")[1][0])[self.load_bus_index][0]  #
    Add a variable for storing the current load at the desired bus so it is remembered between load
    adjustments
31
32         loads_at_buses = np.array(psspy.aloadint(-1, 1, "NUMBER")[1][0])
33         self.nr_of_loads_at_bus = sum(np.where(loads_at_buses == bus_number)[0] > 0)
34
35         self.limits = limits  # The limits at which the unit supplies power, for example freq=49.5 Hz will
    supply 20 MW
36         self.activation_at_limits = activation_at_limits  # How much power the unit supplies at the
    different sensed limits exceeded
37         self.time_to_activate = time_to_activate  # Used for resetting the counter in
    time_to_activate_counter
38         self.time_to_activate_counter = time_to_activate[:]  # Time-delay for each generation step to
    activate upon sensing
39         #  a limit exceeded
40         self.max_time_available = max_time_available  # The amount of time the different load/supply steps
    can be active
41         self.active_since_last = np.zeros((len(self.limits), 1), dtype=bool)  # Bools if the different
    limits are exceeded between each call of the update_pgu() function
42         self.response_remains_active = response_remains_active  # True if increased frequency should cause
    previous
43         # low-frequency response to deactivate
44
45     # Variables supplied later as the object is called
46         self.time = []  # The time for each measurement
47         self.single_channel_data = []  # The raw-data input from the calling function
48
49     # Variables calculated as function is called over and over
50         self.current_power_output = 0
51         self.channel_time = []
52         self.output_power_over_time = []
53
54     # Interaction with UFLS and UVLS?
55         self.power_previous_pgu_call = 0  # Load power at the end of last iteration with PGU
56         #self.power_current_pgu_call = 0  # Load power at new run with PGU
```

```
57          #load_now = 0
58
59      # Simulation time
60          self.current_time = 0  # The current simulation time when the function is called
61          self.time_since_last_call = 0  # The simulation time passed since the last the load was called
62
63
64          for i in range(len(self.limits)):
65              # The values passed from calling function are p.u. frequency deviation from nominal, so limits must be
66              # converted to the same format.
67              self.limits[i] = (self.limits[i] - 50) / 50
68
69          if self._verify_equal_lengths():
70              pass  # No error in initialization
71          else:
72              self.error  # Some kind of faulty initialization, throw error?
73
74      def update_pgu(self, channel_time, single_channel_data):
75          """
76              Function called every stopped time-step in PssPy to control for the loads' activation parameters and to
77              thereafter step loads if conditions are met.
78          :return:
79          """
80          self.time_since_last_call = channel_time[len(channel_time)-1] - self.current_time
81          self.current_time = channel_time[len(channel_time)-1]
82
83          self.channel_time = channel_time  # Superfluous?
84          self.single_channel_data = single_channel_data  # Superfluous?
85
86
87          # Count the amount of remaining time the unit has to supply MWs
88          for i in range(len(self.active_since_last)):
89              if self.active_since_last[i]:
90                  self.max_time_available[i] -= self.time_since_last_call
91
92          # Has been constant power output since last function call; save this power output so it can be plotted later
93          for i in range(len(channel_time) - len(self.output_power_over_time)):  # For use in plotting power output over time
94              self.output_power_over_time.append(self.current_power_output)
95
96          # Check if conditions are exceeded and activate generation as programmed
97          self._activate_freq_response()  # Check if bus frequency is exceeded, and at which level
98
99      def plot(self, save_plots_local_folder):
100         for i in range(len(self.single_channel_data)):
```

```
101             self.single_channel_data[i] = self.single_channel_data[i] * 50 + 50  # Convert p.u. freq.
    deviation to freq
102
103         fig, ax1 = plt.subplots()
104         fig.suptitle("PGU "+str(self.bus_number), fontsize=12)
105         ax1.plot(self.channel_time, self.single_channel_data, "b-")
106         ax1.set_xlabel("Time [s]")
107         ax1.set_ylabel("Frequency [Hz]", color="b")
108         ax1.tick_params("y", colors="b")
109         ax1.grid()
110
111         ax2 = ax1.twinx()
112         ax2.plot(self.channel_time, self.output_power_over_time, color="r")
113         ax2.set_ylabel("Power output [MW]", color="r")
114         ax2.tick_params("y", colors="r")
115         # For when I want frequency on left y-axis, MW output on right y-axis
116         # https://matplotlib.org/examples/api/two_scales.html
117         pass
118
119     def return_bus_number(self):
120         return self.bus_number
121
122 # Private functions
123     def _verify_equal_lengths(self):
124         # Verifies that the different input matrices are of equal length
125         len1, len2, len3, len4 = len(self.limits), len(self.activation_at_limits), len(self.
    time_to_activate), len(self.max_time_available)
126         return ((len1 == len2) and (len3 == len4) and (len2 == len3))
127
128     def _activate_freq_response(self):
129         bus_freq_data = self.single_channel_data
130
131         # Only works for LOW frequencies, not high frequencies
132         end_index = len(bus_freq_data)  # The index of the latest input data
133         last_freq = bus_freq_data[end_index-1]  # -1 due to zero-indexing
134         test_freq = last_freq*50 + 50
135
136         # Count the amount of remaining time till unit activates
137         for i in range(len(self.time_to_activate)):
138             #if min_freq < self.limits[i]:  # Count down the time until the load should be activated
139             if last_freq < self.limits[i]:
140                 self.time_to_activate_counter[i] -= self.time_since_last_call
141             else:  # Limits not exceeded, generation should not be activated and counter is thus reset
142                 self.time_to_activate_counter[i] = self.time_to_activate[i]
143
144         current_power_output = 0
145         for i in range(len(self.activation_at_limits)):
146             if self.max_time_available[i] > 0 and self.time_to_activate_counter[i] <= 0:
147                 current_power_output += self.activation_at_limits[i]  # Activate this power
```

```
148                 self.active_since_last[i] = 1  # Will now be counter on next iteration
149             else:
150                 self.active_since_last[i] = 0
151         self.current_power_output = min(current_power_output, self.max_change)  # Hinders output exceeding
        maximum
152         if self.response_remains_active:
153             self.current_power_output = max(self.current_power_output, self.power_previous_pgu_call)
154         power_adjustment = self.current_power_output - self.power_previous_pgu_call
155         if power_adjustment == 0:  # If no power change happens since last iteration: do nothing
156             return
157         self.power_previous_pgu_call = self.current_power_output
158         load_now = np.array(psspy.alodbuscplx(-1, 1, "MVANOM")[1][0])[self.load_bus_index][0].real
159         new_load_setpoint = (load_now - power_adjustment)/self.nr_of_loads_at_bus
160         for i in range(self.nr_of_loads_at_bus):
161             psspy.load_chng_4(self.bus_number, str(i+1), [_i, _i, _i, _i, _i, _i],
162                               [new_load_setpoint, _f, _f, _f, _f, _f])
```